



# Azlactome functionalization of magnetic nanoparticles using CRP techniques and their bioconjugation

Yingrak Pray-In

## ► To cite this version:

Yingrak Pray-In. Azlactome functionalization of magnetic nanoparticles using CRP techniques and their bioconjugation. Cristallography. Le Mans Université; Mahāwitthayālai Narēsūan (Phitsanulok), 2014. English. NNT : 2014LEMA1037 . tel-01954187

**HAL Id: tel-01954187**

**<https://theses.hal.science/tel-01954187>**

Submitted on 13 Dec 2018

**HAL** is a multi-disciplinary open access archive for the deposit and dissemination of scientific research documents, whether they are published or not. The documents may come from teaching and research institutions in France or abroad, or from public or private research centers.

L'archive ouverte pluridisciplinaire **HAL**, est destinée au dépôt et à la diffusion de documents scientifiques de niveau recherche, publiés ou non, émanant des établissements d'enseignement et de recherche français ou étrangers, des laboratoires publics ou privés.

# Thèse de Doctorat

Yingrak PRAY-IN

*Mémoire présenté en vue de l'obtention du  
grade de Docteur de l'Université du Maine  
sous le label de L'Université Bretagne Loire  
et en cotutelle avec Naresuan University*

École doctorale : ED3MPL

Discipline : Chimie

Spécialité : Chimie des Matériaux

Unité de recherche : IMMM UMR CNRS n°6283

Soutenue le 24 mars 2014

Thèse N° :

## AZLACTONE FUNCTIONALIZATION OF MAGNETIC NANOPARTICLES USING CRP TECHNIQUES AND THEIR BIOCONJUGATION

### JURY

Examineurs :

**Tirayut VILAIVAN**, Associate professor  
Boonjira RUTNAKORNPITUK, assistant professor  
**Sagrario PASCUAL**, Professeur, Université du Maine  
**Pranee PHINYOCHEEP**, Associate professor  
**Panya SUNINTABOON**, assistant Professor

Directeur de Thèse :

**Laurent FONTAINE**, Professeur, Université du Maine.

Co-directeur de Thèse :

**Metha RUTNAKORNPITUK**, Associate professor

**AZLACTONE FUNCTIONALIZATION OF MAGNETIC NANOPARTICLES  
USING CRP TECHNIQUES AND THEIR BIOCONJUGATION**

**YINGRAK PRAY-IN**

**A Thesis Submitted to the Graduate School of Naresuan University and  
Université du Maine  
in Partial Fulfillment of the Requirements  
for the Doctor of Philosophy Degree in Chemistry  
March 2014  
Copyright 2014 by Naresuan University and Université du Maine**

This thesis entitled “Azlactone functionalization of magnetic nanoparticles using CRP techniques and their bioconjugation submitted by Yingrak Pray-in in partial fulfillment of the requirements for the Doctor of Philosophy Degree in Chemistry is hereby approved.

.....Chair

(Professor Tirayut Vilaivan, D. Phil)

.....Committee

(Associate Professor Metha Rutnakornpituk, Ph.D.)

.....Committee

(Assistant Professor Boonjira Rutnakornpituk, Ph.D.)

.....Committee

(Professor Laurent Fontaine, Ph.D.)

.....Committee

(Sagrario Pascual, Ph.D.)

.....Committee

(Associate Professor Pranee Phinyocheep, Ph.D.)

.....Committee

(Assistant Professor Panya Sunintaboon, Ph.D.)

**Approved**

.....

(Professor Rattana Buosonte, Ph.D.)

Dean of Graduate School

March 2014

## **ACKNOWLEDGEMENT**

First, I would like to sincerely thank my research advisor, Associate Professor Dr.Metha Rutnakornpituk and Professor Dr.Laurent Fontaine, for their support, attention, patience, guidance and encouragement throughout the completion of my research. Deeply thanks are also extended to the member of my committee, Professor Dr.Tirayut Vilaivan, Associate Professor Dr.Pranee Phinyocheep, Assistant Professor Dr.Panya Sunintaboon, Assistant Professor Dr.Boonjira Rutnakornpituk and Dr.Sagrario Pascual for their valuable insight and suggestions.

I also appreciate the faculty and graduate students in the Department of Chemistry for always taking time for technical discussions and sharing materials when necessary, particularly Metha Research Group and Uthai Research Group. The staffs at Naresuan University and Université du Maine are excellent at making everything function smoothly and are irreplaceable.

I especially would like to thank the financial support from the Thailand Research Fund (TRF) (DBG5580002), the Franco-Thai Cooperation Program in Higher Education and Research 2009-2010, supported by the Ministry of Foreign Affairs, Ministry of Higher Education and Research of France and the Commission on Higher Education of Thailand and PHC grant (PHC 2009-2010 n° 20609UF). Financial support from the Royal Golden Jubilee for the scholarship (PHD/0207/2551), Office of the Higher Education Commission, Ministry of Education is also gratefully acknowledged.

Finally and certainly not least, I would like to thank Dr.Uthai Wichai and Dr.Véronique Montembault for their suggestions and taking care of me, my family for their support of all my life choices and their love, which is a constant source of strength for everything I do.

Yingrak Pray-in

<b>Title</b>	AZLACTONE FUNCTIONALIZATION OF MAGNETIC NANOPARTICLES USING CRP TECHNIQUES AND THEIR BIOCONJUGATION
<b>Author</b>	Yingrak Pray-in
<b>Advisor</b>	Associate Professor Dr. MethaRutnakornpituk, Ph.D.
<b>Advisor</b>	Professor Dr. Laurent Fontaine, Ph.D.
<b>Academic Paper</b>	Ph.D. Thesis in Chemistry, Naresuan University, 2014
<b>Keywords</b>	Magnetite, nanoparticle, ATRP, RAFT polymerization, PNA, folic acid, antibody

### ABSTRACT

We herein report the surface modification of magnetite nanoparticle (MNP) with copolymers containing active azlactone rings *via* a grafting ‘from’ and grafting ‘onto’ controlled radical polymerization (CRP) for use as a nano-solid support for immobilization with biomolecules. Three different approaches were presented as following.

First, synthesis of poly(poly(ethylene glycol) methyl ether methacrylate-*stat*-2-vinyl-4,4-dimethylazlactone) (PEGMA-*stat*-VDM)-grafted MNP *via* a grafting ‘from’ atom transfer radical polymerization (ATRP) and its application as a platform for conjugating thymine peptide nucleic acid (PNA) monomer were presented. ATRP of PEGMA and VDM was firstly carried out in a solution system to optimize the reaction condition. It was found that 1/0.2/0.2 molar ratio of [ethyl-2-bromoisobutyrate (EBiB)]<sub>0</sub>/ [copper(I) bromide (CuBr)]<sub>0</sub>/[tris-[2-(dimethylamino)ethyl]amine (Me<sub>6</sub>Tren)]<sub>0</sub>, respectively, led to a good control of the copolymerization; the resulting polymers have molecular weight ( $\overline{M}_n$ ) close to the theoretical ones and relatively narrow polydispersity indices (PDIs = 1.11-1.43). The optimal condition was then applied in the surface-initiated ATRP of MNP. The presence of polymeric shell on MNP core was indicated by fourier transform infrared spectroscopy (FTIR) and vibrating sample magnetometry (VSM) techniques. After immobilization of thymine PNA monomer, thermogravimetric analysis (TGA) results showed that there were 4 wt% of the PNA monomer in the complex (1.2  $\mu$ mol/g complex). The presence of the PNA monomer was also confirmed *via* FTIR and VSM.

In the second work, the synthesis of MNP grafted with PEGMA and VDM *via* ATRP for conjugation with folic acid (FA) was studied. A grafting ‘from’ was applied for the copolymerization of PEGMA and VDM from the particle surface with various molar compositions of PEGMA to VDM (0/100, 30/70, 50/50 and 70/30, respectively). The existence of PEGMA and VDM in the structure was characterized by FTIR, TGA and VSM. It was found that the degree of PEGMA and VDM could be finely tuned by varying the molar ratio of PEGMA and VDM in the copolymerization. After the FA conjugation, TEM result indicated that the FA-conjugated MNP having high VDM content exhibited good dispersibility in water.

Third, the synthesis of MNP grafted with poly(ethylene oxide)-*block*-poly(2-vinyl-4,4-dimethylazlactone) (PEO-*b*-PVDM)diblock copolymer *via* a grafting ‘onto’ strategy and its application as recyclable magnetic nano-support for adsorption with antibody were studied. PEO-*b*-PVDM diblock copolymers were first synthesized using a reversible addition-fragmentation chain transfer (RAFT) polymerization and then grafted onto amino-functionalized MNP by coupling with some azlactone rings of the PVDM block. TEM was used to investigate the particle nanoclustering and its distribution. It was found that increasing the PVDM chain length increased the size of MNP nanoclusters from 20 to 150 nm; approximately 10, 50 and 100 particles/cluster for PEO-*b*-PVDM<sub>21</sub>, PEO-*b*-PVDM<sub>41</sub> and PEO-*b*-PVDM<sub>84</sub> diblock copolymer, respectively. Moreover, TEM images and photo correlation spectroscopy (PCS) technique indicated an improvement in the particle dispersibility in water after coating with the copolymers. The nanoclusters with PEO-*b*-PVDM<sub>84</sub> diblock copolymer coating were used as recyclable magnetic nano-supports for adsorption with antibody. The results show that there was 96-99% adsorption ability during eight adsorption-separation-desorption cycles.



## LIST OF CONTENTS

Chapter	Page
<b>I Introduction and literature review</b> .....	1
1.1 Surface modification of MNP.....	2
1.1.1 Surface modification of magnetite nanoparticle (MNP) <i>via</i> atom transfer radical polymerization (ATRP).....	4
1.1.2 Surface modification of magnetite nanoparticle (MNP) <i>via</i> grafting ‘from’ reversible addition-fragmentation chain transfer (RAFT) polymerization.....	12
1.2 Bioconjugation on surface of magnetic nanoparticle.....	18
1.2.1 Surface functionalization of MNP with peptide nucleic acid (PNA).....	22
1.2.2 Surface functionalization of MNP with folic acid (FA).....	25
1.2.3 Surface functionalization of MNP with antibody.....	30
1.3 Chemistry of azlactone compounds.....	34
1.4 Conclusions.....	35
References.....	36
 <b>II Azlactone functionalization of magnetic nanoparticles using ATRP and their bioconjugation</b> .....	40
Abstract.....	40
2.1 Experimental.....	40
2.1.1 Materials.....	40
2.1.2 Characterization.....	41
2.1.3 General procedure for the synthesis of poly(PEGMA- <i>stat</i> - VDM) copolymers <i>via</i> ATRP in solution.....	42
2.1.4 Synthesis of MNP coated with ATRP initiators (BTPAm- coated MNP).....	42

## LIST OF CONTENTS (CONT.)

Chapter	Page
<b>II</b>	
2.1.5 Synthesis of poly(PEGMA- <i>stat</i> -VDM)-coated MNP <i>via</i> ATRP .....	43
2.1.6 Immobilization of thymine PNA monomer on the poly(PEGMA- <i>stat</i> -VDM)-coated MNP .....	44
2.2 Results and discussion .....	44
2.2.1 Synthesis of poly(PEGMA- <i>stat</i> -VDM) <i>via</i> ATRP in solution .....	44
2.2.2 Preparation of poly(PEGMA- <i>stat</i> -VDM)-coated MNP <i>via</i> ATRP .....	49
2.2.3 Immobilization of thymine PNA monomer on poly(PEGMA- <i>stat</i> -VDM)-coated MNP .....	52
2.3 Conclusions .....	57
References .....	58
<b>III    Hydrophilic azlactone-functionalized magnetite nanoparticle for conjugation with folic acid</b> .....	<b>59</b>
Abstract .....	59
3.1 Experimental .....	59
3.1.1 Materials .....	59
3.1.2 Characterization .....	60
3.1.3 Synthesis of 2-vinyl-4,4-dimethylazlactone (VDM) .....	61
3.1.3.1 Synthesis of <i>N</i> -acryloyl-2-methylalanine .....	61
3.1.3.2 Cyclization of <i>N</i> -acryloyl-2-methylalanine to form VDM cyclic .....	61
3.1.4 Synthesis of poly(PEGMA- <i>stat</i> -VDM) copolymer coated on the MNP surface <i>via</i> ATRP .....	62

## LIST OF CONTENTS (CONT.)

Chapter	Page
<b>III</b>	
3.1.5 Immobilization of folic acid (FA) on the surface of poly(PEGMA- <i>stat</i> -VDM)-coated MNP.....	63
3.2 Results and discussion.....	63
3.3 Conclusions.....	73
References.....	74
<b>IV</b>	
<b>Recyclable magnetic nanocluster crosslinked with poly(ethylene oxide)-<i>block</i>-poly(2-vinyl-4,4-dimethylazlactone) copolymer for adsorption with antibody...</b>	<b>75</b>
Abstract.....	75
4.1. Experimental.....	76
4.1.1 Materials.....	76
4.1.2 Characterization.....	76
4.2 Syntheses.....	77
4.2.1 Synthesis of PEO- <i>b</i> -PVDM diblock copolymers by RAFT polymerization.....	77
4.2.2 Synthesis of (3-aminopropyl)triethoxysilane-grafted MNP (APS-grafted MNP).....	78
4.2.3 Formation of PEO- <i>b</i> -PVDM copolymers-MNP nanocluster.....	78
4.2.4 Adsorption efficiency study of the copolymer-MNP nanoclusters with antibody.....	79
4.2.5 Determination of recycling ability of the PEO- <i>b</i> -PVDM copolymer-MNP nanoclusters in adsorption with anti-rabbit IgG antibody.....	80
4.2.6 Antigen recognition capacity study of antibody-adsorbed magnetic nanoclusters.....	81

## LIST OF CONTENTS (CONT.)

Chapter	Page
<b>IV</b>	
4.3 Results and discussion.....	81
4.4 Conclusions.....	91
References.....	93
<b>V</b> <b>Conclusions</b> .....	94
<b>Appendix A</b> .....	97
<b>Appendix B</b> .....	109
<b>Biography</b> .....	117

## LIST OF TABLES

<b>Chapter I</b>	<b>Page</b>
<b>Table 1.1</b> Examples of various MNP surface modifications.....	19
<b>Chapter II</b>	
<b>Table 2.1</b> ATRP of mixtures of PEGMA and VDM using various molar ratios of EBiB initiator and CuBr/Me <sub>6</sub> Tren catalytic complexes in toluene.....	45
<b>Table 2.2</b> Summary of monomers conversions, $\overline{M}_n$ , and PDIs of poly(PEGMA- <i>stat</i> -VDM) copolymers using 100/100/1/0.4/0.4 molar ratio of [PEGMA] <sub>0</sub> /[VDM] <sub>0</sub> /[EBiB] <sub>0</sub> /[CuBr] <sub>0</sub> / [Me <sub>6</sub> Tren] <sub>0</sub> , respectively, in toluene at 30°C.....	52
<b>Chapter III</b>	
<b>Table 3.1</b> Grafting density of carboxyl groups on poly(PEGMA- <i>stat</i> -VDM)-coated MNP after dispersing in water.....	69
<b>Table 3.2</b> Hydrodynamic diameter (D <sub>h</sub> ) and zeta potential of the MNPs in water at pH 7.4, before and after FA conjugation.....	71
<b>Chapter IV</b>	
<b>Table 4.1</b> Diblock copolymers of PEO and PVDM synthesized by RAFT polymerization at 70°C in 1,4-dioxane: experimental conditions and characterizations.....	82
<b>Table 4.2</b> Hydrodynamic diameter (D <sub>h</sub> ), size distribution and zeta potential of the nanoclusters dispersed in 10 mM MES pH 6 solutions....	86

## LIST OF FIGURES

Chapter I	Page
<b>Figure 1.1</b> (a) Electrostatic stabilization of MNPs, and (b) steric stabilization of MNPs by coating with a surfactant or a polymeric shell.....	3
<b>Figure 1.2</b> Surface modification of MNP <i>via</i> grafting ‘from’ and grafting ‘onto’ strategies.....	3
<b>Figure 1.3</b> Schematic mechanism of atom transfer radical polymerization (ATRP).....	4
<b>Figure 1.4</b> Methods for immobilizing ATRP initiators on MNP surfaces in the preparation of functional polymer brushes by surface-initiated ATRP.....	5
<b>Figure 1.5</b> Schematic representation for the synthesis of PMMA-coated MNPs by a surface-initiated ATRP.....	6
<b>Figure 1.6</b> Illustration of the synthesis route of polystyrene-coated MNP with core/shell structure.....	7
<b>Figure 1.7</b> Surface-initiated ATRP of MNP with PEGMA- <i>b</i> -MMA block copolymer brushes.....	8
<b>Figure 1.8</b> Schematic representation for the preparation of P(PEGMA)-coated MNP by a surface-initiated ATRP.....	8
<b>Figure 1.9</b> Surface modification of MNP with PHEMA brush.....	9
<b>Figure 1.10</b> Schematic diagrams of PHEMA brush-modified beads and the protein binding.....	10
<b>Figure 1.11</b> Synthesis of MNP/PDMAEMA nanoparticles.....	10
<b>Figure 1.12</b> Synthesis of PAA-coated MNPs <i>via</i> ATRP reaction and immobilization of FA.....	11
<b>Figure 1.13</b> Proposed mechanism of the RAFT process.....	13
<b>Figure 1.14</b> Synthetic scheme of chain transfer agent-anchored PS and PS-grafted MNP by grafting ‘onto’ strategy.....	14

## LIST OF FIGURES (CONT.)

Chapter I	Page
<b>Figure 1.15</b> RAFT polymerization of <i>N,N'</i> -dimethylaminoethylacrylate (DMAEMA) and oligo(ethylene glycol) methyl ether acrylate (OEG-A) in the presence of phosphonic acid RAFT agent.....	15
<b>Figure 1.16</b> Strategies for the synthesis of PAA-PEO and PAA-PAMPEO copolymers.....	16
<b>Figure 1.17</b> Proposed stabilization of MNP with PAA-PEO and PAA-PAMPEO copolymers.....	16
<b>Figure 1.18</b> (a) Homopolymerization of <i>N</i> -isopropylacrylamide (NIPAAm) by RAFT process and (b) exchange of the surfactant with a mixture of PNIPAAm and biotin-PNIPAAm in dioxane on the MNP.....	17
<b>Figure 1.19</b> Synthesis of poly(OEG-A) and PNIPAAm having phosphonic acid end-group and ethylpyridyl disulfide end-groups.....	18
<b>Figure 1.20</b> Chemical structures of A) DNA, B) aegPNA, C) acpcPNA and D) hydrogen bonding of nucleotides <i>via</i> Watson-Crick base pairing rules.....	23
<b>Figure 1.21</b> Preparation of PNA-functionalized magnetic nanoparticles (MNPs).....	24
<b>Figure 1.22</b> Functionalized gold shell–cobalt ferrite nanoparticles with thio-lated PNA for use as a PNA/DNA biosensor.....	25
<b>Figure 1.23</b> (A) Chemical scheme for the synthesis of a trifluoroethyl ester terminal PEG silane, (B) immobilization of FA and PEG on MNP surface.....	26
<b>Figure 1.24</b> TEM micrographs of MNP modified with (A) TFEE terminal PEG silane, (B) amine-terminated PEG, and (C) FA- <i>t</i> -BOC-terminal PEG silane.....	27

## LIST OF FIGURES (CONT.)

Chapter I	Page
<p><b>Figure 1.25</b> (A) Synthesis of folate-NHS (10) and (B) surface modification of nanoparticles with FA (11) or (C) PEG-FA conjugate (13).....</p> <p><b>Figure 1.26</b> The surface modification of MNPs with FA.....</p> <p><b>Figure 1.27</b> Modification of MNP with MA (MAM) and with FA (FAMAM).....</p> <p><b>Figure 1.28</b> (A) Synthesis of Azide-Functionalized MNPs, (B) Synthesis of Alkyne-Bound FA, and (C) Synthesis of FA-Functionalized MNPs <i>via</i> Click Reaction.....</p> <p><b>Figure 1.29</b> Chemical structure of amphiphilic polymer.....</p> <p><b>Figure 1.30</b> SDS-PAGE of HER2 from SK-BR3 cell lysate.....</p> <p><b>Figure 1.31</b> Schematic diagram of the process for preparing the magnetite fine particles encapsulated with a polymer.....</p> <p><b>Figure 1.32</b> 2-Vinyl-4,4-dimethylazlactone (VDM) monomer.....</p> <p><b>Figure 1.33</b> Azlactone-ring opening reaction and proposed mechanism.....</p>	<p>27</p> <p>28</p> <p>29</p> <p>30</p> <p>31</p> <p>32</p> <p>33</p> <p>34</p> <p>34</p>
<p><b>Chapter II</b></p>	
<p><b>Figure 2.1</b> The <math>\ln([M]_0/[M])</math> vs time plot and monomers conversions vs time plot of ATRP of PEGMA and VDM using <math>[PEGMA]_0/[VDM]_0/[EBiB]_0/[CuBr]_0/[Me_6Tren]_0</math> molar ratio = 50/50/1/1/1, in toluene at 50°C.....</p> <p><b>Figure 2.2</b> Dependence of <math>\overline{M}_n</math> and <math>\overline{M}_w/\overline{M}_n</math> (PDI) with monomer conversion of ATRP of PEGMA and VDM using <math>[PEGMA]_0/[VDM]_0/[EBiB]_0/[CuBr]_0/[Me_6Tren]_0</math> molar ratio = 50/50/1/1/1, in toluene at 50°C.....</p>	<p>46</p> <p>47</p>



## LIST OF FIGURES (CONT.)

Chapter II	Page
<p><b>Figure 2.3</b> The <math>\ln([M]_0/[M])</math> vs time plot and monomers conversions vs time plot of ATRP of PEGMA and VDM using <math>[PEGMA]_0/[VDM]_0/[EBiB]_0/[CuBr]_0/[Me_6Tren]_0</math> molar ratio = 50/50/1/0.5/0.5, in toluene at 30°C.....</p>	47
<p><b>Figure 2.4</b> Dependence of <math>\overline{M}_n</math> and <math>\overline{M}_w/\overline{M}_n</math> (PDI) with monomer conversion of ATRP of PEGMA and VDM using <math>[PEGMA]_0/[VDM]_0/[EBiB]_0/[CuBr]_0/[Me_6Tren]_0</math> molar ratio = 50/50/1/0.5/0.5, in toluene at 30°C.....</p>	48
<p><b>Figure 2.5</b> The <math>\ln([M]_0/[M])</math> vs time plot and monomers conversion vs time plot of ATRP of PEGMA and VDM using <math>[PEGMA]_0/[VDM]_0/[EBiB]_0/[CuBr]_0/[Me_6Tren]_0</math> molar ratio = 50/50/1/0.2/0.2, in toluene at 30°C.....</p>	49
<p><b>Figure 2.6</b> Dependence of <math>\overline{M}_n</math> and <math>\overline{M}_w/\overline{M}_n</math> (PDI) with monomer conversion of ATRP of PEGMA and VDM using <math>[PEGMA]_0/[VDM]_0/[EBiB]_0/[CuBr]_0/[Me_6Tren]_0</math> molar ratio = 50/50/1/0.2/0.2, in toluene at 30°C.....</p>	49
<p><b>Figure 2.7</b> FTIR spectra of (A) bare MNP, (B) BTPAm-coated MNP and (C) poly(PEGMA-<i>stat</i>-VDM)-coated MNP.....</p>	51
<p><b>Figure 2.8</b> FTIR spectra of (A) thymine PNA monomer, (B) poly(PEGMA-<i>stat</i>-VDM)-coated MNP and (C) poly(PEGMA-<i>stat</i>-VDM)-coated MNP immobilized with thymine PNA monomer.....</p>	53
<p><b>Figure 2.9</b> TEM images of (A) oleic acid-coated MNP (prepared from toluene dispersion), (B) poly(PEGMA-<i>stat</i>-VDM)-coated MNP (prepared from DMF dispersion) and (C) poly(PEGMA-<i>stat</i>-VDM)-coated MNP immobilized with thymine PNA monomer (prepared from DMF dispersion).....</p>	54

## LIST OF FIGURES (CONT.)

Chapter II	Page
<p><b>Figure 2.10</b> TGA curves of (A) bare MNP, (B) BTPAm-coated MNP, (C) poly(PEGMA-<i>stat</i>-VDM)-coated MNP and (D) poly(PEGMA-<i>stat</i>-VDM)-coated MNP immobilized with thymine PNA monomer.....</p>	55
<p><b>Figure 2.11</b> <i>M-H</i> curves of A) bare MNP, B) BTPAm-coated MNP, C) poly(PEGMA-<i>stat</i>-VDM)-coated MNP and (D) poly(PEGMA-<i>stat</i>-VDM)-coated MNP immobilized with thymine PNA monomer.....</p>	56
<p><b>Chapter III</b></p>	
<p><b>Figure 3.1</b> FTIR spectra of poly(PEGMA-<i>stat</i>-VDM)-coated MNPs having molar ratio of PEGMA to VDM of A) 0/100, B) 30/70, C) 50/50 and D) 70/30, respectively.....</p>	65
<p><b>Figure 3.2</b> TEM images of poly(PEGMA-<i>stat</i>-VDM)-coated MNPs having molar ratio of PEGMA to VDM of A) 0/100, B) 30/70, C) 50/50 and D) 70/30, respectively.....</p>	66
<p><b>Figure 3.3</b> TGA curves of A) bare MNP, B) BTPAm-coated MNP and poly(PEGMA-<i>stat</i>-VDM)-coated MNPs having C) 0/100, D) 30/70, E) 50/50 and F) 70/30 molar ratios of PEGMA to VDM, respectively.....</p>	67
<p><b>Figure 3.4</b> <i>M-H</i> curves of A) bare MNP, B) BTPAm-coated MNP and poly(PEGMA-<i>stat</i>-VDM)-coated MNPs having C) 0/100, D) 30/70, E) 50/50 and F) 70/30 molar ratios of PEGMA to VDM.....</p>	68
<p><b>Figure 3.5</b> TEM images of the poly(VDM)-coated MNP, (A-D) before and (A'-D') after the FA conjugation. The MNPs were coated with the copolymers having (A, A') 0/100, (B, B') 30/70, (C, C') 50/50 and (D, D') 70/30 molar ratios of PEGMA to VDM, respectively. All TEM samples were prepared from aqueous dispersions.....</p>	72

## LIST OF FIGURES (CONT.)

Chapter III	Page
<p><b>Figure 3.6</b> (A) TGA thermograms of a) poly(VDM)-coated MNP without FA and b) FA-poly(VDM)-coated MNP and (B) UV-visible absorption spectra of a) poly(VDM)-coated MNP without FA b) FA-poly(VDM)-coated MNP and c) FA.....</p>	73
<p><b>Chapter IV</b></p>	
<p><b>Figure 4.1</b> Overlay SEC trace of (a) PEO<sub>44</sub>-CTA, (b) PEO<sub>44</sub>-<i>b</i>-PVDM<sub>21</sub> copolymer, (c) PEO<sub>44</sub>-<i>b</i>-PVDM<sub>41</sub> copolymer and (d) PEO<sub>44</sub>-<i>b</i>-PVDM<sub>84</sub> copolymer.....</p>	82
<p><b>Figure 4.2</b> A) <sup>1</sup>H NMR spectrum of PEO<sub>44</sub>-<i>b</i>-PVDM<sub>41</sub> copolymer in CDCl<sub>3</sub> and B) FTIR spectrum of PEO<sub>44</sub>-<i>b</i>-PVDM<sub>41</sub> copolymer.....</p>	83
<p><b>Figure 4.3</b> FTIR spectra of A) APS-grafted MNPs, B) PEO-<i>b</i>-PVDM copolymer and C) PEO-<i>b</i>-PVDM-MNP nanoclusters.....</p>	84
<p><b>Figure 4.4</b> TEM images of A) APS-grafted MNP, B) PEO<sub>44</sub>-<i>b</i>-PVDM<sub>21</sub>-MNP nanoclusters, C) PEO<sub>44</sub>-<i>b</i>-PVDM<sub>41</sub>-MNP nanoclusters and D) PEO<sub>44</sub>-<i>b</i>-PVDM<sub>84</sub>-MNP nanoclusters.....</p>	85
<p><b>Figure 4.5</b> TGA thermograms of A) bare MNPs, B) APS-grafted MNPs, C) PEO<sub>44</sub>-<i>b</i>-PVDM<sub>21</sub>-MNP nanoclusters, D) PEO<sub>44</sub>-<i>b</i>-PVDM<sub>41</sub>-MNP nanoclusters and E) PEO<sub>44</sub>-<i>b</i>-PVDM<sub>84</sub>-MNP nanoclusters.....</p>	87
<p><b>Figure 4.6</b> Calibration curve of BGG standard.....</p>	88
<p><b>Figure 4.7</b> Adsorption efficiency of PEO<sub>44</sub>-<i>b</i>-PVDM<sub>84</sub>-MNP nanoclusters for ionic adsorption with anti-rabbit IgG antibody.....</p>	89
<p><b>Figure 4.8</b> Recycling efficiency of PEO<sub>44</sub>-<i>b</i>-PVDM<sub>84</sub>-MNP nanoclusters in the ionic adsorption of anti-rabbit IgG antibody after 8-recycling process....</p>	90

## LIST OF FIGURES (CONT.)

Chapter IV	Page
<p><b>Figure 4.9</b> Scheme showing the indirect method used to visualize the antigen recognition capability; A) 10 mM MES pH 6, B) 1% BSA in 10 mM MES pH 6, C) anti-rabbit IgG-HRP, D) anti-rabbit IgG-adsorbed MNP nanoclusters immobilized with IgG and anti-rabbit IgG-HRP, E) anti-rabbit IgG-adsorbed MNP nanoclusters immobilized with IgG, F) anti-rabbit IgG-adsorbed MNP nanoclusters without IgG (blocked with BSA) and G) MNP nanoclusters.....</p>	91

## LIST OF SCHEMES

<b>Chapter II</b>	<b>Page</b>
<b>Scheme 2.1</b> Surface modification of MNP with poly(PEGMA- <i>stat</i> -VDM) copolymer <i>via</i> ATRP reaction.....	43
<b>Scheme 2.2</b> Immobilization of thymine PNA monomer onto poly(PEGMA- <i>stat</i> -VDM)-coated MNP.....	44
 <b>Chapter III</b>	
<b>Scheme 3.1</b> Synthesis of poly(PEGMA- <i>stat</i> -VDM)-coated MNPs <i>via</i> surface-initiated ATRP reaction.....	62
<b>Scheme 3.2</b> Immobilization of FA onto poly(PEGMA- <i>stat</i> -VDM)-coated MNP.....	63
 <b>Chapter IV</b>	
<b>Scheme 4.1</b> Synthesis of PEO- <i>b</i> -PVDM diblock copolymers by RAFT polymerization.....	78
<b>Scheme 4.2</b> Synthesis of PEO- <i>b</i> -PVDM copolymers-MNP nanocluster.....	79
<b>Scheme 4.3</b> Schematic illustration of an adsorption-separation-desorption cycle of the recyclable copolymer-MNP nanocluster in adsorption with antibody (anti-rabbit IgG).....	80

## ABBREVIATIONS

A	adenine
Ab	antibody
acpc	<i>d</i> -prolyl-2-aminocyclopentanecarboxylic acid
ACVA	4,4'-azobis(4-cyanovaleric acid)
aeg	<i>N</i> -(2-aminoethyl)-glycine
AIBN	2,2'-azobisisobutyronitrile
aminobutyl NTA	<i>N</i> <sub>α</sub> <i>N</i> <sub>α</sub> -bis (carboxymethyl)-L-lysine hydrate
anti-HER2 or anti-HER2/neu	Ab against human epithelial growth factor receptor 2
APS	(3-aminopropyl)triethoxysilane
ATRP	atom transfer radical polymerization
BIB	α-bromoisobutyric acid
BIBB	α-bromoisobutyryl bromide
BMPA	2-bromo-2-methyl(propionic acid)
Bpy	2,2'-byridine
BTPAm	2-bromo-2-methyl- <i>N</i> -(3-(triethoxysilyl) propyl) propanamide
C	cytosine
CEPA	2-carboxyethyl phosphonic acid
CTA	chain transfer agent
CTCs	circulating cancer cells
CTCS	2-(4-chlorosulfonyl-phenyl) ethyl trichlorosilane
CTS	[4-(chloromethyl)phenyl] trichlorosilane
CPA	3-chloropropionic acid
CRP	controlledfree radical polymerization
DCC	1,3-dicyclohexylcarbodiimide
DCSPA	2-[(dodecyl sulfanyl)-carbonothioyl]sulfanylpropanoic acid
DMAEMA	2-( <i>N,N</i> -dimethylamino) ethyl methacrylate
DMAP	4-dimethylaminopyridine

## ABBREVIATIONS

DMF	<i>N,N</i> -dimethylformamide
DMP	2-dodecylsulfanylsulfanylthiocarbonylsulfanyl-2-methyl propionic acid
DMSO	dimethyl sulfoxide
DNA	deoxyribonucleic acid
EBB	DL-ethyl 2-bromobutyrate
EDA	ethylene diamine
EDC	1-[3-(dimethylamino)propyl]-3-ethylcarbodiimide hydrochloride
FA	folic acid
FA-EDBE	$\gamma$ - { <i>N</i> -{2-[2-(2-aminoethoxy) ethoxy]ethyl} folic acid
FeSO <sub>4</sub>	Iron(II) sulfate
G	glycine
HEMA	2-hydroxyethyl methacrylate
His-tagged	polyhistidine-tagged
IAA	Fe(3-allylacetylacetonate) <sub>3</sub>
MA	maltotrionic acid
MAM	maltotrionic acid (MA)-coated MNP
MMA	Methyl methacrylate
$\overline{M}_n$	Number averaged molecular weight
MNP	Magnetite nanoparticle
MRI	magnetic resonance imaging
M <sub>s</sub>	saturation magnetization
NHS	<i>N</i> -hydroxysuccinimide
OEG-A	oligo(ethylene glycol) methyl ether acrylate
PAA	poly(acrylic acid)
PAA-PAMPEO	poly(acrylic acid)-b-poly(acrylate methoxy poly(ethyleneoxide))
PAA-PEO	poly(acrylic acid)-b-poly(ethylene oxide)
PDI	polydispersity index
PEG	poly(ethylene glycol)

## ABBREVIATIONS

PEGMA	poly(ethylene glycol) methacrylate
PEGMA-b-MMA	poly(ethylene glycol)methacrylate-b-methy methacrylate block copolymer
PEO	poly(ethylene oxide)
PDMAEMA	poly(2-dimethylamino) ethyl methacrylate
PHEMA	poly(2-hydroxyethyl methacrylate)
PMDETA	<i>N,N,N',N'',N''</i> -pentamethylenetriamine
PMMA	poly(methyl methacrylate)
PNA	peptide nucleic acid
PNIPAAm	poly(N-isopropylacrylamide)
poly(OEG-A)	poly(oligoethyleneglycol acrylate)
poly( <i>t</i> -BA)	poly( <i>t</i> -butyl acrylate)
P(PEGMA)	poly(poly(ethylene glycol)monomethacrylate)
PS	poly(styrene)
RAFT	reversible addition-fragmentation chain transfer
RNA	ribonucleic acid
SA	succinic anhydride
SAED	selected area electron diffraction
SERS	surface-enhanced raman scattering
T	thymine
TEA	triethylamine
TEOS	tetraethyl orthosilicate
TFEE	bistrifluoroethyestersilane
TGA	thermogravimetric analysis
VDM	2-vinyl-4,4-dimethylazlactone
VSM	vibrating sample magnetometer
XRD	X-ray Diffraction



## CHAPTER I

### INTRODUCTION AND LITERATURE REVIEW

Magnetite nanoparticle ( $\text{Fe}_3\text{O}_4$ , MNP) is a black, ferromagnetic mineral containing both Fe(II) and Fe(III) components that have gained much attention in both scientific and technological fields due to the strong ferromagnetic behavior, less sensitivity to oxidation and relatively low toxicity compared to many other materials (e.g., iron, nickel and cobalt). It is a crystal complex composing of 1:2 molar ratio of Fe (II) to Fe (III) in its structure [1-2]. Several potential applications of MNP in biotechnology have been recently reported such as magnetic resonance imaging contrast (MRI), drug delivery, biomolecular magnetic separation, and medical diagnosis [3-7]. Surface-modification of the MNP core with a suitable and functional organic polymer shell is a method of choice to obtain biocompatible nanoparticle and to enhance dispersibility of the particles in aqueous and organic solvents. In addition, the organic layer on its surface can provide a platform for incorporating biological functional molecules, such as amino acid, protein and enzyme [8-10]. Therefore, surface modification and functionalization with a shell of organic polymers have been widely studied.

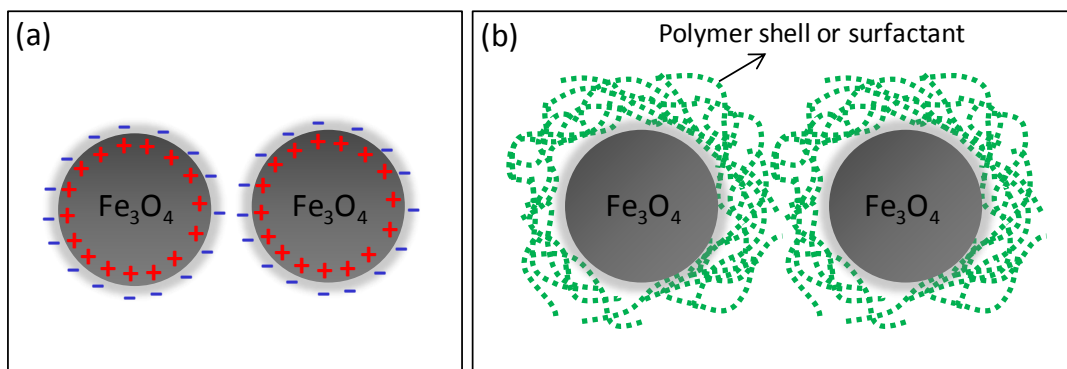
The objective of this research is to modify the MNP surface with the polymeric layer containing azlactone functional groups (2-vinyl-4,4-dimethylazlactone, VDM) *via* a controlled radical polymerization (CRP), such as atom transfer radical polymerization (ATRP) and reversible addition-fragmentation chain transfer (RAFT) polymerization, using either grafting ‘from’ or grafting ‘onto’ techniques. In addition, applications of the azlactone-functionalized MNP for bioconjugation have also been demonstrated. In the first approach (Chapter II), surface-initiated ATRP of the copolymer between poly(ethylene glycol) methacrylate (PEGMA) and VDM (poly(PEGMA-*stat*-VDM)) from MNP was studied. The application of the surface-modified MNP as a scavenger for thymine peptide nucleic acid (PNA) monomer was also demonstrated. In the second approach (Chapter III), the MNPs coated with poly(PEGMA-*stat*-VDM) having various azlactone functionalities were used as a scavenger for folic acid (FA), a cancer cell targeting agent. In the third approach

(Chapter IV), the copolymer between poly(ethylene oxide) (PEO) and VDM (PEO-*co*-PVDM) was synthesized *via* RAFT polymerization in solutions and then grafted ‘onto’ the MNP surface. The particles were used as magnetic nanosolid support for adsorption of antibody.

Therefore, in this chapter, surface modifications of MNP *via* CRP reactions, such as ATRP and RAFT polymerizations, are described in details. The studies in the applications of the MNP for bioconjugations, such as PNA, FA and antibody, are also discussed. In addition, the background of azlactone compounds was then reviewed.

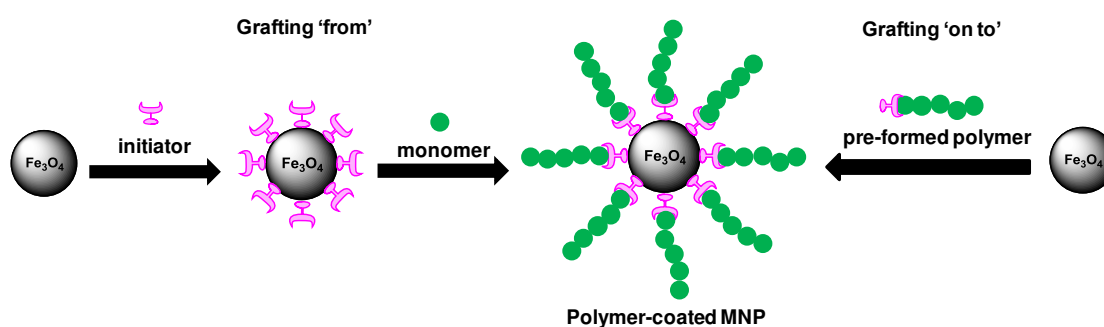
### 1.1 Surface modification of MNP

Because MNP is in nano-scale that has a high surface area-to-volume ratio, it is thus not stable, leading to aggregation in dispersions due to various attractive forces among the particles such as Van der Waals force, gravitational force and magnetic force [11-12]. Large clusters of aggregates take place during or after the synthesis of the MNP because of these attractive forces in order to minimize the total surface energy. Therefore, stabilization of MNPs by surface modification is necessary to protect them from aggregation. Electrostatic and steric stabilizations are typically used for stabilization of the MNPs. In the case of electrostatic stabilization, an electrical double layer of charges is created around the MNPs, resulting in repulsive forces between the particles (Figure 1.1 (a)) [13]. While in the steric stabilization strategy, the MNPs are coated by surfactant such as oleic acid, citric acid and sodium oleate [13]. The particles can be coated with surfactants during and after the synthesis to reduce the surface tension [14]. Polymers are also used as a surfactant by grafting to the particle surface (Figure 1.1 (b)). These polymer shells can increase the steric repulsive force that will prevent the particle agglomeration [13]. In addition, stabilization and surface modification of the MNP with small organic molecules, or polymers, not only prevents uncontrollable aggregation and protects them from the aggregation, but also allows them to be dispersible in various organic solvents or water.



**Figure 1.1** (a) Electrostatic stabilization of MNPs, and (b) steric stabilization of MNPs by coating with a surfactant or a polymeric shell

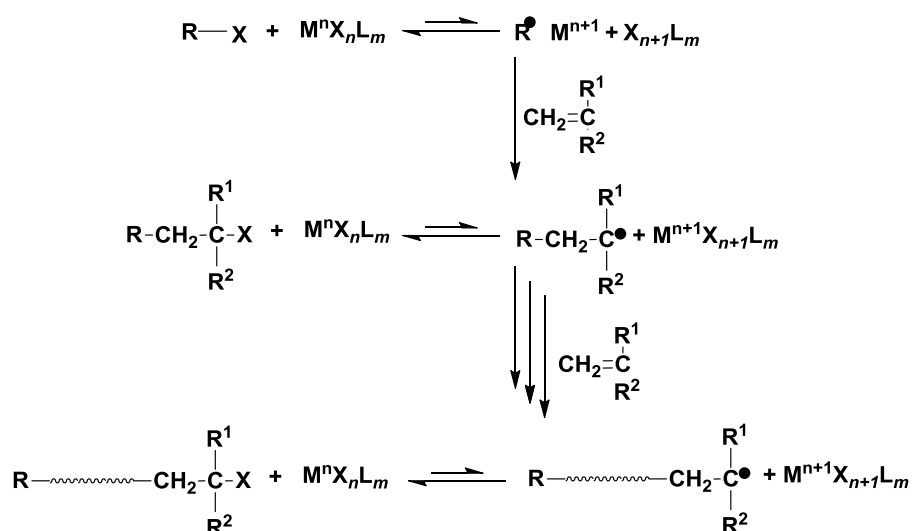
The attachment of polymer chains to the MNP surface can be performed *via* the interaction between the hydroxyl groups on the bare MNP surface and suitable functional groups of polymer chains or active compounds. Two alternative strategies: grafting ‘onto’ and ‘from’ are used to prepare polymer-coated MNP. In the case of grafting ‘from’ strategy, the polymer chain is grown from the initiator-functionalized particle surface, while in the grafting ‘onto’ strategy, a pre-formed polymer with an appropriate functional group is grafted onto the particle surface [15]. The combination of these two strategies with CRP technique has widely used for preparation of polymer-coated particles. Figure 1.2 shows the use of grafting ‘onto’ and ‘from’ strategies to prepare polymer-coated MNP.



**Figure 1.2** Surface modification of MNP *via* grafting ‘from’ and grafting ‘onto’ strategies

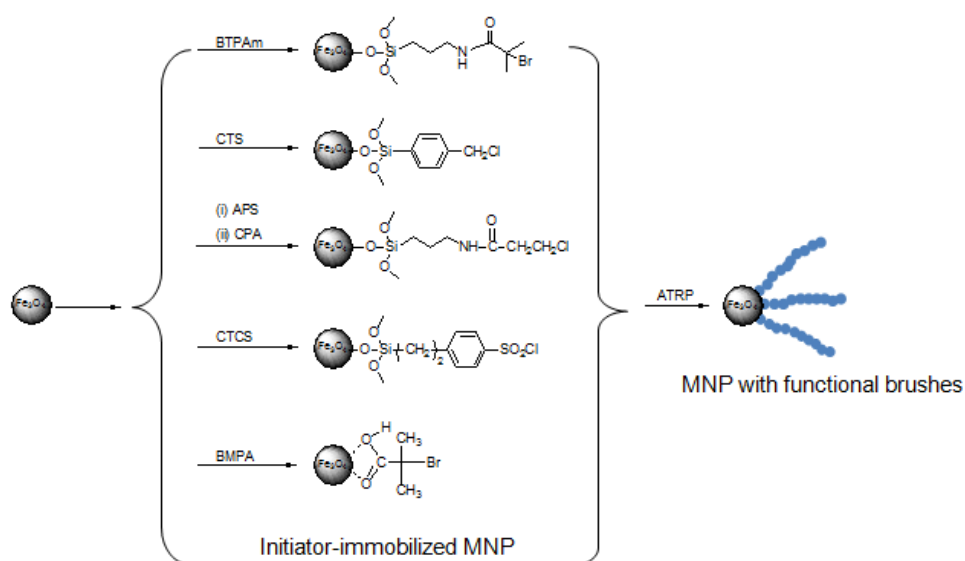
### 1.1.1 Surface modification of magnetite nanoparticle (MNP) *via* atom transfer radical polymerization (ATRP)

ATRP is one of several kinds of CRP, which does not require stringent experimental condition. A wide range of functional monomers such as styrene [16], methacrylate [17], acrylates [18] and *N*-isopropylacrylamide [19] can be used to prepare the polymer with a controllable fashion and narrowly dispersed molecular weights. Figure 1.3 presents the general mechanism of ATRP. In the polymerization, initiating radical species ( $R^\bullet$ ) and an oxidized metal complex ( $M^{n+1}X_{n+1}L_m$ ) will be activated from the carbon-halogen bond in an organic halide ( $R-X$ ) *via* one-electron oxidation of the metal center ( $M^nX_nL_m$ ). After that  $R^\bullet$  is reacted with the halogen on the oxidized metal to regenerate  $R-X$  or added to the monomer to generate a radical species  $[R-CH_2-C(R^1)(R^2)^\bullet]$ . The adduct  $[R-CH_2-C(R^1)(R^2)-X]$  of  $R-X$  and monomer will be then generated *via* an abstraction of a halogen atom from  $M^{n+1}X_{n+1}L_m$ . The carbon-halogen bond of the adduct is subsequently activated by the metal complex, similarly to  $R-X$ , to result in a similar carbon-halogen bond at the polymer terminal *via* a repetitive set of the reactions. The important factors of this reaction are the low concentration of the radical intermediates at a given time and the fast but reversible transformation into the dormant species rather than the addition to monomers [20].



**Figure 1.3** Schematic mechanism of atom transfer radical polymerization (ATRP) [20]

Immobilization of ATRP initiators on nanoparticle surface has prevalently studied. Various methods for immobilizing ATRP initiators on MNP surfaces in the preparation of functional polymer brushes by surface-initiated ATRP are shown in Figure 1.4 A variety of functional molecules such as phosphonate [21], carboxylic acid [22] and alkoxy silanes [16, 23-25] based initiator have been used as efficient ATRP initiators from MNP surface.

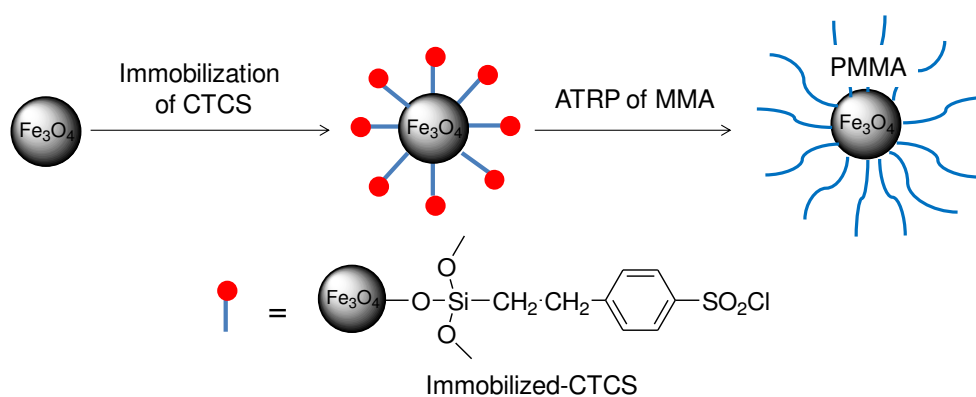


**Figure 1.4** Methods for immobilizing ATRP initiators on MNP surfaces in the preparation of functional polymer brushes by surface-initiated ATRP (BTPAm: 2-bromo-2-methyl-*N*-(3-(triethoxysilyl) propyl) propanamide; CTS: [4-(chloromethyl) phenyl] trichlorosilane; APS: (3-aminopropyl)triethoxysilane; CPA: 3-chloropropionic acid; CTCS: 2-(4-chlorosulfonylphenyl)ethyl trichlorosilane; BMFA: 2-bromo-2-methyl propionic acid [16, 23-25]

Several groups have recently applied a grafting ‘from’ strategy for preparation of polymeric layers on surface of MNP. The advantages of this strategy are that the as-synthesized polymer possesses low polydispersity index (PDI), controllable molecular weight, functionality, composition distribution, and desired polymer architecture.

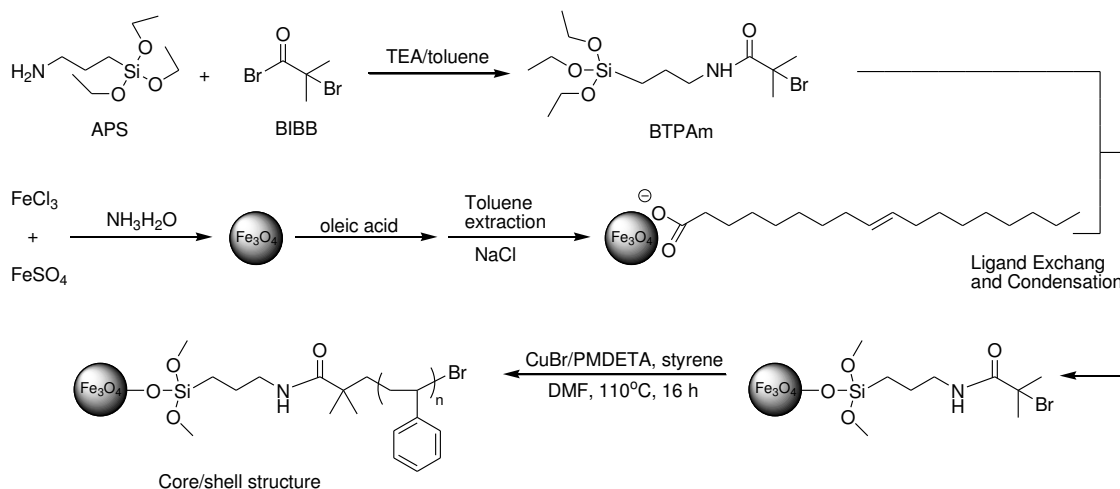
Marutani *et al.* have reported the synthesis of MNP coated with a well-defined poly(methyl methacrylate) (PMMA) (Figure 1.5) [23]. The ATRP initiator, 2-(4-chlorosulfonylphenyl)ethyl trichlorosilane (CTCS) was chemically bound on the

particle surface through the self-assembled monolayer-deposition method. Methyl methacrylate (MMA) monomer was polymerized *via* the surface-initiated ATRP in the presence of *p*-toluenesulfonyl chloride as a free (sacrificial) initiator. The polymerization of MMA on CTCS-functionalized MNP progressed in a living fashion, displaying the first-order kinetics of monomer consumption as well as in the solution in the presence of the free initiator. Moreover, the molecular weight ( $\overline{M}_n$ ) and PDIs were closely with those of the free polymer. This result indicated that the properties of the polymer grafted on the MNP can be determined from the free polymer in the solution.



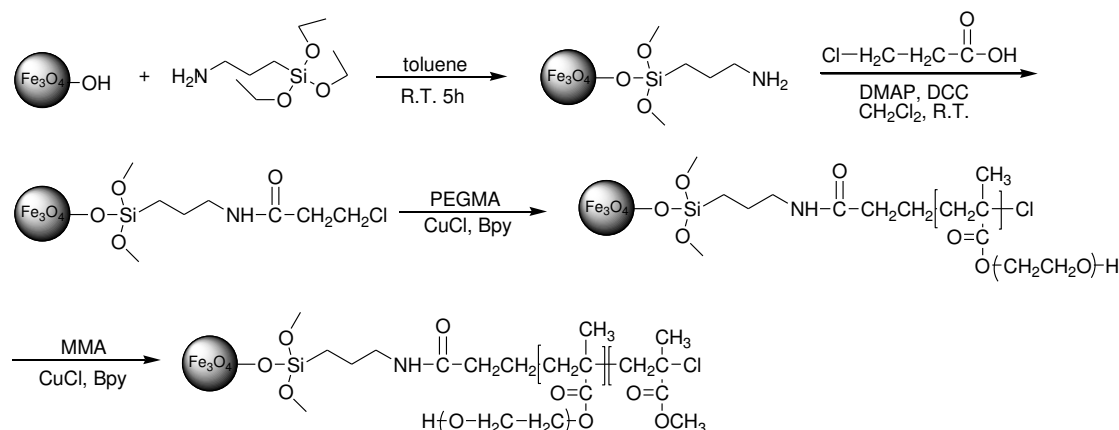
**Figure 1.5** Schematic representation for the synthesis of PMMA-coated MNPs by a surface-initiated ATRP [23]

Sun *et al.* have reported the preparation of MNP/polystyrene core/shell nanoparticles by a surface-initiated ATRP (Figure 1.6) [16]. In the first step, 2-bromo-2-methyl-*N*-(3-(triethoxysilyl) propyl) propanamide (BTPAm), an ATRP initiator was covalently bound onto the MNP surfaces using the combination of ligand exchange and condensation reactions. Then, styrene monomers were grafted from the initiating site *via* an ATRP reaction using copper(I) bromide/*N,N,N',N'',N''*-pentamethylenetriamine (CuBr/PMDETA) as a catalytic complex. The ATRP of styrene showed the characteristics of a controlled/“living” polymerization.



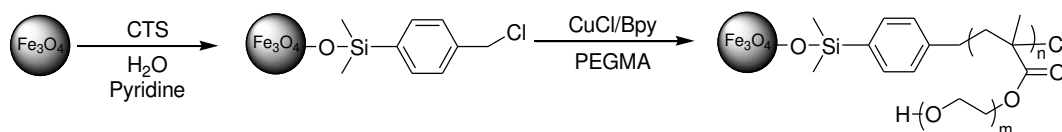
**Figure 1.6** Illustration of the synthesis route of polystyrene-coated MNP with core/shell structure (TEA: triethylamine; BIBB:  $\alpha$ -bromoisobutyryl bromide;  $\text{FeCl}_3$ : iron(III) chloride;  $\text{FeSO}_4$ : iron(II) sulfate; NaCl: sodium chloride; CuBr: copper(I) bromide; PMDETA:  $N,N,N',N'',N'''$ -pentamethylenetriamine); DMF:  $N,N$ -dimethylformamide [16]

Zhou *et al.* have reported the synthesis of poly(ethylene glycol)methacrylate-*b*-methy methacrylate block copolymer (PEGMA-*b*-MMA) brushes on MNP *via* a surface-initiated ATRP (Figure 1.7) [24]. In the first step, MNP was coated with a thin layer of silica of (3-aminopropyl)triethoxysilane to prevent the oxidation and dissolution of the particle. The ATRP initiator (3-chloropropionic acid) was then immobilized onto the silica surface *via* amidation reaction. PEGMA macromonomer was grafted from the immobilized initiators to give the macroinitiators for the ATRP of the MMA second block. It was found that the biocompatibility of the particles was considerably improved by introducing a monolayer of PEGMA to its surface. Moreover, the capability of the modified particles in resistance to the proteins non-specific adsorption was higher than the uncoated particles.



**Figure 1.7** Surface-initiated ATRP of MNP with PEGMA-*b*-MMA block copolymer brushes (DMAP: 4-dimethylaminopyridine; DCC: 1,3-dicyclohexylcarbodiimide; CuCl: copper(I) chloride; Bpy: 2,2'-bipyridine) [24]

Hu, *et al.* have presented the surface modification of MNP through the growth of poly(poly(ethylene glycol)monomethacrylate) (P(PEGMA)) using a [4-(chloromethyl) phenyl] trichlorosilane (CTS) as a silane ATRP initiator (Figure 1.8) [25]. The modified nanoparticles were well dispersible in aqueous solution. The saturation magnetization values of the P(PEGMA)-immobilized nanoparticles were 19 emu/g and 11 emu/g after 2 and 4 h polymerization, respectively, compared to 52 emu/g for the pristine MNPs. This method provides opportunities for grafting a layer of hydrophilic polymer brushes onto the MNPs surface.

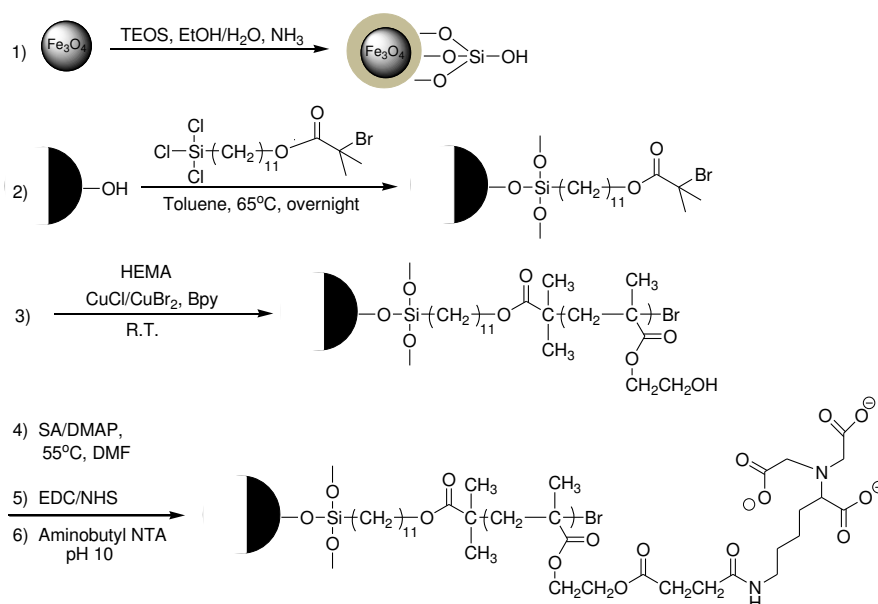


**Figure 1.8** Schematic representation for the preparation of P(PEGMA)-coated MNP by a surface-initiated ATRP [25]

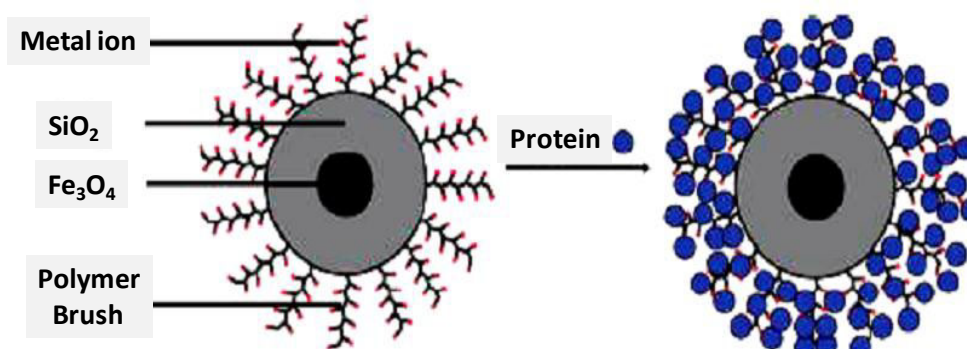
Xu *et al.* have presented the synthesis of MNP with poly(2-hydroxyethyl methacrylate) (PHEMA) brushes through ATRP from surface-immobilized initiators (Figure 1.9) [26]. The PHEMA-grafted particle was subsequently functionalized with nitrilotriacetate- $\text{Ni}^{2+}$  to give magnetic beads for selective capture of polyhistidine-



tagged (His-tagged) protein from cell extracts (Figure 1.10). First, the MNP was coated with silica and then immobilized with ATRP initiators *via* silanization. The immobilized initiators were used to polymerize HEMA monomer to give PHEMA-grafted MNP. After that, the polymer brushes were further reacted with succinic anhydride (SA) and  $N_\alpha, N_\alpha$ -bis (carboxymethyl)-L-lysine hydrate (aminobutyl NTA). It was found that His-tagged protein can be rapidly isolated from a cell extract with high purity by using this particle. The 50 nm thickness of polymer brushes can reduce the diffusion limitation and allow protein capture in a short period of time (5 min). Furthermore, the polymer brush-modified particles provide high protein recoveries and can be recycled.

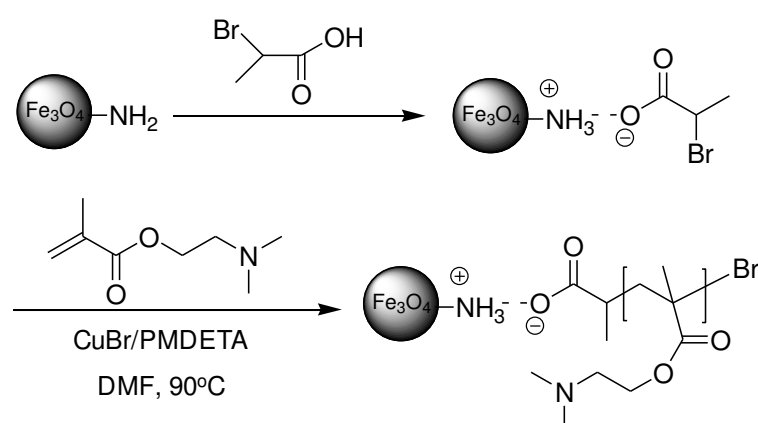


**Figure 1.9** Surface modification of MNP with PHEMA brush (TEOS: tetraethyl orthosilicate; EtOH: ethanol; HEMA: 2-hydroxyethyl methacrylate; CuCl: copper(I) chloride;  $\text{CuBr}_2$ : copper(II) bromide; Bpy: 2,2'-bipyridyl; DMAP: 4-dimethylaminopyridine; DMF:  $N,N$ -dimethylformamide; EDC: 1-[3-(dimethylamino)propyl]-3-ethylcarbodiimide hydrochloride; NHS:  $N$ -hydroxysuccinimide) [26]



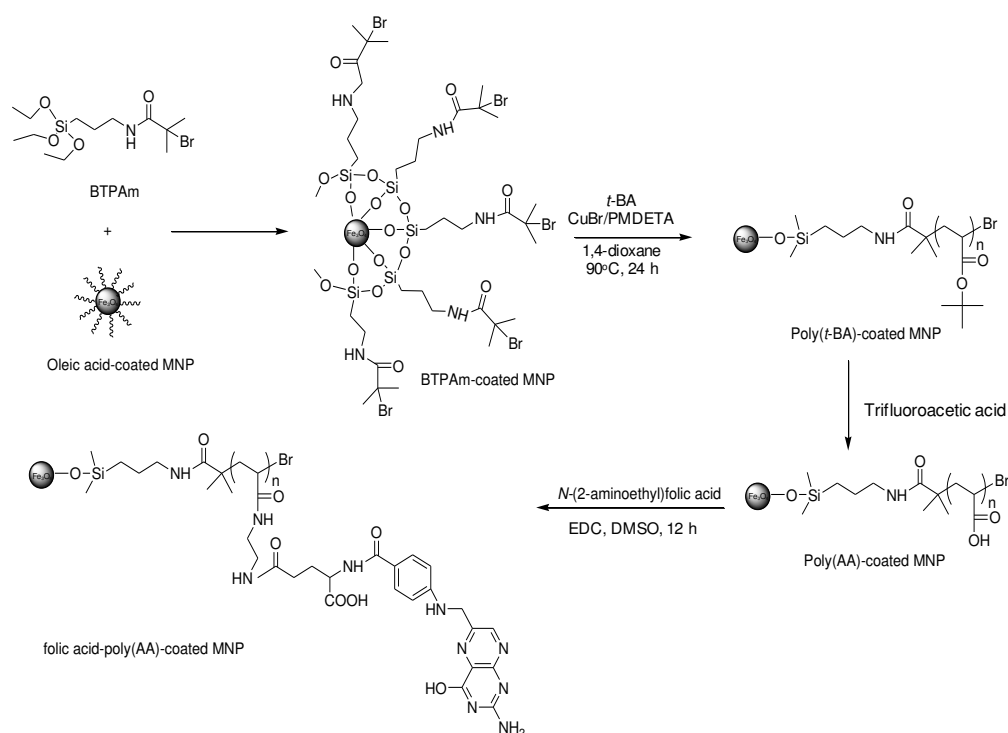
**Figure 1.10** Schematic diagrams of PHEMA brush-modified beads and the protein binding [26]

Zhou *et al.* have functionalized MNP with pH-sensitive poly(2-dimethylamino) ethyl methacrylate (PDMAEMA) for use as a drug carriers and controllable release (Figure 1.11) [27]. The MNP/PDMAEMA core-shell nanoparticles were synthesized by two-step methods; 1) grafting of  $\alpha$ -bromoisobutyric acid (BIB) onto the MNP and 2) polymerization of 2-(*N,N*-dimethylamino) ethyl methacrylate (DMAEMA) monomer from the immobilized-initiators *via* ATRP reaction in the presence of DL-ethyl 2-bromobutyrate (EBB) as a sacrificial initiator (free initiator). The core-shell nanoparticles were capable to load drugs into the polymer shell. The release rate of the drugs can be efficiently controlled by adjusting the pH value of the MNP dispersion.



**Figure 1.11** Synthesis of MNP/PDMAEMA nanoparticles (CuBr: copper(I) bromide; PMDETA: *N,N,N',N'',N'''*-pentamethylenetriamine) [27]

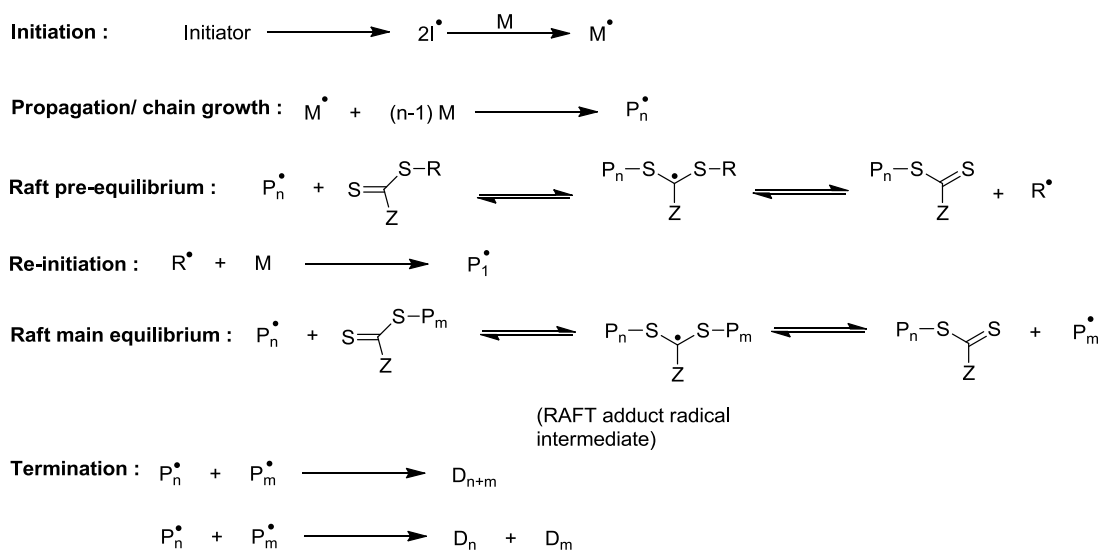
Furthermore, Rutnakornpituk *et al.* have presented the surface modification of MNP with poly(*t*-butyl acrylate) (P(*t*-BA)) *via* ATRP, followed by a hydrolysis of *t*-BA groups to obtain poly(acrylic acid) (PAA) and finally immobilization of folic acid (FA) on its surface (Figure 1.12) [28]. FA was successfully activated with ethylene diamine (EDA) to obtain primary amine-terminated folic acid derivative. This logical strategy enhanced the reactivity of FA to efficiently react with carboxylic acid overexpressed on the surface of PAA-coated MNPs through amidization reaction. Moreover, PAA on MNP surface can also provide stabilization mechanisms through both steric and electrostatic repulsion.



**Figure 1.12** Synthesis of PAA-coated MNPs *via* ATRP reaction and immobilization of FA (CuBr: copper(I) bromide; PMDETA: *N,N,N',N'',N'''*-pentamethylenetriamine; EDC: 1-[3-(dimethylamino)propyl]-3-ethylcarbodiimide hydrochloride; DMSO: dimethyl sulfoxide) [28]

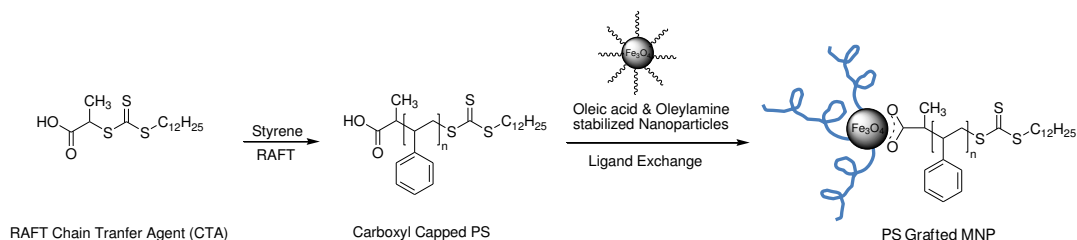
### 1.1.2 Surface modification of magnetite nanoparticle (MNP) *via* grafting ‘from’ reversible addition-fragmentation chain transfer (RAFT) polymerization

The RAFT process utilizes classic free radical initiators and monomers but also includes the presence of chain transfer agent (CTA) in the reaction. This technique, similar to other CRP techniques, produces polymers with controllable molecular weight with narrow PDIs. Figure 1.13 presents the proposed mechanism of RAFT polymerization by Thang *et al.* in 1998. The reaction initiated from a decomposition of radical initiator such as peroxide or azo to form two radical fragments ( $I^\bullet$ ), which can react with monomers to yield propagating species ( $M^\bullet$ ) (initiation step). After that, the longer propagating radicals ( $P_n^\bullet$ ) are generated by the reaction between the initiating radicals ( $M^\bullet$ ) and monomer ( $M$ ) (propagation/chain growth step). A polymeric propagating radical ( $P_n^\bullet$ ) then reacts with the RAFT agent to form a RAFT adduct radicals. This step may undergo a fragmentation reaction in either way to give either the starting species or radical ( $R^\bullet$ ) and a polymeric RAFT agent ( $S=((Z)S-P_n)$ ). This is a reversible step that the intermediate RAFT adduct radical is able to lost either the R group ( $R^\bullet$ ) or the polymeric species ( $P_n^\bullet$ ) (RAFT pre-equilibrium). Then, the leaving group radical ( $R^\bullet$ ) reacts with another monomer to initiate more active polymer chain (re-initiation step). In the next step, the main RAFT equilibrium begins by the same mechanism of the RAFT pre-equilibrium step. However, in this stage, this process takes place only between propagating chains and macro RAFT agents, resulting in a rapid change of dithioester cap. This process ensures that each chain has the same possibility of growth and decreases in termination reactions. Polymerization is mainly terminated *via* a re-combination process to form dead polymers ( $D_{n+m}$ ,  $D_n$ ,  $D_m$ ). Ideally, the RAFT adduct radical is sufficiently hindered such that it does not undergo termination reactions [29].



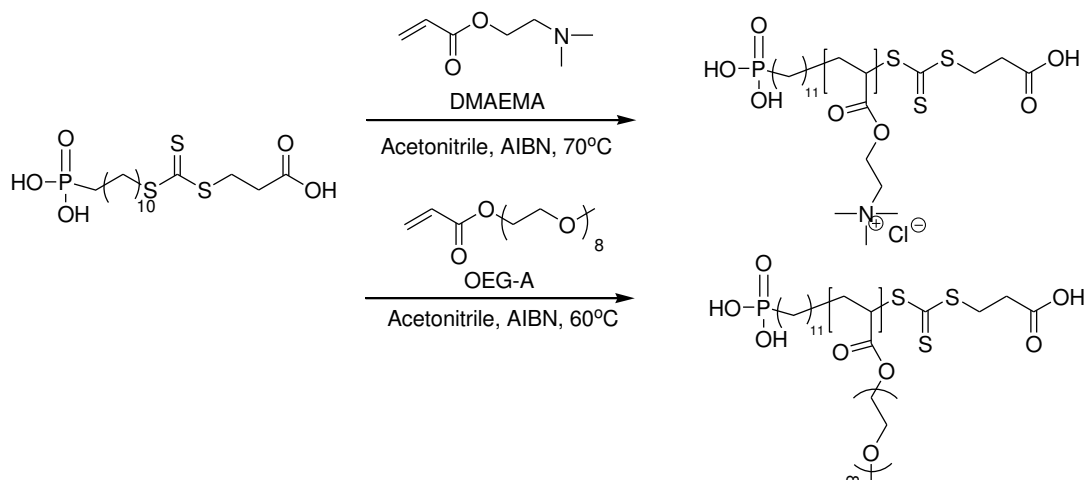
**Figure 1.13** Proposed mechanism of the RAFT process [29]

Many works have applied RAFT polymerization technique to modify MNP surface. In 2012, Jiao *et al.* have presented the synthesis of poly(styrene) (PS)-grafted MNP by grafting ‘onto’ strategy [30]. PS containing a carboxyl group and RAFT agent was first synthesized using 2-[(dodecyl sulfanyl)-carbonothioyl]sulfanylpropanoic acid (DCSPA) as a RAFT agent in the presence of an azobisisobutyronitrile (AIBN) initiator (Figure 1.14). The carboxyl-capped PS was coupled with the MNP stabilized with oleic acid and oleylamine by a ligand-exchange reaction (Figure 1.14). The PDI of the resulting polymer was narrow (1.06-1.28), indicating the characteristics of RAFT polymerization. The grafting density of the polymer brushes on the MNPs was controlled by adjusting the ratio of PS to the MNP in the reaction. The results indicated that the nanostructure of the particles can be changed by varying the grafting density and chain lengths of PS.



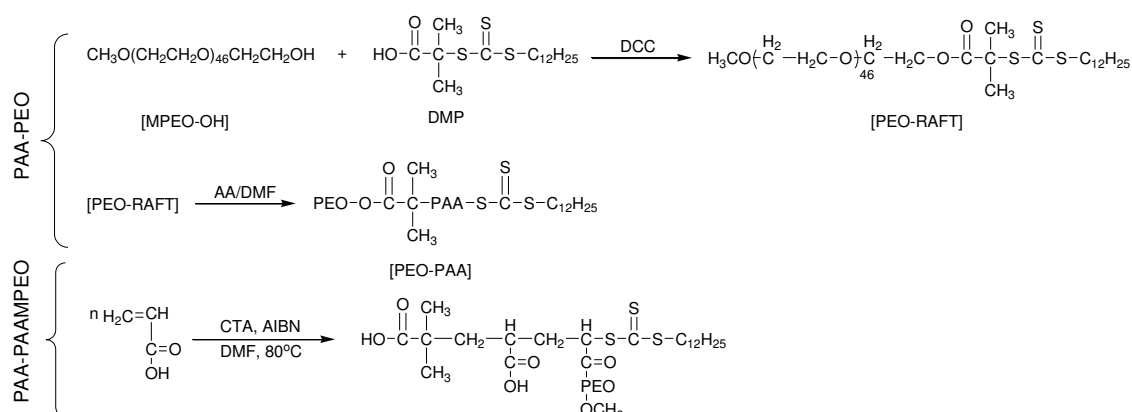
**Figure 1.14** Synthetic scheme of chain transfer agent-anchored PS and PS-grafted MNP by grafting ‘onto’ strategy [30]

Boyer *et al.* have modified MNP surface *via* a grafting ‘onto’ strategy using phosphonic acid-terminated polymer synthesized by RAFT polymerization [31]. First, oligo(ethylene glycol) methyl ether acrylate (OEG-A) and *N,N'*-dimethylaminoethylacrylate (DMAEA) were polymerized in the presence of an  $\alpha$ -phosphonic acid RAFT agent. Two types of polymers:  $\alpha$ -phosphonic acid-P(OEG-A) and  $\alpha$ -phosphonic acid-P(DMAEA), were obtained (Figure 1.15). It was found that the  $\overline{M}_n$  values of the polymers were nearly with those of the targeted  $\overline{M}_n$  values. The narrow PDIs were also observed (PDIs below 1.3). Moreover, the first-order kinetics of the monomer consumption confirmed the controlled characteristics of CRP. Each polymer was conjugated to the MNP surface to yield P(OEG-A)-coated MNP and P(DMAEMA)-coated MNP. It was found that the MNP coated with these two polymers were well dispersible in aqueous solutions. In addition, it was also tested that these surface-modified MNPs were non-toxic to human neuroblastoma cells and capable of complexing siRNA.

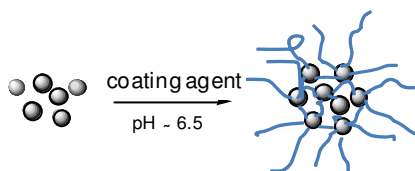


**Figure 1.15** RAFT polymerization of *N,N'*-dimethylaminoethylacrylate (DMAEMA) and oligo(ethylene glycol) methyl ether acrylate (OEG-A) in the presence of phosphonic acid RAFT agent [31]

Aqil *et al.* have prepared diblock copolymer based on poly(acrylic acid) (PAA) for use as a polymeric surfactant of MNP [32]. Two types of diblock copolymers, poly(acrylic acid)-*b*-poly(ethylene oxide) (PAA-PEO) and poly(acrylic acid)-*b*-poly(acrylate methoxy poly(ethyleneoxide)) (PAA-PAMPEO), were synthesized by RAFT polymerization with 2-dodecylsulfanylsulfanylthiocarbonylsulfanyl-2-methyl propionic acid (DMP) as a chain transfer agent (CTA) (Figure 1.16). The molecular weight of the copolymers increased linearly with monomer conversion and their PDIs were lower than 1.15, indicating the characteristics of RAFT polymerization. After that PAA-PEO and PAA-PAMPEO were used separately to stabilize MNP by PAA containing block copolymers (Figure 1.17).



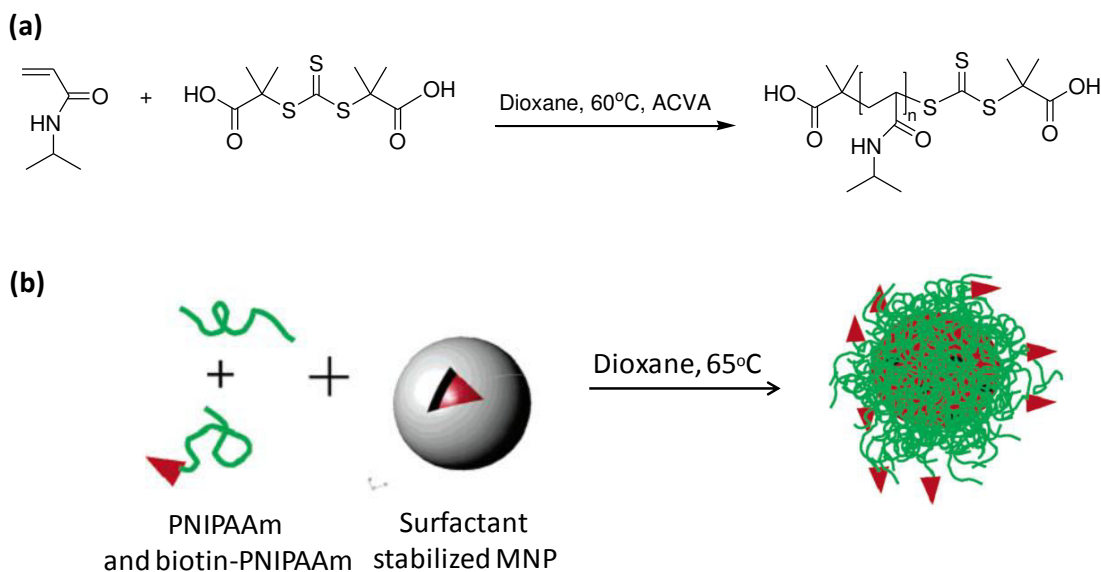
**Figure 1.16** Strategies for the synthesis of PAA-PEO and PAA-PAMPEO copolymers [32]



**Figure 1.17** Proposed stabilization of MNP with PAA-PEO and PAA-PAMPEO copolymers [32]

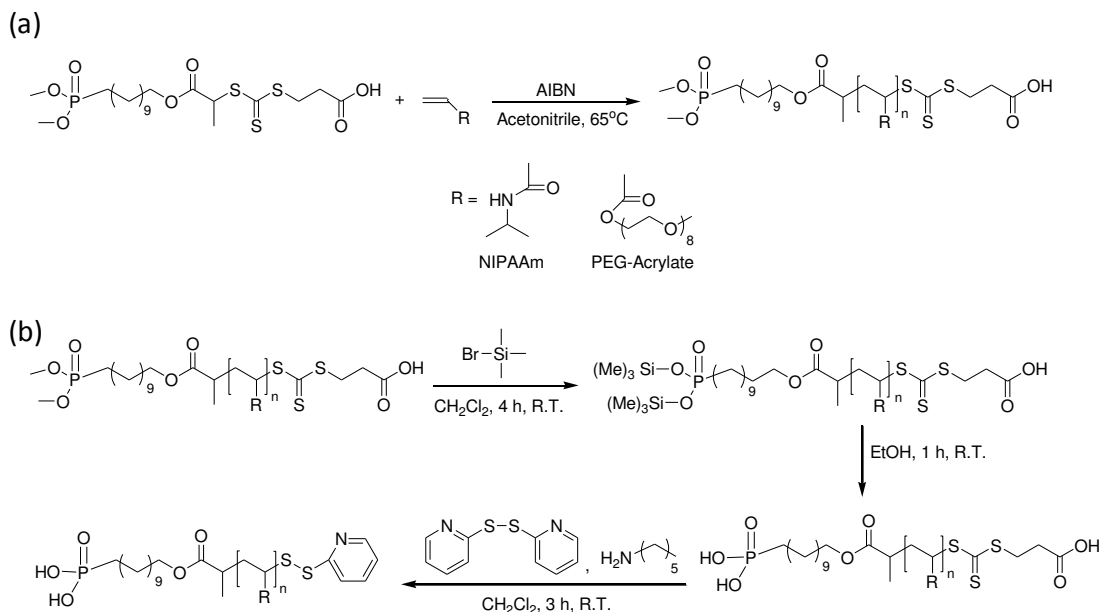
Narain *et al.* have reported the synthesis of monodisperse biotinylated poly(*N*-isopropylacrylamide) (PNIPAAm)-coated MNP for bioconjugation with streptavidin. PNIPAAm was first synthesized by RAFT polymerization using *S,S'*-bis( $\alpha,\alpha'$ -dimethyl- $\alpha''$ -acetic acid)trithiocarbonate and 4,4'-azobis(4-cyanovaleric acid) (ACVA) as a CTA and initiator, respectively (Figure 1.18 (a)) [33]. Biotin was then conjugated at one end of the polymer chain to yield biotin-PNIPAAm through the coupling reaction between PNIPAAm and a PEO maleimide-activated biotin. The mixture of PNIPAAm and biotin-PNIPAAm was mixed with the particle in an attempt to yield biotin-PNIPAAm-coated MNP *via* the interaction between carboxylate groups of the polymers and the particle surface (Figure 1.18 (b)). The binding of biotin-coated particle to streptavidin was observed by fluorescence and surface plasmon resonance. It was found that the biotin-coated particles have a high affinity to bind with streptavidin in solution or when the streptavidin was immobilized on the surface.





**Figure 1.18** (a) Homopolymerization of *N*-isopropylacrylamide (NIPAAm) by RAFT process and (b) exchange of the surfactant with a mixture of PNIPAAm and biotin-PNIPAAm in 1,4-dioxane on the MNP [33]

Furthermore, stabilization and bioconjugation of MNP with hetero-telechelic polymers synthesized by RAFT polymerization were reported [Boyer *et al.* [34]]. Water soluble telechelic polymers of poly(oligoethyleneglycol acrylate) P(OEG-A) and PNIPAAm were first synthesized using trithiocarbonate compounds containing a dimethyl group as a CTA in the presence of AIBN initiator (Figure 1.19 (a)). After modification of one terminal of the polymers to obtain phosphonic acid end-groups and another terminal to obtain ethylpyridyl disulfide end-groups, the phosphonic acid can conjugate to the particle surface, resulting in stable particles dispersible in water. It was found that the particles grafted with P(OEG-A) having  $\overline{M}_n$  larger than 10,000 g/mol were stable in phosphate buffers for several days. Additionally, the particles grafted with P(OEG-A) having  $\overline{M}_n = 62,000$  g/mol were stable in varying concentration of bovine serum albumin (BSA) in phosphate buffer solution. It was found that reduced glutathione (as a model peptide) and NGR motif (as a tumor targeting peptide) were successfully conjugated onto the polymer-stabilized MNP by the  $\omega$ -dithiopyridine functionality of the polymer.

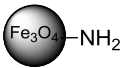
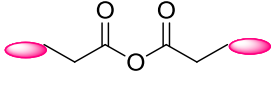
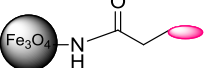
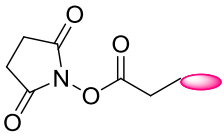
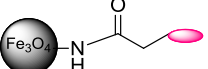
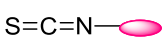
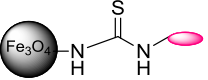
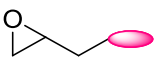
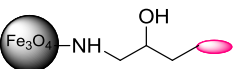
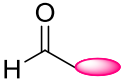
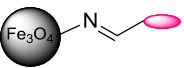
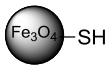
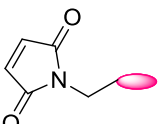
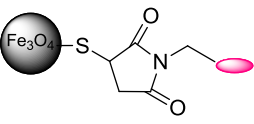
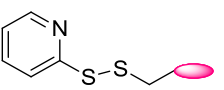
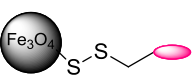


**Figure 1.19** Synthesis of P(OEG-A) and PNIPAAm having phosphonic acid end-group and ethylpyridyl disulfide end-groups [34]

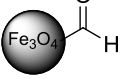
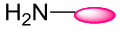
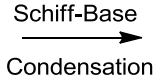
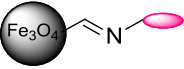
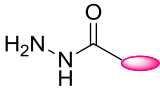

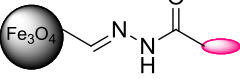
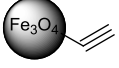
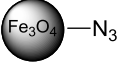

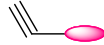
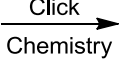
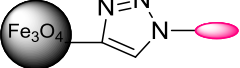
## 1.2 Bioconjugation on surface of magnetic nanoparticle

Besides the creation of hydrophilic polymers on magnetic nanoparticle surface and making them stable against agglomeration in water, surface modification with polymeric surfactant can also provide a platform for functionalization with bioentities. Various chemical approaches have been used for conjugation of biomolecules on particle surfaces such as targeting agent, therapeutic and imaging reporter molecules. These can be achieved by covalent linkage approaches (direct nanoparticle conjugation, click chemistry, covalent linker chemistry) and physical interactions (electrostatic, hydrophilic/hydrophobic interactions). Table 1.1 shows some examples of strategies that can be used for surface modification.

**Table 1.1** Examples of various MNP surface modifications

Covalent bonding attachment			
1. Direct nanoparticle conjugation			
Nanoparticle	Reactive ligand	Conjugate	Typical ligands
 <b>Amine</b>	 <b>Anhydride</b>		Activated small molecules, dyes, peptides, proteins or antibodies (Ref. [35-38], [40])
	 <b>Succinimidyl ester</b>		
	 <b>Isothiocyanate</b>		
	 <b>Epoxide</b>		
	 <b>Aldehyde</b>	Schiff-Base Condensation 	
 <b>Sulfhydryl</b>	 <b>Maleimide</b>		Activated dyes, peptides, proteins or antibodies (Ref. [39])
	 <b>Pyridyl Disulfide</b>		

**Table 1.1** (cont.)

<b>Covalent bonding attachment</b>			
1. Direct nanoparticle conjugation			
Nanoparticle	Reactive ligand	Conjugate	Typical ligands
 <b>Aldehyde</b>	 <b>Amine</b>	 	Amine-containing or hydrazide activated small molecules, dyes, peptides, proteins or antibodies (Ref. [41-42])
	 <b>Hydrazide</b>	 	
 <b>Alkyne</b> or  <b>Azide</b>	 <b>Azide</b> or  <b>Alkyne</b>	 	Activated small molecules, dyes, peptides, proteins or antibodies (Ref. [35], [43-44])

**Table 1.1** (cont.)

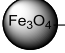
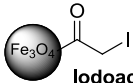

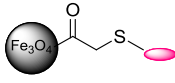
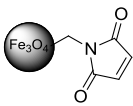

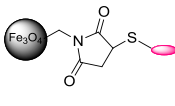
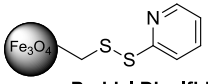

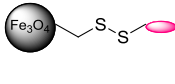
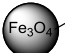
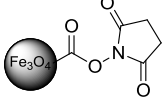

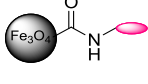
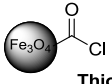

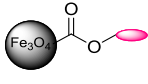


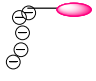
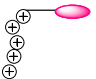
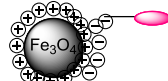
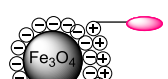
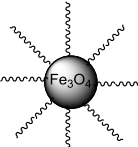
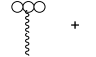
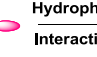
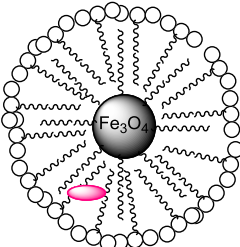
2. Linker chemistry conjugation				
Starting nanoparticle	Linker chemistry	Reactive ligand	Conjugate	Typical ligands
 <b>Amine</b>	 <b>Iodoacetyl</b>	+ HS- 		Activated small molecule, peptides, proteins, antibodies or aptamers (Ref. [38-39])
	 <b>Maleimide</b>	+ HS- 		
	 <b>Pyridyl Disulfide</b>	+ HS- 		
 <b>Carboxyl</b>	 <b>EDC or DCC/NHS</b>	+ H <sub>2</sub> N- 		Amine-containing molecules (Ref. [28], [39], [45-46])
	 <b>Thionyl Chloride</b>	+ HO- 		

Table 1.1 (cont.)

Physical interaction attachment			
Starting nanoparticle	Ligand	Functionalized nanoparticle	Typical ligand
 or  <b>Charged surface</b>	 +  <b>Electrostatic Interaction</b>	 	Modified peptides, proteins or antibodies, DNA or RNA (Ref. [47-48])
 <b>Hydrophobic surface</b>	 +  <b>Hydrophobic Interaction</b>		Hydrophobic molecules (Ref. [49])

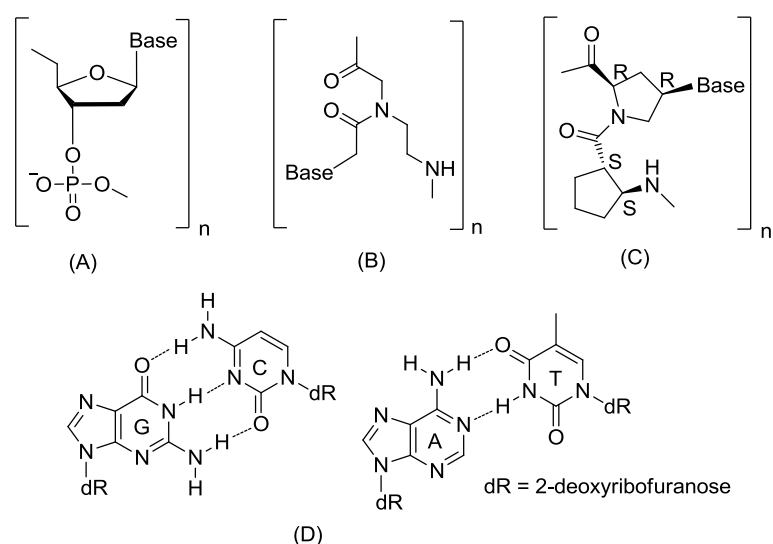
Various biological molecules such as antibodies, proteins, targeting ligands, PNA, DNA and FA, can be chemically bound to nanoparticle surfaces through those linkages. Because the current work involved the immobilization of PNA, FA or antibodies on MNP surfaces, introduction to PNA, FA and antibodies-immobilized nanoparticles have been reviewed.

### 1.2.1 Surface functionalization of MNP with peptide nucleic acid (PNA)

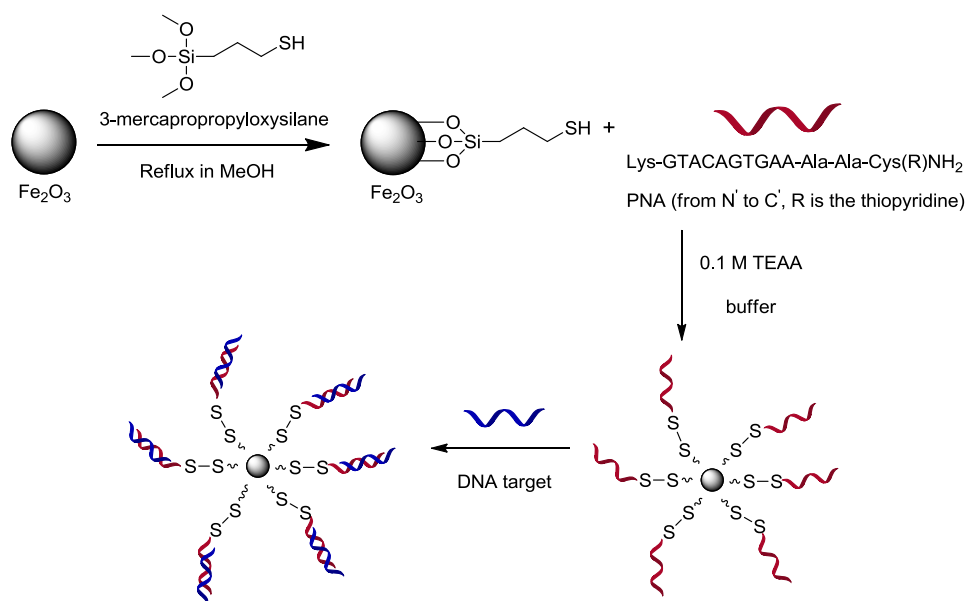
Peptide nucleic acid (PNA) is a synthetic deoxyribonucleic acid (DNA) mimic in which the phosphate backbone is replaced by repeating units of a flexible pseudo-peptide polymer such as *N*-(2-aminoethyl)-glycine units or *d*-prolyl-2-aminocyclopentanecarboxylic acid units that linked by peptide bonds, so called aegPNA [50] and acpcPNA [51], respectively (Figure 1.20). Because the PNA backbone contains no charged phosphate groups, the hybridization between PNA and

DNA strands is stronger than between DNA and DNA strands due to the lack of electrostatic repulsion. Hybridization between DNA and PNA abides by the Watson-Crick base pairing rule; adenine (A) bonds with thymine (T) and cytosine (C) bonds with glycine (G) (Figure 1.20).

In addition, PNA is not recognized by nuclease and protease, making it resistant to enzyme degradation. These unique properties of PNA have led to the development of a wide range of biological assays, especially in the field of PNA-based hybridization technology. In the recent years, many research lines have been developed the modification of magnetic nanoparticle with PNA for use as a PNA probe to separate DNA or ribose nucleic acid (RNA). For example, Wang *et al.* have reported the preparation of PNA-functionalized magnetic nanoparticles (MNPs) for hybridizing with DNA (Figure 1.21) [52]. First, 4-pyridyldithiol-derivertized PNA was used to attach to 3-mercaptopropyl-oxysilane-coated MNPs *via* a thiol-disulfide exchange reaction. After that, it was used as a PNA probe to separate perfect-match DNA from non-complementary DNA. The hybridization of PNA probe with target DNA was characterized using surface-enhanced Raman scattering (SERS). The results showed that PNA probe can be able to hybridize with the perfect-match DNA target and did not bind with non-complementary DNA.



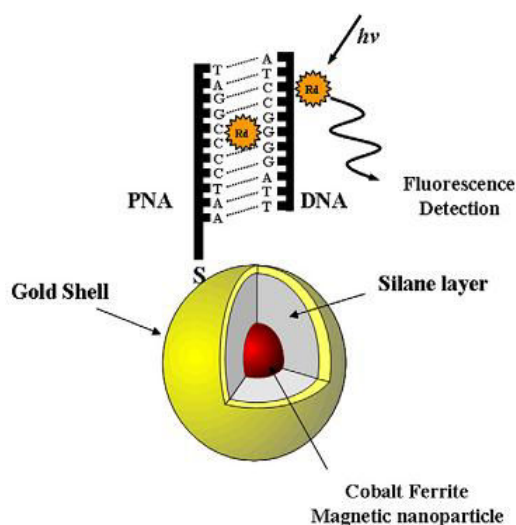
**Figure 1.20** Chemical structures of A) DNA, B) aegPNA, C) acpcPNA and D) hydrogen bonding of nucleotides *via* Watson-Crick base pairing rules



**Figure 1.21** Preparation of PNA-functionalized magnetic nanoparticles (MNPs) [52]

Pita *et al.* have reported the synthesis of PNA functionalized-monodispersed water-soluble gold-covered magnetic nanoparticles for use as a PNA/DNA biosensor [53]. PNA was immobilized onto the particle surface *via* a thiol chemistry to obtain PNA-modified nanoparticle. After that, this PNA probe was used to hybridize with complementary DNA molecules in solutions (Figure 1.22). The PNA/DNA hybridization was monitored by the detection of Rhodamine 6G (an external fluorescent molecule). It was found that this nanoparticle can be used as a biosensor to detect the complementary DNA. Moreover, the magnetic feature of the particles facilitated the separation process in each step of the reactions.





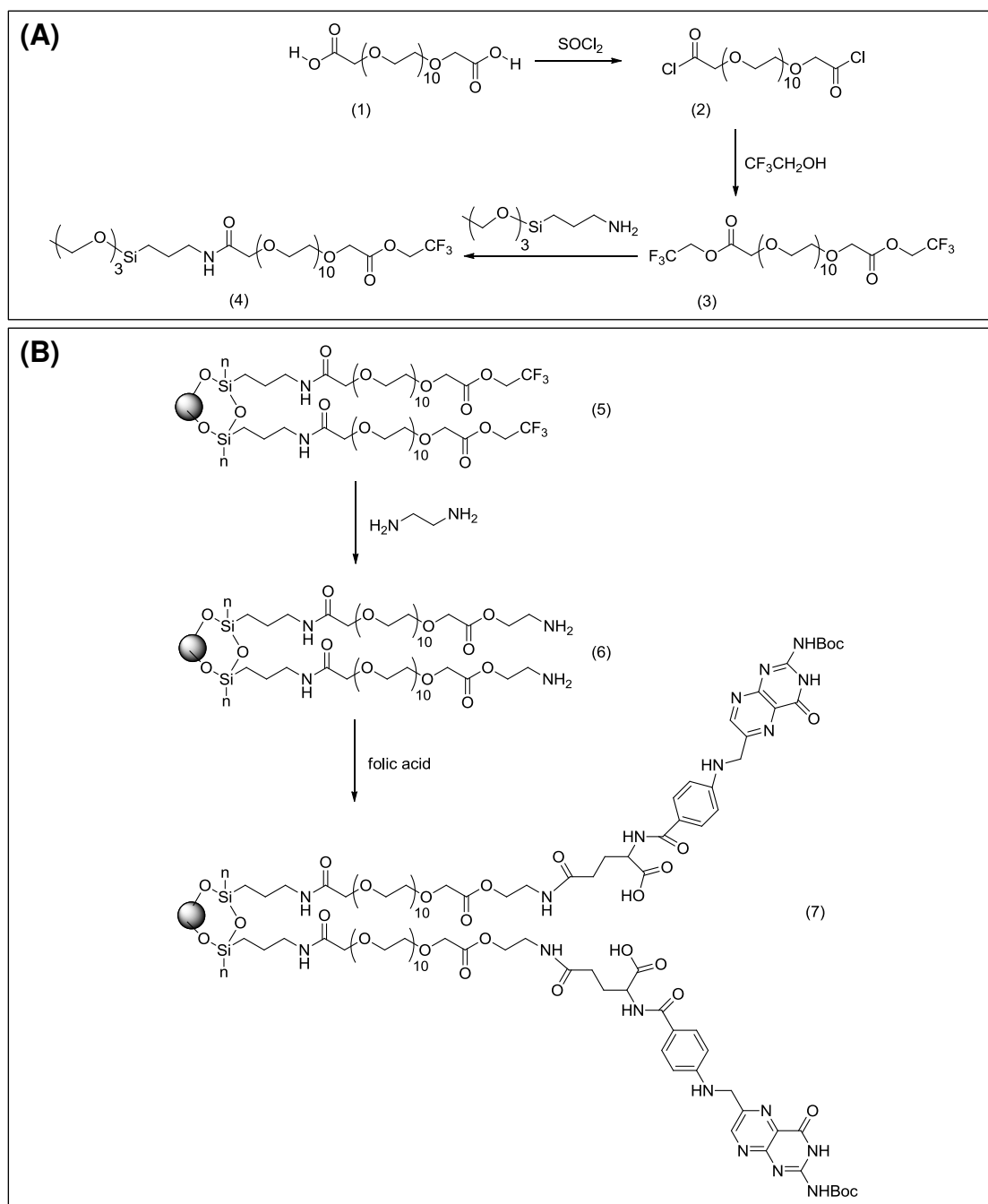
**Figure 1.22** Functionalized gold shell–cobalt ferrite nanoparticles with thio-lated PNA for use as a PNA/DNA biosensor [53]

### 1.2.2 Surface functionalization of MNP with folic acid (FA)

Folic acid (FA) has become an attractive candidate molecule for targeting cancer cells because folate receptor is overexpressed on the surface of cancer cells. Hence, utilization of FA-mediated nanoparticles or molecules to a target folate receptor is markedly being recognized as an potential strategy for improving the therapeutic indices of anticancer drugs. In addition, folate receptors are considered appropriate for tumor selective drug delivery because it provides preferential sites that differentiate tumor cells from normal cells. [54].

Many works have been reported the applications of MNP as a solid support for immobilization of FA for potential use in cancer cell treatment. In 2004, Kohler *et al.* have presented the synthesis of MNP grafted with trifluoroethylester-terminal poly(ethylene glycol) (PEG) silane for conjugation with FA [55]. The trifluoroethylestersilane (4) was synthesized by modifying a PEG diacid (1) to form the corresponding bistrifluoroethylestersilane (TFEE) (3), followed by a reaction with (3-aminopropyl)triethoxysilane (APS). The APS coupled with PEG chains (4) were used to modify the surface of MNP to obtain the primary amine on its surface (6). Figure 1.23 shows the chemical scheme for surface modification of nanoparticles with TFEE silane and subsequently conjugating with ethylenediamine using carboxylic acid

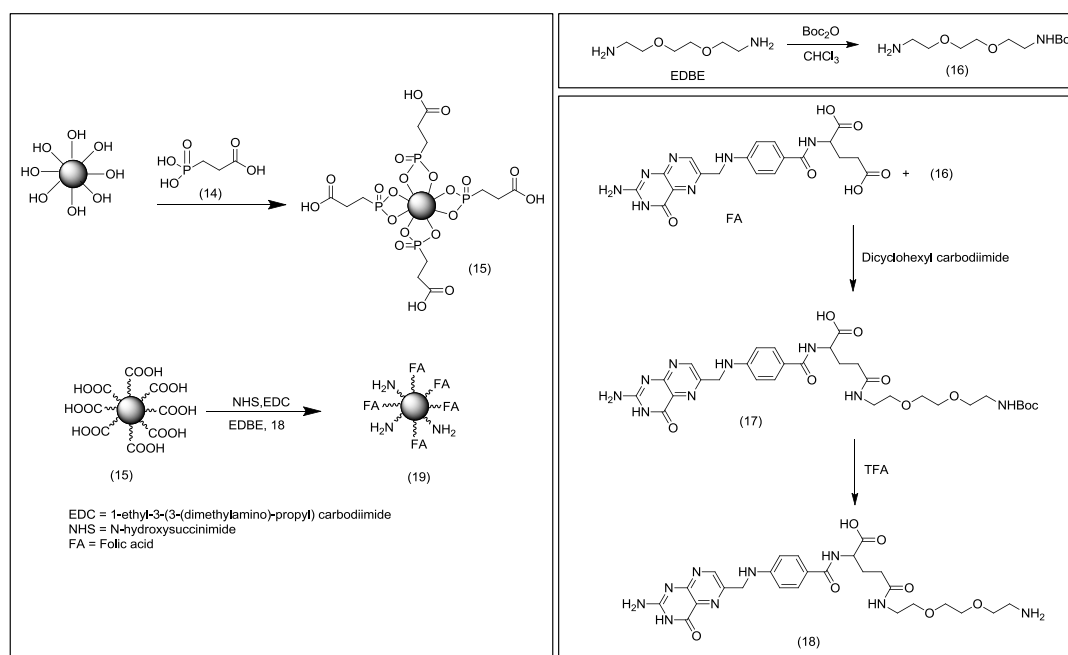
end groups of the derivatized folic acid. The results from TEM analysis showed the well-dispersed nanoparticles both before and after coating with PEG and FA (Figure 1.24).



**Figure 1.23** (A) Chemical scheme for the synthesis of a trifluoroethyl ester terminal PEG silane, (B) immobilization of FA and PEG on MNP surface [55]



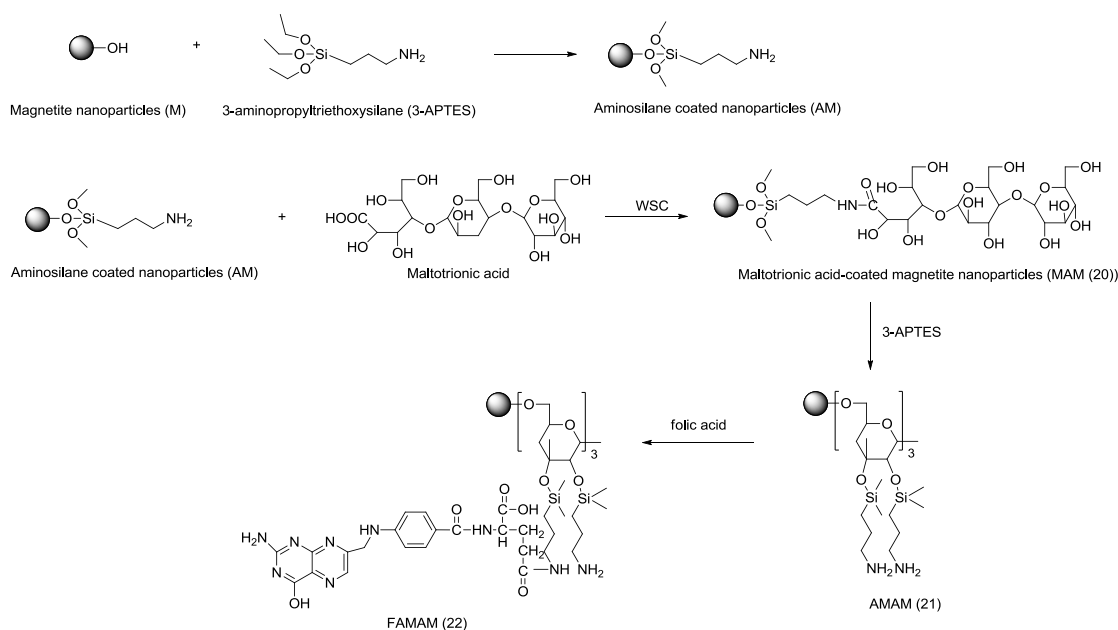
Furthermore, Mohapatra *et al.* have presented surface modification of MNP with FA for targeting human cervixes carcinogen HeLa cell [45]. In the first step, 2-carboxyethyl phosphonic acid (CEPA, (14)) was immobilized on the particle surface to form carboxyl group-terminated nanoparticles (15). In the second step,  $\gamma$ -N-{2-[2-(2-aminoethoxy) ethoxy]ethyl} folic acid (FA-EDBE, (18)) was then immobilized through amidiation between amine ( $-\text{NH}_2$ ) groups of FA-EDBE and carboxyl groups on the particle surface (Figure 1.26). They found that the FA-conjugated particles (19) had a hydrodynamic size of 58 nm with PDI less than 0.2. Change of pH (4.5–8.5) of the medium did not significantly change the hydrodynamic diameter of the samples. Moreover, the nanoparticles had the ability to target human cervixes carcinoma HeLa cell and low cytotoxicity even at relatively high concentration (0.2 mg/mL).



**Figure 1.26** The surface modification of MNPs with FA [45]

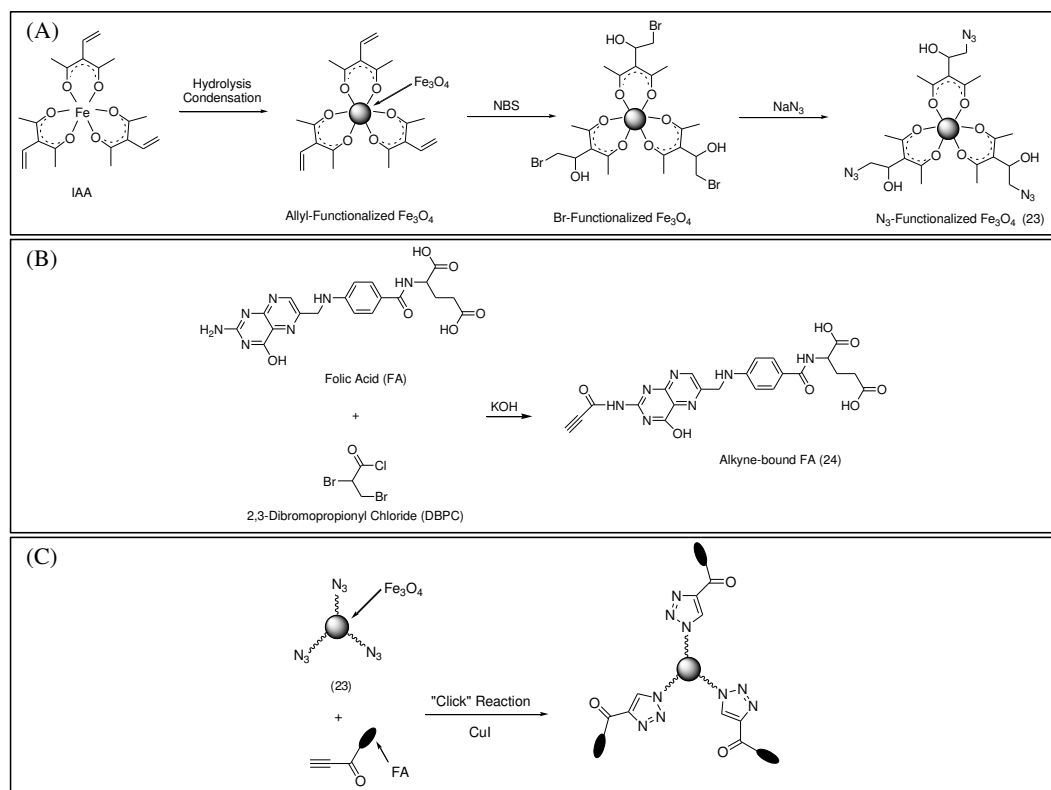
In 2006, Selim *et al.* have demonstrated a novel approach for preparing highly hydrophilic, uniform, superparamagnetic and nontoxic maltotrionic acid (MA)-coated MNP (MAM, (20)) (Figure 1.27) [56]. MA provided an improvement in biocompatibility, monodispersity and non-specific intracellular uptake of the nanoparticles. FA was then conjugated to the MAM to preferentially target KB cells (cancer cells) having folate receptors expressed on their surfaces and to facilitate the

MNPs in their transit across the cell membrane. The results of cell culture experiments indicated that MAM (20) and MAM conjugate with FA (FAMAM, (22)) were biocompatible. The fluorescence and confocal microscope results showed that MAM and FAMAM were internalized into breast cancer cell (KB cells). The amount of uptake of FAMAM was much higher than that of MAM. This result suggests that the modification of MNP with both MA and FA could be used to facilitate the nanoparticle uptake to specific KB cells for molecular imaging.



**Figure 1.27** Modification of MNP with MA (MAM) and with FA (FAMAM) [56]

In addition, Hayashi *et al.* have reported the synthesis of FA-functionalized MNPs *via* click chemistry [44]. First, azide-functionalized MNPs (23) were synthesized from Fe(3-allylacetylacetonate)<sub>3</sub> (IAA) through *in situ* hydrolysis and ligand modification (Figure 1.28A). Alkyne-terminated folic acid (alkyne-FA, (24)), synthesized from a coupling reaction between 2,3-dibromopropionyl chloride and FA, was then immobilized onto the azide-functionalized MNPs (Figure 1.28B and 1.28C). This strategy prevented to loss of the  $\alpha$ -carboxyl group of FA, which is essential for high-affinity binding to folate receptors on human tumors.



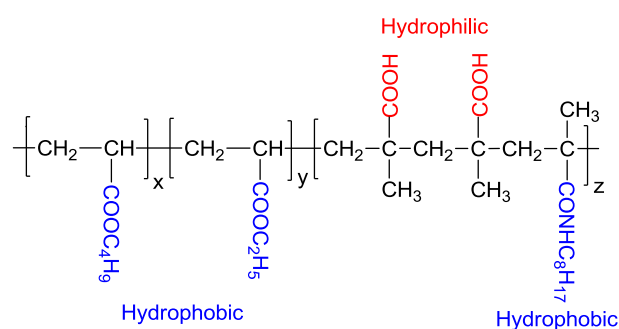
**Figure 1.28** (A) Synthesis of Azide-Functionalized MNPs, (B) Synthesis of Alkyne-Bound FA, and (C) Synthesis of FA-Functionalized MNPs *via* Click Reaction [44]

### 1.2.3 Surface functionalization of MNP with antibody

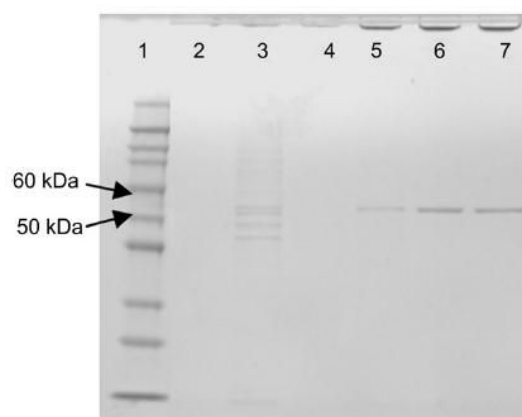
Antibodies or immunoglobulins (Ig), biological products that are parts of the specific immune system, usually possess pathogenic or toxin neutralizer properties. Also, they show the recruitment of immune elements such as complement, improving phagocytosis, cytotoxicity antibody dependent by natural killer cells. In addition, they could carry several elements such as toxins, drugs, fluorochroms, or even nanoparticles, etc., and be used in several diagnostic procedures and therapy to destroy a specific target. The conjugation of antibodies to nanoparticles can generate a hybrid product that merges the properties of both. For instance, they combine the special thermal, imaging, drug carrier, or magnetic characteristics of nanoparticles with the specific and selective recognition abilities of antibodies [57].

Xu *et al.* have demonstrated the separation of circulating cancer cells (CTCs) from fresh whole blood using an antibody-conjugated MNP (Ab-MNP). First, MNP was modified with amphiphilic polymer (Figure 1.29) to yield the water dispersible

MNP having reactive carboxyl groups on its surface [58]. After that, the MNP was conjugated with Ab against human epithelial growth factor receptor 2 (anti-HER2 or anti-HER2/neu) through amidation between amine groups ( $-\text{NH}_2$ ) of the Ab and carboxyl groups ( $-\text{COOH}$ ) of MNP surface to form Ab-MNP. The Ab-MNP was used to isolate HER2 from human breast cancer cell line SK-BR3. The Sodium dodecyl sulfate polyacrylamide gel electrophoresis (SDS-PAGE) results in Figure 1.30 show that Ab-MNP can selectively separate HER2 protein based on the retarded migration of the Ab-MNP on Lane 5, 6 and 7 in comparison with Lane 2 (the original cell lysate) or Lane 3 (the whole protein extract). It was also found that carboxylated MNP without anti-HER2 conjugated cannot separate HER2 (Lane 4). These results confirm that the capture of the HER2 was only obtained when MNP was conjugated with the specific antibody.



**Figure 1.29** Chemical structure of amphiphilic polymer [58]



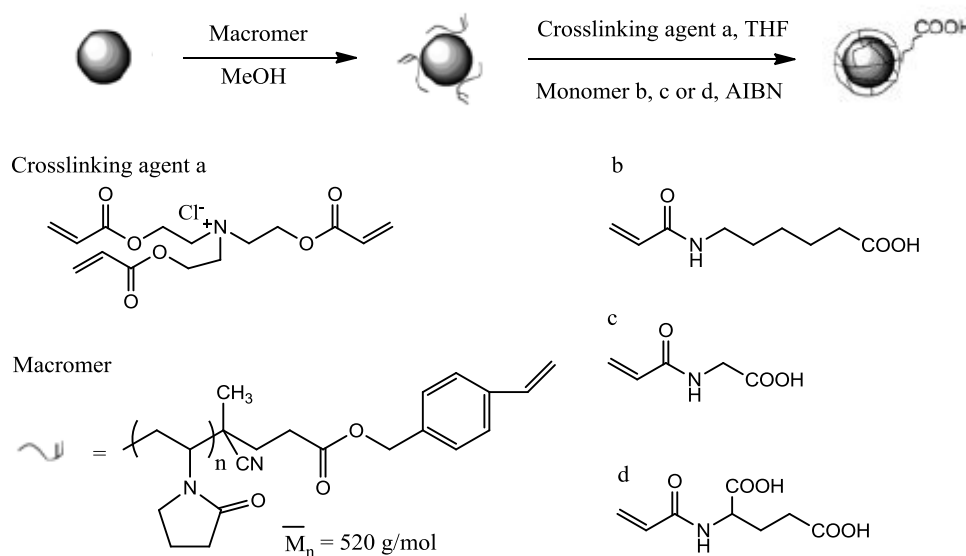
**Figure 1.30** SDS-PAGE of HER2 from SK-BR3 cell lysate. Lane 1: Marker; Lane 2:  $10^6$  SK-BR3 cell lysate; Lane 3: whole protein extract using Norgen kit; Lane 4: control-carboxyl functionalized MNP for capture; Lane 5: Ab-MNP for capture from non-purified SK-BR3 cell lysate; Lane 6: Ab-MNP capture from purified whole protein extracted from  $10^5$  SK-BR3; and Lane 7: Ab-MNP captured HER2 from purified whole protein extracted from  $10^6$  SK-BR3 [58]

Roque *et al.* have studied the attachment strategy of antibody on the surface of MNP (covalent and physical adsorptions) [59]. First, bare MNP and the commercial MNP, Sicastar- M<sup>®</sup>-NH<sub>2</sub> functionalized with glutaraldehyde were used to immobilize antibody (goat IgG) *via* physical adsorption and covalent attachment, respectively. After that, the particles were bind with a complementary antibody labeled with fluorescein isothiocyanate (FITC) (anti-goat IgG). According to fluorescence microscopy results, the covalent attachment of the antibody to MNP was efficient with very low non-specific interactions. On the other hand, the physical adsorption of the antibody was not successful with the presence of non-specific interactions, indicated by observation of the secondary antibody labeled with FITC.

Moon *et al.* have reported the preparation of polymer-coated MNP with various carboxyl vinyl monomers including *N*-acryloylaminohexanate, *N*-acryloylglycine and *N*-acryloyl-*L*-glutamic acid by radical polymerization for application as an immunoassay magnetic marker [60]. First, a hydrophilic macromer having a vinyl group at the terminal poly(*N*-vinyl-2-pyrrolidone) was adsorbed on the particle surface. Then, a carboxyl vinyl monomer and a crosslinking agent (tris(2-acryloyl-oxoethyl)ammonium chloride) were added to initiate a copolymerization



reaction (Figure 1.31). Finally, the particle was conjugated with antibody *via* a reaction between the carboxyl groups on the particle surface and amino groups of antibody. It was found that the particles were dispersed stably in aqueous media. In addition, the particles exhibited high antibody binding ability and high magnetic sensitivity properties which are suitable for use as magnetic markers.



**Figure 1.31** Schematic diagram of the process for preparing the magnetite fine particles encapsulated with a polymer [60]

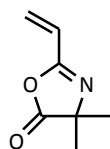
Puertas *et al.* have recently reported a synthesis of carboxylated MNP for ionic adsorption with antibodies through their richest positive charged regions [48]. The adsorption of antibody was applicable at the pH lower than its isoelectric point and the antibodies could be easily eluted by increasing the ionic strength and/or changing the net charge of the antibodies by changing the solution pH.

The reaction of biomolecules with MNP containing reactive functional groups may require the presence of a catalyst to achieve high yields and it can be accompanied by the formation of a side-product, making purification of the resulting polymer tedious. In the context of biological applications, such reactions should be avoided whenever possible, since the catalyst and/or by-product can be toxic. Therefore, utilization of MNP coated with reactive polymers containing functional

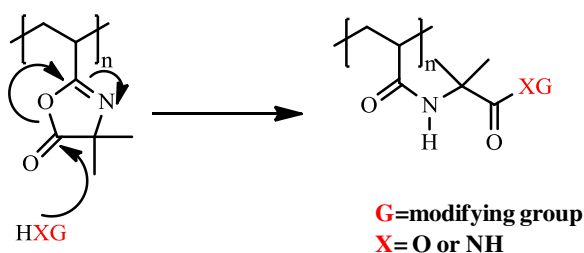
groups that do not require a catalyst to react with biomolecules is very interesting. Therefore, the background of azlactone compounds is then reviewed.

### 1.3 Chemistry of azlactone compounds

2-Vinyl-4,4-dimethylazlactone (VDM, Figure 1.32) is a vinyl azlactone monomer that has attracted much attention recently because the azlactone ring is sensitive toward nucleophiles, such as amines ( $-\text{NH}_2$ ), hydroxyls ( $-\text{OH}$ ), and thiols ( $-\text{SH}$ ), resulting in rapid and efficient covalent bond formation and leaving no by-product (Figure 1.33).



**Figure 1.32** 2-Vinyl-4,4-dimethylazlactone (VDM) monomer [61]



**Figure 1.33** Azlactone-ring opening reaction and proposed mechanism

Because of these advantages, many research works have reported the preparation of (co)polymer templates based on VDM. Rasmussen *et al.* have shown that highly cross-linked functional polymeric particles can be obtained by conventional free radical polymerization of VDM with appropriate comonomer [62]. The synthesized copolymers can be used as a scavenger for immobilization of protein A for affinity column chromatography. Fréchet *et al.* reported the preparation of grafted polyVDM macroporous monolithic disks for use as scavengers of amines [63]. Fontaine *et al.* reported the preparation of PVDM grafted onto electron-beam activated poly(propylene) films and fabrics [64]. These materials were efficient for

immobilization of sericin, a natural protein issued from silk degumming. Additionally, Sun *et al.* reported the use of azlactone-functionalized polymers as reactive templates for the synthesis of a series of amine functionalized-polymers [65]. These materials can be used as cationic polymers for DNA delivery. Recently, Fontaine *et al.* have synthesized PVDM brushes from a polymeric resin using a surface-initiated ATRP [66]. Wang resin, a styrene-based resin, was first immobilized with an ATRP initiator, followed by VDM polymerization from the resin surface. The VDM-functionalized resin was efficiently used as a nucleophilic scavenger to remove benzylamine from solutions.

#### **1.4 Conclusions**

In this chapter, we reviewed some important works regarding the utilization of CRP techniques such as ATRP and RAFT polymerization to prepare the polymeric layer on MNP surface. As discussed above, the progress in the modification methods have now allowed us to finely tailor almost all aspects of MNP properties, such as size, size distribution, physiology stability, hydrodynamic diameter and conjugation ability, etc.

## References

1. Cornell, R.M.; Schwertmann, U. *The Iron Oxides*. Weinheim: VCH, **1996**; p 4.
2. LaConte, L.; Nitin, N.; Bao, G. *Nanotoday*. **2005**, 8, 32-38.
3. Hong, R.Y.; Feng, B. ; Chen, L.L.; Liu, G.H.; Li, H.Z.; Zheng, Y.; Wei, D.G. *Biochem Eng J* **2008**, 42, 290-300.
4. Yuan, Q.; Venkatasubramanian, R.; Hein, S.; Misra, R.D.K. *Acta Biomater* **2008**, 4, 1024-1037.
5. Xu, F.; Geiger, J. H.; Baker, G. L.; Bruening, M. L. *Langmuir* **2011**, 27, 3106-3112.
6. Xu, H.; Aguilar, Z.P.; Yang, L.; Kuang, M.; Duan, H.; Xiong, Y.; Wei, H.; Wang, A. *Biomaterial* **2011**, 32, 9758-9765.
7. Schladt, T.D.; Schneider, K.; Schild, H.; Tremel, W. *Dalton Trans* **2011**, 40, 6315-6343.
8. Ebrahiminezhad, A .; Ghasemi, Y .; Rasoul-Amini, S.; Barar, J.; Davaran, S. *Colloids Surf B* **2013**, 102, 534-539.
9. Wang, T. H.; Lee, W. C. *Biotechnol. Bioprocess Eng* **2003**, 8, 263-267.
10. Johnson, P.A.; Park, H.J.; Driscoll, A.J. *Methods Mol Biol* **2011**, 679,183-191.
11. Kim, D.K.; Zhang, Y.; Voit, W.; Rao, R.V.; Muhamed, M. *J Magn Magn Mater* **2001**, 225, 30-36.
12. Rosensweig, R.E. *Ferrohydrodynamics* Cambridge University Press: Cambridge, **1985**; p 344.
13. Kim, D.K.; Mikhaylova, M; Zhang, Y.; Muhamed, M. *Chem Mater* **2003**, 15, 1617-1627.
14. Nalwa, H.S., *Encyclopedia of Nanoscience and Nanotechnology* American Scientific Publishers: California, **2004**; Vol. 1, p 815-848.
15. Li, C.; Benicewicz, B.C. *Macromolecules* **2005**, 38, 5929-5936.
16. Sun, Y.; Ding, X.; Zheng, Z.; Cheng, X.; Hu, X.; Peng, Y. *Eur Polym J* **2007**, 43, 762-772.
17. Mendonça, P.V.; Serra, A.C.; Coelho, J.F.J.; Popov, A.V.; Guliashvili, T. *Eur Polym J* **2011**, 47, 1460-1466.
18. Lacerda, P.S.S.; Barros-Timmons, A.M.M.V.; Freire, C.S.R.; Silvestre, A.J.D.; Neto, C.P. *Biomacromolecules* **2013**, 14, 2063-2073.
19. Lu, X.; Zhang, L.; Meng, L.; Liu, Y. *Polym Bull* **2007**, 59, 195-206.

20. Kamigaito, M.; Ando, T.; Sawamoto, M. *Chem Rev* **2001**, 101, 3689-3745.
21. Calitz, F.M.; Tonge, M.P.; Sanderson, R.D. *Macromolecules* **2003**, 36, 5-8.
22. Ding, S.; Xing, Y.; Radosz, M.; Shen, Y. *Macromolecules* **2006**, 39, 5921-5928.
23. Marutani, E.; Yamamoto, S.; Ninjabadgar, T.; Tsujii, Y.; Fukuda, T.; Takano, M. *Polymer* **2004**, 45, 2231-2235.
24. Zhou, Y.; Wang, S.; Ding, B.; Yang, Z. *Chem Eng J* **2008**, 138, 578-585.
25. Hu, F.; Neoh, K.G.; Cen, L.; Kang, E.T. *Biomacromolecules* **2006**, 7, 809-816.
26. Xu, F.; Geiger, H.J.; Baker, G.L.; Gruening, M.L. *Langmuir* **2011**, 27, 3106-3112.
27. Zhou, L.; Yuan, J.; Yuan, W.; Sui, X.; Wu, S.; Li, Z.; Shen, D. *J. Magn Magn Mater* **2009**, 321, 2799-2804.
28. Rutnakornpituk, M.; Puangsin, N.; Theamdee, P.; Rutnakornpituk, B.; Wichai, U. *Polymer* **2011**, 52, 987-995.
29. Chiefari, J.; Chong, Y.K.; Ercole, F.; Krstina, J.; Jeffery, J.; Le, T.P.T.; Mayadunne, R.T.A.; Meijs, G.F.; Moad, C.L.; Moad, G.; Rizzardo, E.; Thang, S.H. *Macromolecules* **1998**, 31, 5559-5562.
30. Jiao, Y.; Akcora, P. *Macromolecules* **2012**, 45, 3463-3470.
31. Boyer, C.; Priyanto, P.; Davis, T.P.; Pissuwan, D.; Bulmus, V. Kavallaris, M.; Teoh, W.Y.; Amal, R.; Carroll, M.; Woodward, R.; St Pierre, T. *J Mater Chem* **2010**, 20, 255-265.
32. Aqil, A.; Vasseur, S.; Duguet, E.; Passirani, C.; Benoît, J.P.; Roch, A.; Müller, R.; Jérôme, R.; Jérôme, C. *Eur Polym J* **2008**, 44, 3191-3199.
33. Narain, R.; Gonzales, M.; Hoffman, A.S.; Stayton, P. S.; Krishnan, K.M. *Langmuir* **2007**, 23, 6299-6304.
34. Boyer, C.; Bulmus, V.; Priyanto, P.; Teoh, W.Y.; Amal, R.; Davis, T.P. *J Mater Chem* **2009**, 19, 111-123.
35. Das, M.; Bandyopadhyay, D.; Mishra, D.; Datir, S.; Dhak, P.; Jain, S.; Maiti, T. K.; Basak, A.; Pramanik, P. *Bioconjugate Chem* **2011**, 22, 1181-1193.
36. Zhang, Y.; Zhang, J. *J Colloid Interface Sci* **2005**, 283, 352-357.
37. Wang, N.; Guan, Y.; Yang, L.; Jia, L.; Wei, X.; Liu, H.; Guo, C. *J Colloid Interface Sci* **2013**, 395, 50-57.

38. Sun, E.Y.; Josephson, L.; Kelly, K.A.; Weissleder, R. *Bioconjugate Chem* **2006**, 17, 109-113.
39. Weissleder, R.; Kelly, K.; Sun, E.Y.; Shtatland, T.; Josephson, L. *Nat Biotechnol* **2005**, 23, 1418-1423.
40. Culita, D.C.; Patron, L.; Oprea, O.; Bartha, C.; Palade, P.; Teodorescu, V.; Filoti, G. *J Nanopart Res* **2013**, 15, 1-15.
41. Cao, J.; Wang, Y.; Yu, J.; Xia, J.; Zhang, C.; Yin, D.; Häfeli, U. O. *J Magn Magn Mater* **2004**, 277, 165–174.
42. Xie, M.; Xu, Y.; Liu, J.; Zhang, T.; Zhang, H. *J Nano Mat* **2012**, 2012, 1-943.
43. Socaci, C.; Rybka, M.; Magerusan, L.; Nan, A.; Turcu, R.; Liebscher, J. *J Nanopart Res* **2013**, 15, 1-14.
44. Hayashi, K.; Moriya, M.; Sakamoto, W.; Yogo, T. *Chem Mater* **2009**, 21, 1318-1325.
45. Mohapatra, S.; Mallick, S.K.; Maiti, T.K.; Ghosh, S.K.; Pramanik, P. *Nanotechnology* **2007**, 18, 1-9.
46. Chen, D.; Jiang, M.; Li, N.; Gu, H.; Xu, Q.; Ge, J.; Xia, X.; Lu, J. *J Mater Chem* **2010**, 20, 6422-6429.
47. Theppaleak, T.; Rutnakornpituk, B.; Wichai, U.; Vilaivan, T.; Rutnakornpituk, M. *J Biomed Nanotech* **2013**, 9, 1-12.
48. Puertas, S.; Batalla, P.; Moros, M.; Polo, E.; Del Pino, P.; Guisan, J.M.; Grazú, V.; de la Fuente J.M. *ACS Nano* **2011**, 28, 4521-4528.
49. Rutnakornpituk, M.; Meerod, S.; Boontha, B.; Wichai, U. *Polymer* **2009**, 50, 3508–3515.
50. Nielsen, P.E.; Egholm, M.; Berg, R.H.; Buchardt, O. *Science* **1991**, 254, 1497-1500.
51. Ananthanawat, C.; Vilaivan, T.; Mekboonsonglarp, W.; Hoven V.P. *Biosens Bioelectro* **2009**, 24, 3544-3549.
52. Wang, F.; Shen, C.A.; Feng, J.; Yang, H. *Microchim Acta* **2006**, 153, 15-20.
53. Pita, M.; Abad, J.M.; Vaz-Dominguez, C.; Briones, C.; Mateo-Martí, E.; Martín-Gago, J.A.; Morales, M.P.; Fernández, V.M. *J. Colloid Interface Sci* **2008**, 321, 484-492.
54. Vana, P.; Nguyen, D.H. *Polym Adv Technol* **2006**, 17, 625-633.

55. Kohler, N.; Fryxell, G.E.; Zhang, M. *J Am Chem Soc* **2004** 126, 7206-7211.
56. Selim, K.M.K.; Lee, J.H.; Kim, S.J.; Xing, Z.; Kang, I.K.; Chang, Y.; Guo, H. *Macromol Res* **2006**, 14, 646-653.
57. Arruebo, M.; Valladares, M.; González-Fernández, Á. *J Nano Mat* **2009**, 1-24.
58. Xu, H.; Aguilar, Z.P.; Yang, L.; Kuang, M.; Duan, H.; Xiong, Y. Wei, H.; Wang, A. *Biomaterials* **2011** 32, 9758-9765.
59. Roque, A.C.; Bispo, S.; Pinheiro, A.R.; Antunes, J.M.; Gonçalves, D.; Ferreira, H.A. *J Mol Recognit* **2009**, 22, 77-82.
60. Moon, J.M.; Kim, B.S.; Choi, Y.S.; Lee, J.O.; Nakahara, T.; Yoshinaga, K. *Macromol Res* **2010**, 18, 793-799.
61. Taylor, L.D.; Kolesinski, H.S.; Mehta, A.C.; Locytell, L.; Larson, P.S. *Macromol Chem Phys* **1982**, 3, 779-782.
62. Rasmussen, J.K.; Heilmann, S.M.; Krepski, L.R.; Jensen, K.M.; Mickelson, J.; Johnson, K. (Zeimet). *React Polym* **1991/1992**, 16, 199-212.
63. Fréchet J.M.J.; Tripp, J.A.; Stein, J.A.; Svec, F. *Org Lett* **2000**, 2, 195-198.
64. Fontaine, L.; Lemele, T.; Brosse, J.C.; Sennyey, G.; Senet, J.P.; Wattiez, D. *Macromol Chem Phys* **2002**, 203, 1377-1384.
65. Sun, B.; Liu, X.; Buck, M.E.; Lynn, D.M. *Chem Commun* **2010**, 46, 2016-2018.
66. Fournier, D.; Pascual, S.; Montembault, V.; Haddleton, D.M.; Fontaine, L. *J Comb Chem* **2006**, 8, 522-530.

## CHAPTER II

# AZLACTONE FUNCTIONALIZATION OF MAGNETIC NANOPARTICLES USING ATRP AND THEIR BIOCONJUGATION\*

### Abstract

Surface modification of magnetite nanoparticle (MNP) with poly(poly(ethylene glycol) methyl ether methacrylate-*stat*-2-vinyl-4,4-dimethylazlactone) copolymers (poly(PEGMA-*stat*-VDM)) *via* atom transfer radical polymerization (ATRP) and its application to anchor thymine peptide nucleic acid (PNA) monomer are reported. ATRP of PEGMA and VDM was first performed in a solution system to optimize the reaction condition and the optimal condition was then applied in the surface-initiated ATRP of MNP. Fourier transform infrared (FTIR) spectroscopy indicated the presence of the copolymer in the MNP complexes. After immobilization of thymine PNA monomer, thermogravimetric analysis (TGA) results indicated that there were 4 wt% of the PNA monomer in the complex (1.2 mmol/g complex). The existence of the PNA monomer in the complex was also confirmed *via* FTIR and vibrating sample magnetometry (VSM). The MNP complex with active surface might be efficiently used as magnetically guidable nanosolid support for PNA oligomers and other molecules containing affinity functional groups.

### 2.1 Experimental

#### 2.1.1 Materials

Unless otherwise stated, all reagents were used without further purification: iron(III) acetylacetonate (Fe(acac)<sub>3</sub>, 99.9%, Acros), benzyl alcohol (98%, Unilab), oleic acid (Fluka), copper(I) bromide (99.999%, Aldrich), triethylamine (TEA, 97%, Carlo Erba), ethyl-2-bromoisobutyrate (EBiB, 98%, Aldrich), and thymine PNA (Acros). Poly(ethylene glycol) methyl ether methacrylate (PEGMA, Aldrich) with average molecular weight  $\overline{M}_n = 300 \text{ g.mol}^{-1}$  was purified by passing through basic alumina and stored at -4°C after purification. 2-Vinyl-4,4-dimethylazlactone (VDM,

\*This work has been published in Polymer, 2012, 53, 113-120.



99.4%, ISOCHEM) was distilled *in vacuo* and stored at -15°C after purification. Tris-[2-(dimethylamino) ethyl]amine (Me<sub>6</sub>Tren) [1] and 2-bromo-2-methyl-*N*-(3-(triethoxysilyl) propyl) propanamide (BTPAm) [2] were prepared according to previously reported procedures. Dichloromethane (CH<sub>2</sub>Cl<sub>2</sub>), ethanol, methanol and diethyl ether were dried with P<sub>2</sub>O<sub>5</sub> and distilled prior to use. *N,N*-dimethylformamide (DMF, 99.8%, Aldrich), toluene (99.8%, Sigma-Aldrich) and deuterated chloroform (CDCl<sub>3</sub>, 99%, Euriso-Top) were used as received.

### 2.1.2 Characterization

Proton Nuclear Magnetic Resonance (<sup>1</sup>H NMR) spectra were obtained from a Bruker AC 200-MHz spectrometer using CDCl<sub>3</sub> as a solvent. Molar masses and molar mass distributions were determined *via* size exclusion chromatography (SEC) at 35°C on a system equipped with a Spectra System AS1000 autosampler with a guard column (Polymer Laboratories, PL gel 5 µm guard, 50 × 7.5 mm) followed by two columns (Polymer Laboratories, two PL gel 5 µm Mixed – D columns, 2 × 300 × 7.5 mm). Polystyrene standards (580-483 × 10<sup>3</sup> g.mol<sup>-1</sup>) were used to calibrate the SEC. Fourier transform infrared (FTIR) analyses were recorded using a Nicolet Avatar 370 DTGS spectrometer in the attenuated total reflection (ATR) mode. Elemental analysis was performed by the Service Central d'Analyses du Centre National de Recherche Scientifique, Gif-sur-Yvette (France). Transmission electron microscopy (TEM) images were taken using a Philips Tecnai 12 operated at 120 kV equipped with Gatan model 782 CCD camera. The particles were re-suspended in toluene or DMF with sonication before deposition on a TEM grid. Magnetic properties of the particles were measured at room temperature using a Standard 7403 Series, Lakeshore vibrating sample magnetometer (VSM). Magnetic moment of each sample was investigated over a range of ± 10000 G of applied magnetic fields using 30 min sweep time. Thermogravimetric analysis (TGA) was performed on SDTA 851 Mettler-Toledo at the temperature ranging between 25-600°C at a heating rate of 20°C/min under oxygen atmosphere.

### 2.1.3 General procedure for the synthesis of poly(PEGMA-*stat*-VDM) copolymers *via* ATRP in solution

An example of the synthesis of poly(PEGMA-*stat*-VDM) using EBiB/CuBr/Me<sub>6</sub>Tren/PEGMA/VDM of 1/1/1/50/50 is illustrated. CuBr (0.0287 g, 0.2 mmol) was added to a Schlenk tube equipped with a stir bar. After sealing with a rubber septum, the Schlenk tube was deoxygenated with three vacuum/argon fill cycles. A degassed solution of PEGMA (6 g, 20 mmol), VDM (2.78 g, 20 mmol), toluene (70 % v/v, 6 mL), EBiB (0.039 g, 0.2 mmol) and DMF (5 % v/v, 0.4 mL) (used as an internal standard) was added to the Schlenk tube containing CuBr *via* a cannula. The resulting solution was further degassed using freeze/pump/thaw cycles *in vacuo*. Degassed Me<sub>6</sub>Tren (0.046 g, 0.2 mmol) was added ( $t = 0$ ) to the Schlenk tube and it was then placed in an oil bath preheated to a desired temperature. The samples were withdrawn periodically *via* a degassed syringe for conversion measurements and SEC analyses.

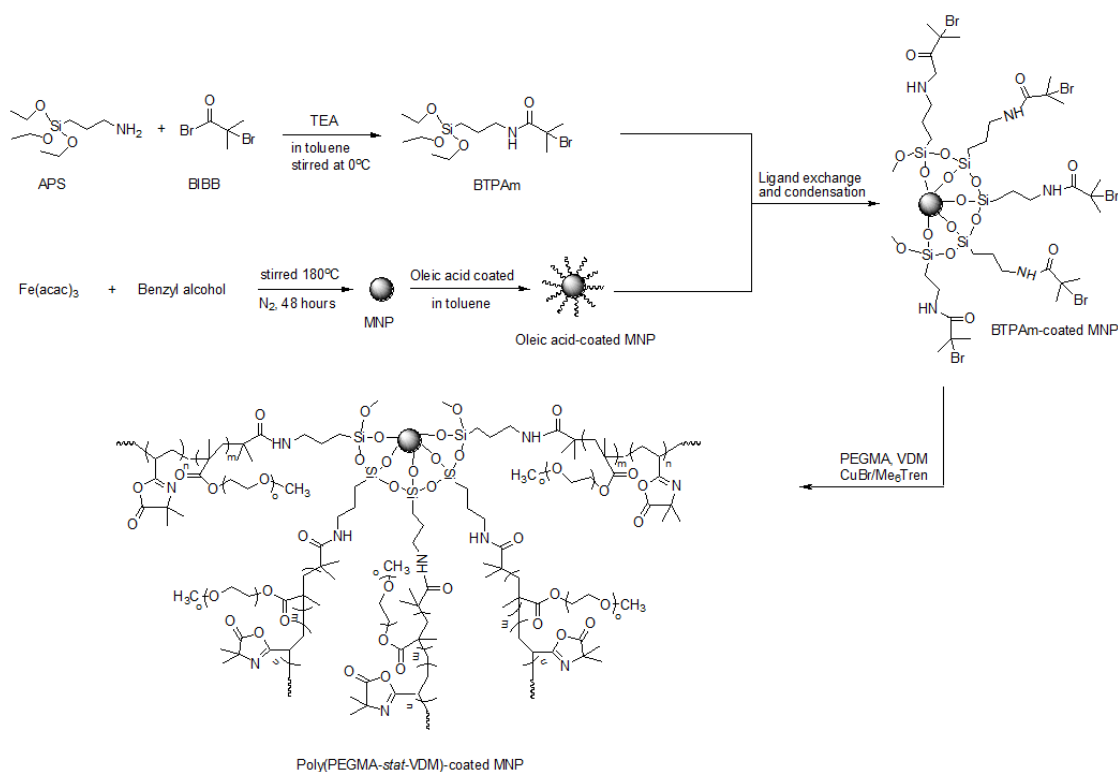
### 2.1.4 Synthesis of MNP coated with ATRP initiators (BTPAm-coated MNP)

BTPAm-coated MNP was prepared *via* a three-step reaction; (1) synthesis of MNP core, (2) coating the MNP with oleic acid and (3) grafting BTPAm onto the oleic acid-coated MNP. MNP was synthesized *via* a thermal decomposition reaction according to the procedure previously reported [3]. Namely, Fe(acac)<sub>3</sub> (5 g, 14.05 mmol) and benzyl alcohol (90 mL) were mixed in a three-necked round bottomed flask equipped with a mechanical stirrer and septum. The mixture was set at 180°C for 48 h with nitrogen flow. After the reaction, the precipitant was removed from the dispersion using an external magnet and washed with ethanol and CH<sub>2</sub>Cl<sub>2</sub> repeatedly to remove benzyl alcohol. The particles were then dried at room temperature under reduced pressure. To prepare oleic acid-coated MNP, a MNP-toluene dispersion (0.8 g of dried MNP in 30 mL of toluene) was sonicated for 1 h. Oleic acid (4 mL) was then slowly dropped into the dispersion and sonicated for 3 h under nitrogen atmosphere. To immobilize BTPAm onto the MNP surface, the oleic acid-coated MNP dispersed in toluene was mixed with BTPAm using TEA as a catalyst. The reaction was carried out at room temperature for 24 h under nitrogen atmosphere. The dispersion was precipitated in methanol and washed with toluene to remove oleic acid and ungrafted

BTPAm from the dispersion. The Br loading calculated from elemental analysis (%Br = 0.71%) was estimated to  $8.89 \times 10^{-2} \text{ mmol.g}^{-1}$

### 2.1.5 Synthesis of poly(PEGMA-*stat*-VDM)-coated MNP *via* ATRP (Scheme 2.1)

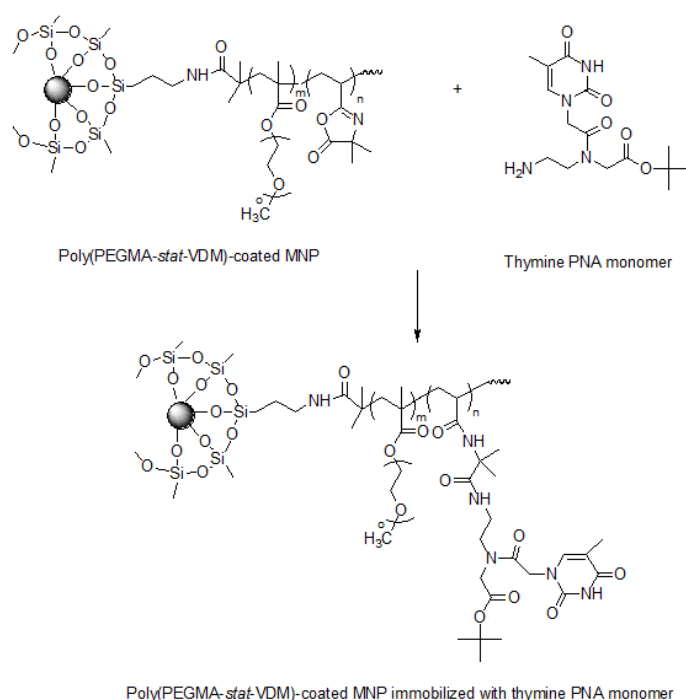
BTPAm-coated MNP dispersed in toluene was sonicated for 20 min and degassed using argon. This suspension was then added to a degassed Schlenk tube containing CuBr, PEGMA, VDM, EBiB (used as a free initiator) and DMF (used as internal standard) *via* a cannula. Degassed Me<sub>6</sub>Tren ligand was added to the above dispersion ( $t=0$ ) and the mixture was set in an oil bath preheated at 30°C. The samples were withdrawn periodically *via* a degassed syringe to monitor the monomer conversions *via* <sup>1</sup>H NMR spectroscopy and to determine molecular characteristics of the copolymer *via* SEC analyses. At the end of the copolymerization, the surface-modified MNP were separated from the mixture by external magnet, precipitated into diethyl ether and dried *in vacuo*. The as-synthesized poly(PEGMA-*stat*-VDM)-coated MNP was obtained as a fine black powder.



**Scheme 2.1** Surface modification of MNP with poly(PEGMA-*stat*-VDM) copolymer *via* ATRP reaction

### 2.1.6 Immobilization of thymine PNA monomer on the poly(PEGMA-*stat*-VDM)-coated MNP (Scheme 2.2)

Thymine PNA monomer (10 mg) was added into a dispersion of poly(PEGMA-*stat*-VDM)-coated MNP (10 mg) in DMF (10 mL). The mixture was sonicated at room temperature for 6 h under argon atmosphere. The particle was then collected using an external magnet and washed with DMF repeatedly to remove ungrafted thymine PNA monomer from the particle surface.



**Scheme 2.2** Immobilization of thymine PNA monomer onto poly(PEGMA-*stat*-VDM)-coated MNP

## 2.2 Results and discussion

### 2.2.1 Synthesis of poly(PEGMA-*stat*-VDM) via ATRP in solution

In the present work, a statistical copolymer of PEGMA and VDM was first synthesized in toluene using CuBr/Me<sub>6</sub>Tren catalytic complex in the presence of EBiB as an initiator. CuBr and Me<sub>6</sub>Tren were selected as a catalytic complex in the present work. Fontaine *et al.* have reported that using Me<sub>6</sub>Tren ligand led to a good control in polymerization of VDM: the experimental molecular weights were comparable to the theoretical values and narrow polydispersities were obtained [4]. Molar ratio of

CuBr/Me<sub>6</sub>Tren/EBiB was studied in order to determine the best experimental conditions to obtain a good control in molecular weight and molecular weight distribution. The selected reaction conditions would then be used for surface-initiated ATRP of PEGMA and VDM from magnetite nanoparticles, which would be then used for immobilizing thymine PNA monomer on their surface.

A EBiB/CuBr/Me<sub>6</sub>Tren molar ratio of 1/1/1 has successfully been used in our group to synthesize well-defined (co) polymers based on VDM in solution [4]. Therefore, in this work, poly(PEGMA-*stat*-VDM) was synthesized *via* ATRP of PEGMA and VDM monomers using the same catalytic/initiator system and similar catalyst/ligand ratios. Table 2.1 shows the summary of the statistical copolymerizations of 50/50/1 molar ratio of PEGMA/VDM/EBiB at various CuBr/Me<sub>6</sub>Tren ratios.

**Table 2.1** ATRP of mixtures of PEGMA and VDM using various molar ratios of EBiB initiator and CuBr/Me<sub>6</sub>Tren catalytic complexes in toluene

entry	EBiB/ CuBr /Me <sub>6</sub> Tren	Temp ( °C)	time (min)	conv <sup>a</sup> (%)		$\overline{M}_{n,th}^b$ (g/mol)	$\overline{M}_{n,SEC}^c$ (g/mol)	PDI <sup>c</sup>
				PEGMA	VDM			
1	1/1/1	50	30	83	90	18705	29400	2.17
2	1/0.5/0.5	30	90	70	82	16199	18600	1.72
3	1/0.2/0.2	30	90	52	61	12039	14400	1.35

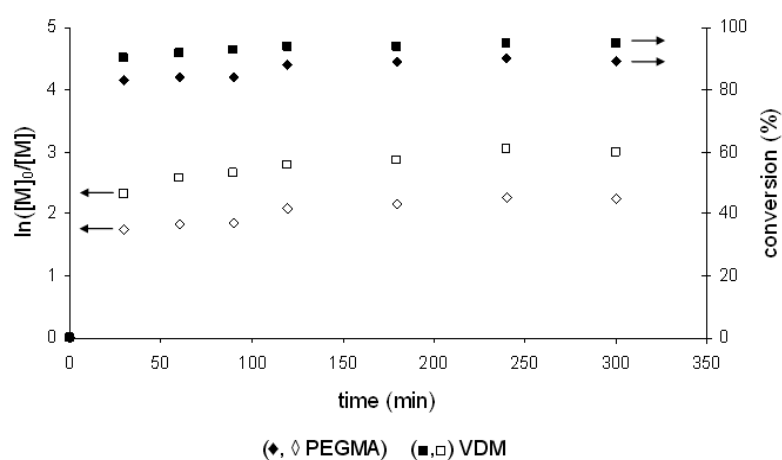
<sup>a</sup> Calculated *via* <sup>1</sup>H NMR spectroscopy.

<sup>b</sup>  $\overline{M}_{n,th} = ([\text{PEGMA}]_0/[\text{EBiB}]_0 \times \text{conv.}_{\text{PEGMA}} \times M_{\text{PEGMA}}) + ([\text{VDM}]_0/[\text{EBiB}]_0 \times \text{conv.}_{\text{VDM}} \times M_{\text{VDM}})$ .

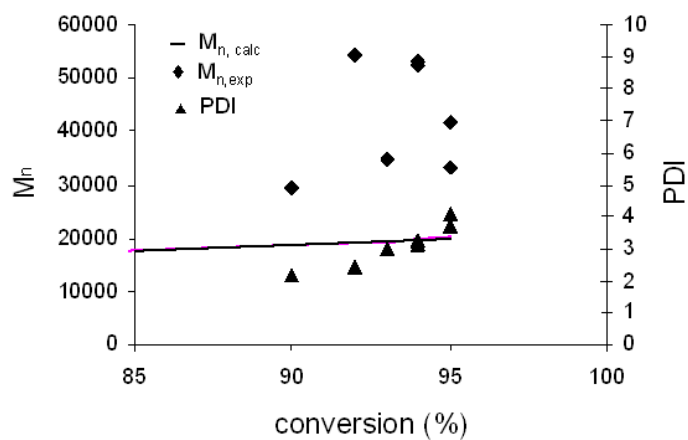
<sup>c</sup> Measured *via* SEC (calibrated with polystyrene standard).

A preliminary experiment was performed in toluene at 50°C using [EBiB]<sub>0</sub>/[CuBr]<sub>0</sub>/[Me<sub>6</sub>Tren]<sub>0</sub> ratio of 1/1/1 (entry 1, Table 2.1). Figure 2.1 shows that conversions of PEGMA and VDM reached 83% and 90%, respectively, after 30 min of polymerization time. Moreover, the ln([M]<sub>0</sub>/[M]) *vs* time plot shows a curvature and reaches a plateau after 30 min of the reaction, indicating the presence of irreversible terminations. This phenomenon is confirmed by the relative broad polydispersity indices obtained (PDIs = 2.17) (Figure 2.2). A decrease of

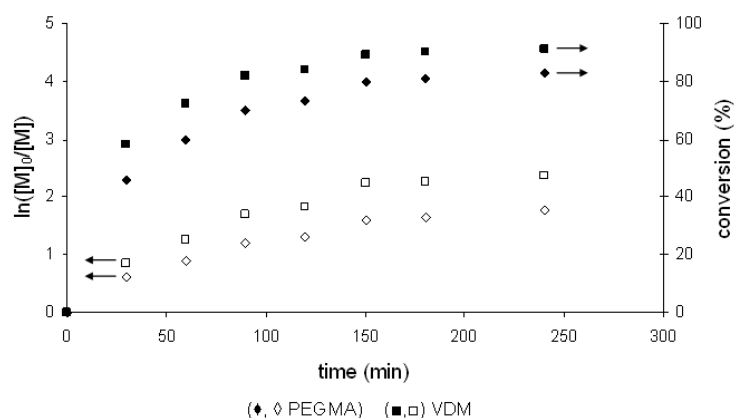
$[\text{EBiB}]_0/[\text{CuBr}]_0/[\text{Me}_6\text{Tren}]_0$  ratio to 1/0.5/0.5 and a decrease of the reaction temperature to 30°C resulted in a decrease of PEGMA and VDM conversion to 70% and 82%, respectively (after 90 min, entry 2, Table 2.1 and Figure 2.3). However, the polydispersity indices were still high (PDIs = 1.40 - 2.19) for a controlled radical polymerization (Figure 2.4). In addition, the  $\ln([M]_0/[M])$  vs time plot again shows a decrease of active species concentration, which is compatible with the presence of irreversible terminations (Figure 2.3).



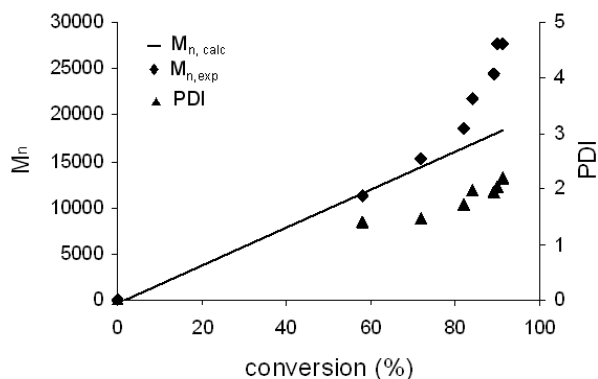
**Figure 2.1** The  $\ln([M]_0/[M])$  vs time plot and monomers conversions vs time plot of ATRP of PEGMA and VDM using  $[\text{PEGMA}]_0/[\text{VDM}]_0/[\text{EBiB}]_0/[\text{CuBr}]_0/[\text{Me}_6\text{Tren}]_0$  molar ratio = 50/50/1/1/1, in toluene at 50°C



**Figure 2.2** Dependence of  $\overline{M}_n$  and  $\overline{M}_w/\overline{M}_n$  (PDI) with monomer conversion of ATRP of PEGMA and VDM using  $[PEGMA]_0/[VDM]_0/[EBiB]_0/[CuBr]_0/[Me_6Tren]_0$  molar ratio = 50/50/1/1/1, in toluene at 50°C



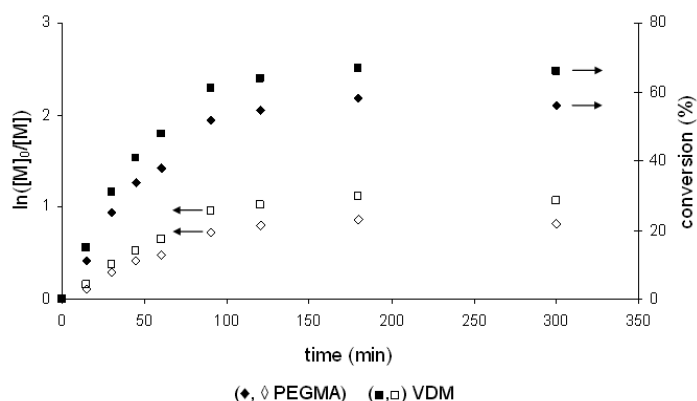
**Figure 2.3** The  $\ln([M]_0/[M])$  vs time plot and monomers conversions vs time plot of ATRP of PEGMA and VDM using  $[PEGMA]_0/[VDM]_0/[EBiB]_0/[CuBr]_0/[Me_6Tren]_0$  molar ratio = 50/50/1/0.5/0.5, in toluene at 30°C



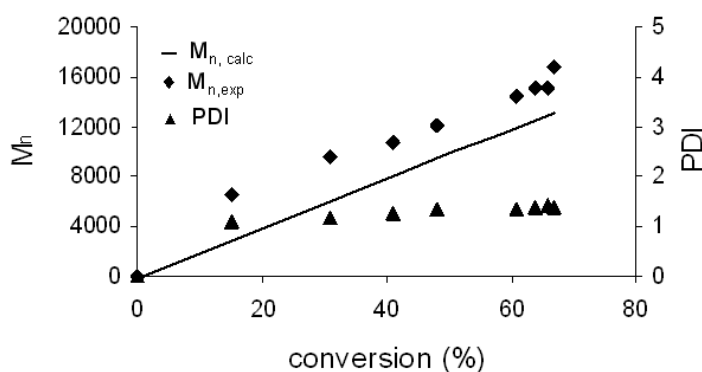
**Figure 2.4** Dependence of  $\overline{M}_n$  and  $\overline{M}_w/\overline{M}_n$  (PDI) with monomer conversion of ATRP of PEGMA and VDM using [PEGMA]<sub>0</sub>/[VDM]<sub>0</sub>/[EBiB]<sub>0</sub>/[CuBr]<sub>0</sub>/[Me<sub>6</sub>Tren]<sub>0</sub> molar ratio = 50/50/1/0.5/0.5, in toluene at 30°C

When a 1/0.2/0.2 molar ratio of [EBiB]<sub>0</sub>/[CuBr]<sub>0</sub>/[Me<sub>6</sub>Tren]<sub>0</sub> was used, the  $\ln([M]_0/[M])$  vs time plot was linear at the beginning, indicating that the concentration of active species was constant in the first step of the polymerization (Figure 2.5). At 90 min, 52% of PEGMA conversion and 61% of VDM conversion were reached (entry 3, Table 2.1). The polydispersity index in this case decreased to 1.35 and the  $\overline{M}_n$  values increased with the monomer conversion, and they are somewhat closed to the theoretical values (Figure 2.6). This experiment clearly shows that a decrease of the catalytic complex-to-initiator ratio allows a better control of the ATRP of PEGMA and VDM in toluene.





**Figure 2.5** The  $\ln([M]_0/[M])$  vs time plot and monomers conversion vs time plot of ATRP of PEGMA and VDM using  $[\text{PEGMA}]_0/[\text{VDM}]_0/[\text{EBiB}]_0/[\text{CuBr}]_0/[\text{Me}_6\text{Tren}]_0$  molar ratio = 50/50/1/0.2/0.2, in toluene at 30°C



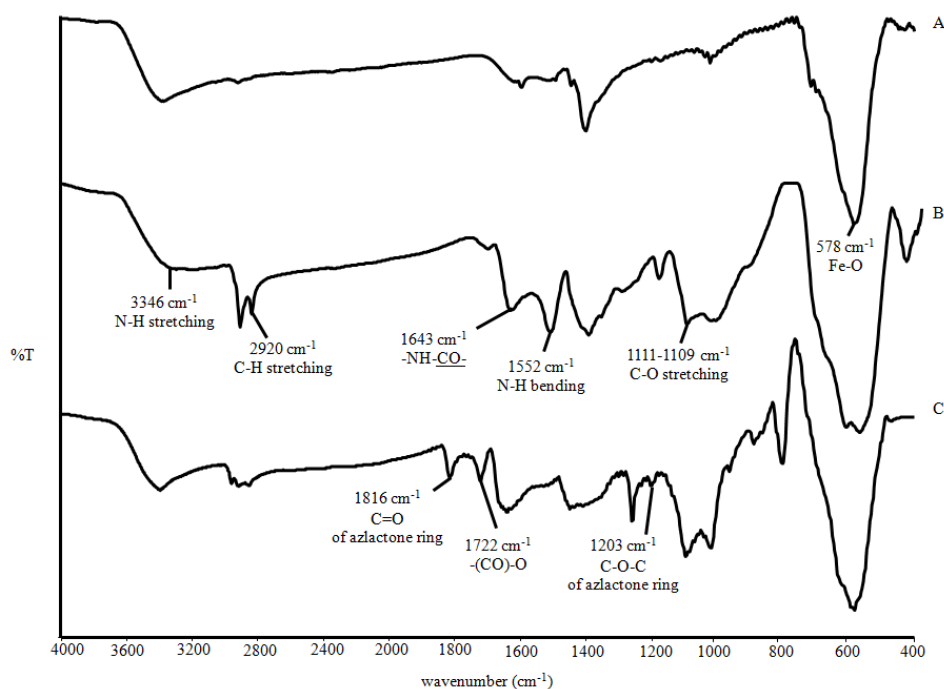
**Figure 2.6** Dependence of  $\overline{M}_n$  and  $\overline{M}_w/\overline{M}_n$  (PDI) with monomer conversion of ATRP of PEGMA and VDM using  $[\text{PEGMA}]_0/[\text{VDM}]_0/[\text{EBiB}]_0/[\text{CuBr}]_0/[\text{Me}_6\text{Tren}]_0$  molar ratio = 50/50/1/0.2/0.2, in toluene at 30°C

### 2.2.2 Preparation of poly(PEGMA-*stat*-VDM)-coated MNP *via* ATRP

To perform ATRP from MNP surface, 2-bromo-2-methyl-*N*-(3-(triethoxysilyl) propyl) propanamide (BTPAm), a molecule containing an ATRP initiating site, was first immobilized onto the particle surface *via* silanization reaction using the triethoxy silane group of BTPAm. FTIR spectrum of BTPAm-coated MNP shows characteristic absorption signals of BTPAm: C-O (1111-1109  $\text{cm}^{-1}$ ), N-H (3346  $\text{cm}^{-1}$ ), NH-CO (1643  $\text{cm}^{-1}$ ), indicating the anchorage of BTPAm (Figure 2.7B).

Then, to prepare statistical copolymers based on PEGMA and VDM grafted onto MNP surface, the optimal condition established previously for ATRP in solution were used. Because the MNP-supported copolymers could not be studied by NMR technique, the free initiator EBiB (also called “sacrificial” initiator) was added to the reaction to easily monitor the reaction progress. Such a strategy was previously applied for ATRP of polystyrene (PS) on Wang resin [5]. It was found that the macromolecular characteristics (molar masses and PDIs) of PS formed in solution and on Wang resin were similar. Therefore, monomer conversions and copolymer compositions, discussed in the latter section, were investigated from the free copolymers *via* NMR spectroscopy. The reaction was carried out in toluene at 30°C using [PEGMA]<sub>0</sub>/[VDM]<sub>0</sub>/[EBiB]<sub>0</sub>/[BTPAm-coated MNP]<sub>0</sub>/[CuBr]<sub>0</sub>/[Me<sub>6</sub>Tren]<sub>0</sub> in a 100/100/1/1/0.4/0.4 molar ratio. This molar ratio was adjusted in accordance with the fact that there were both ATRP initiating sites (BTPAm) grafted on particle surface and a free initiator (EBiB) in this system. After the ATRP reactions, the particles in the dispersion were magnetically separated from the mixture. The aggregate was used in FTIR and VSM characterizations, and the supernatant containing the free copolymers was used in SEC and NMR analyses.

Figure 2.7C shows FTIR spectrum of poly(PEGMA-*stat*-VDM)-coated MNP compared with those of bare MNP (Figure 2.7A) and BTPAm-coated MNP (Figure 2.7B). Poly(PEGMA-*stat*-VDM)-coated MNP exhibited a characteristic signal of azlactone rings of VDM units at 1816 cm<sup>-1</sup> (-C=O stretching), 1203 cm<sup>-1</sup> (C-O-C stretching) and that of PEGMA at 1722 cm<sup>-1</sup> (-C=O stretching) (Figure 2.7C), indicating the presence of the copolymer in the complex. A broad and strong band of Fe-O from MNP cores was also observed at 578 cm<sup>-1</sup>.



**Figure 2.7** FTIR spectra of (A) bare MNP, (B) BTPAm-coated MNP and (C) poly(PEGMA-*stat*-VDM)-coated MNP

Table 2.2 shows the monomer conversion,  $\overline{M}_n$  and polydispersity indices (PDIs) of poly(PEGMA-*stat*-VDM) produced by the free initiator. It was found that the monomer conversions of PEGMA and VDM in BTPAm-coated MNP reached 24% and 29%, respectively, after 24 h of reaction, while those in the solution system with the same reaction conditions proceeded in a much shorter time (25% and 31%, respectively, in 30 min reaction) (see Table A3 in the appendix A). This phenomenon has been previously observed in the surface-initiated ATRP of VDM from the Wang resin solid support [5].  $\overline{M}_n$  gradually increased when the reaction conversions increased, indicating the growth of the copolymer chains. In all cases, the  $\overline{M}_{n,SEC}$  values were higher than the theoretical ones and their distributions were narrow (PDIs = 1.09-1.21) throughout the reaction (Table 2.2).

**Table 2.2** Summary of monomers conversions,  $\overline{M}_n$ , and PDIs of poly(PEGMA-*stat*-VDM) copolymers using 100/100/1/0.4/0.4 molar ratio of [PEGMA]<sub>0</sub>/[VDM]<sub>0</sub>/[EBiB]<sub>0</sub>/[CuBr]<sub>0</sub>/ [Me<sub>6</sub>Tren]<sub>0</sub>, respectively, in toluene at 30°C

time (min)	conv <sup>a</sup> (%)		$\overline{M}_{n,th}^b$ (g/mol)	$\overline{M}_{n,SEC}^c$ (g/mol)	PDI <sup>c</sup>
	PEGMA	VDM			
0	0	0	0	0	0
30	13	16	3062	3800	1.20
45	14	17	3282	4100	1.21
60	15	20	3640	5400	1.19
90	18	22	4229	7700	1.14
120	18	25	4438	7900	1.13
150	20	24	4668	8000	1.13
180	22	28	5246	8100	1.13
1440	24	29	5616	8300	1.09

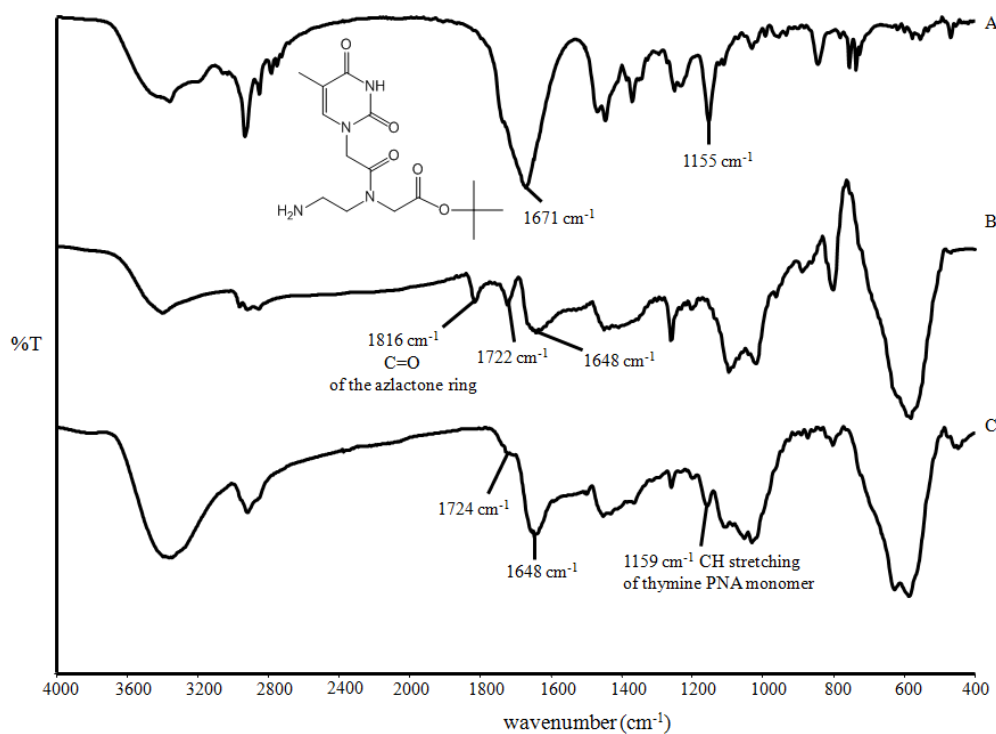
<sup>a</sup> Determined via <sup>1</sup>H NMR spectroscopy (monomer depletion monitored relative to DMF used as an internal standard). <sup>b</sup>  $\overline{M}_{n,th} = ([\text{PEGMA}]_0/[\text{EBiB}]_0 \times \text{conv}_{\text{PEGMA}} \times M_{\text{PEGMA}}) + ([\text{VDM}]_0/[\text{EBiB}]_0 \times \text{conv}_{\text{VDM}} \times M_{\text{VDM}})$ . <sup>c</sup> Measured by SEC (calibrated with polystyrene standard).

### 2.2.3 Immobilization of thymine PNA monomer on poly(PEGMA-*stat*-VDM)-coated MNP

The as-synthesized poly(PEGMA-*stat*-VDM)-coated MNP containing active azlactone functional groups were then used as a magnetically guidable-nanoscale amine support. In this study, thymine PNA monomer was selected as a model compound for grafting onto the particle surface. It is anticipated that these novel copolymer-coated MNPs can be used as a nanosolid support for PNA oligomer immobilization. Because precedents have reported the utilization of PNA oligomer as a probe for detection of DNA sequences [6-9], the attachment of PNA oligomers on these copolymer-coated MNP is warrant for further studies.

The immobilization process of thymine PNA monomer on the particle surface was performed in anhydrous DMF at room temperature for 6 h (Scheme 2.2). Figure 2.8C shows the disappearance of cyclic carbonyl of azlactone rings at 1816 cm<sup>-1</sup> [5]

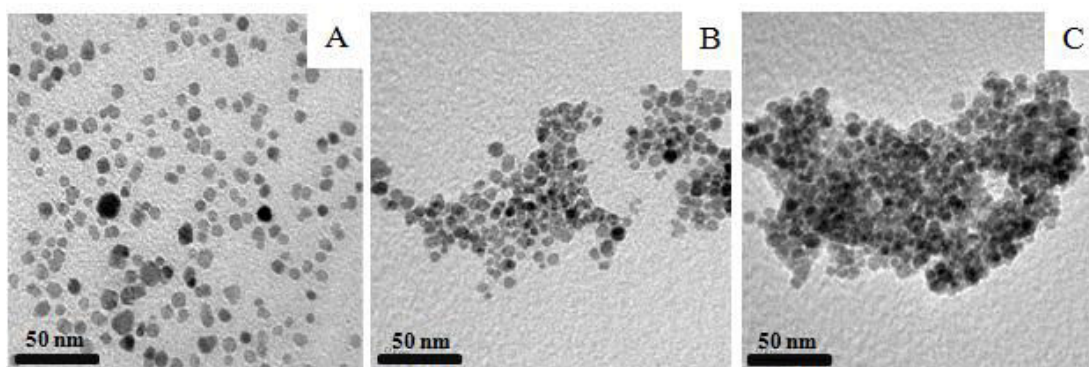
and the appearance of a signal at  $1159\text{ cm}^{-1}$  corresponding to a C-H bending of thymine [10], indicating the presence of thymine PNA monomer in the complex.



**Figure 2.8** FTIR spectra of (A) thymine PNA monomer, (B) poly(PEGMA-*stat*-VDM)-coated MNP and (C) poly(PEGMA-*stat*-VDM)-coated MNP immobilized with thymine PNA monomer

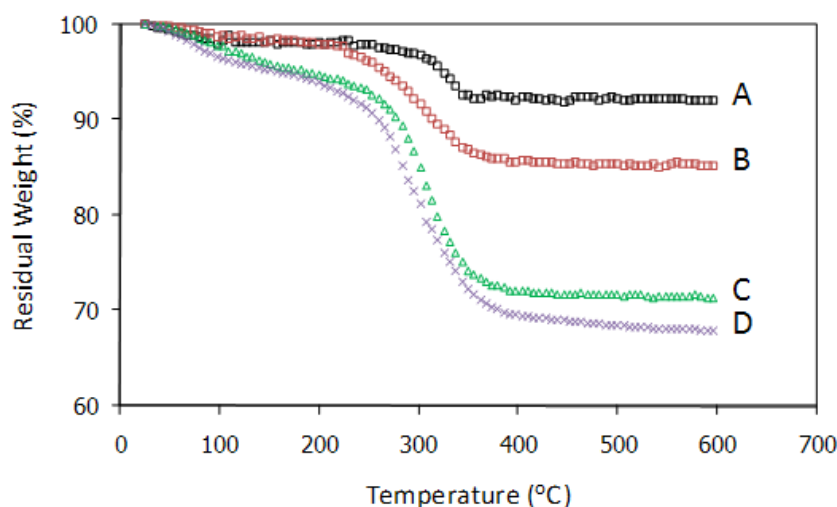
TEM images of MNP complexes at each step of the reaction are shown in Figure 2.9. Bare MNP was not well dispersible in any solvent due to the lack of polymer coating. After coating with oleic acid, the particles were well dispersible in toluene; the TEM image shown in Figure 2.9A was prepared from the particle dispersion in toluene. The particle size was in the range of 7-14 nm with the average diameter of 9 nm. After surface modification of the particle with poly(PEGMA-*stat*-VDM) in DMF, there was some nanoscale aggregation of about 30-50 particles/cluster (Figure 2.9B). After immobilization of thymine PNA monomer on their surface, more aggregation of the particles was observed (about 100 particles/cluster) (Figure 2.9C). The presence of hydrophobic thymine PNA monomer units on surface of the complexes might promote the particle aggregation in DMF. Although there was some

nano-aggregation observed in TEM, these complexes were still visually re-dispersible in various solvents, such as THF, DMF and toluene, probably due to the presence of the polymeric thin film on their surface. A TEM image showing the presence of polymeric thin films on the particle surface was illustrated in the appendix A.



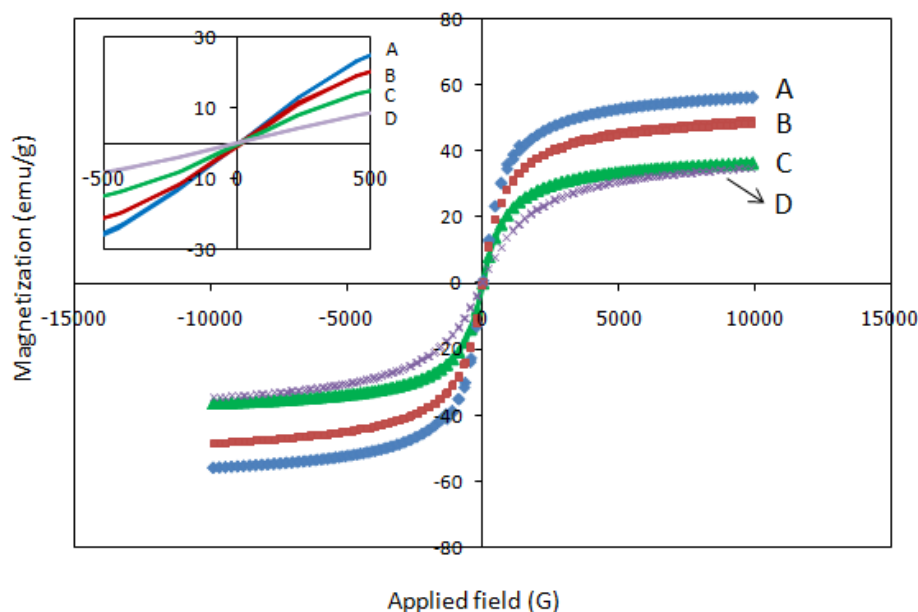
**Figure 2.9** TEM images of (A) oleic acid-coated MNP (prepared from toluene dispersion), (B) poly(PEGMA-*stat*-VDM)-coated MNP (prepared from DMF dispersion) and (C) poly(PEGMA-*stat*-VDM)-coated MNP immobilized with thymine PNA monomer (prepared from DMF dispersion)

TGA studies were carried out to determine the mass loss of the organic components in the grafted-MNP. The MNP complexes in each step of the reaction showed their distinctive TGA curves, giving rise to the information of the amount of BTPAm, poly(PEGMA-*stat*-VDM) and thymine PNA monomer in the grafted-MNP (Figure 2.10). The slight loss in mass of bare MNP was attributed to the residual benzyl alcohol used as the reaction solvent in the MNP preparation step. According to the TGA results, there were about 6 wt% of BTPAm and 17 wt% of poly(PEGMA-*stat*-VDM) copolymer in the complexes. After the immobilization step of thymine PNA monomer, an increase in weight loss as compared to the one before the grafting reaction was observed (Figure 2.10D), indicating that there were about 4 wt% thymine PNA monomer grafted to the grafted-MNP. This number corresponds to about 1.2  $\mu\text{mol}$  of thymine PNA monomer per gram of the grafted-MNP (An example of the calculation is show in the appendix A). This was a supportive result to FTIR that thymine PNA monomer existed in the copolymer-coated MNP.



**Figure 2.10** TGA curves of (A) bare MNP, (B) BTPAm-coated MNP, (C) poly(PEGMA-*stat*-VDM)-coated MNP and (D) poly(PEGMA-*stat*-VDM)-coated MNP immobilized with thymine PNA monomer

The  $M$ - $H$  curves measured at room temperature of the particles in each step of the reaction are illustrated in Figure 2.11. As illustrated in the inset, all samples showed no hysteresis at room temperature. The decrease of saturation magnetization ( $M_s$ ) from 56 emu/g of bare MNP to 49 emu/g of BTPAm-coated MNP was attributable to the presence of BTPAm thin layer on the particle surface, resulting in the decrease of the percentage of MNP core in the complex (Figure 2.11). Likewise, the  $M_s$  values of poly(PEGMA-*stat*-VDM)-coated MNP (36 emu/g) and poly(PEGMA-*stat*-VDM)-coated MNP immobilized with thymine PNA monomer (34 emu/g) were significantly lower than those of the BTPAm-coated MNP, which was again devoted to the decrease of MNP content in the complexes owing to the copolymer/thymine coating. This was in good agreement with the FTIR result indicating the presence of the copolymer in the complex. When taking the percentage of magnetite in the complex into account, the  $M_s$  values in emu/g magnetite basis were in the range of 46-56 emu/g magnetite (see Table A4 in the appendix A). The slight drop in the  $M_s$  values in emu/g magnetite basis was attributed to the use of organic solvents, e.g. DMF, in surface modification reactions, which might, to some extent, affect the magnetic properties of MNP core.



**Figure 2.11** *M-H* curves of A) bare MNP, B) BTPAm-coated MNP, C) poly(PEGMA-*stat*-VDM)-coated MNP and (D) poly(PEGMA-*stat*-VDM)-coated MNP immobilized with thymine PNA monomer. The expansion in the range of  $\pm 500$  G of applied field is shown in the inset.

The crystal structures of each complex were also investigated. From XRD studies, the position and relative intensities of all diffraction signals of bare MNP and poly(PEGMA-*stat*-VDM)-coated MNP matched well with the characteristic peaks of magnetite crystal [10] ( $2\theta = 30.2^\circ, 35.6^\circ, 43.3^\circ, 53.7^\circ, 57.2^\circ$  and  $62.7^\circ$ ) obtained from the standard  $\text{Fe}_3\text{O}_4$  powder diffraction data (see Figure A7 in the appendix A). Due to the limited amount of the as-synthesized poly(PEGMA-*stat*-VDM)-coated MNP immobilized with thymine PNA monomer, determination of its crystal structure *via* the XRD technique was not possible. Selected area electron diffraction (SAED) was thus performed to study the crystal structure information of the MNP immobilized with thymine PNA monomer (see Figure A8 in the Appendix A). Its SAED pattern revealed that the particles were crystalline and the *d*-values of the SAED were in good agreement with those observed in  $\text{Fe}_3\text{O}_4$  [11].



### 2.3 Conclusions

This work presented the surface modification of MNP with the statistical copolymer between PEGMA and VDM *via* ATRP to obtain the particles containing active functional groups on its surface. Hydrophilic PEGMA provided good dispersibility to the particle in polar solvents and azlactone rings served as active functional groups for further chemical attachment with nucleophiles of interest. Surface-initiated ATRP of the copolymer *via* a grafting ‘from’ strategy from the particle produced the active polymer layer with a predicable and controllable fashion. The nanosolid supports were successfully used for immobilization of thymine PNA monomers on its surface. The results signified the feasibility to functionalize the surface of these novel azlactone-based nanoparticles with a broad range of other nucleophilic scavengers such as hydroxyl- and thiol-containing compounds.

## References

1. Ciampolini, M.; Nardi, N. *Inorg Chem* **1966**, 5, 41.
2. Sun, Y.; Ding, X.; Zheng, Z.; Cheng, X.; Hu, X.; Peng, Y. *Eur Polym J* **2007**, 43, 762-772.
3. Rutnakornpituk, M.; Puangsin, N.; Theamdee, P.; Rutnakornpituk, B.; Wichai, U. *Polymer* **2011**, 52, 987-995.
4. Fournier, D.; Pascual, S.; Fontaine, L. *Macromolecules* **2004**, 37, 330-335.
5. Fournier, D.; Pascual, S.; Montembault, V.; Haddleton, D.M.; Fontaine, L. *J Comb Chem* **2006**, 8, 522-530.
6. Ananthanawat, C.; Vilaivan, T.; Hoven, V.P.; Su, X. *Biosens Bioelectron* **2010**, 25, 1064-1069.
7. Huang, B.; Hou, J.; Lin, S.; Chen, J.; Hong, H. *Harmful Algae* **2008**, 7, 495-503.
8. Masuko, M. *Nucleic Acids Res* **2003**, 3, 145-146.
9. Perry-O'Keefe, H.; Rigby, S.; Oliveira, K.; Sørensen, D.; Stender, H. Coull, J. *J Microbiol Methods* **2001**, 47, 281-292.
10. Singh, J.S. *J Mol Struct* **2008**, 876, 127-133.
11. Moisescu, C.; Bonneville, S.; Tobler, D.; Ardelean, I.; Benning, L.G. *Mineral Mag* **2008**, 72, 333-336.

## CHAPTER III

### HYDROPHILIC AZLACTONE-FUNCTIONALIZED MAGNETITE NANOPARTICLE FOR CONJUGATION WITH FOLIC ACID\*

#### Abstract

Herein we report the synthesis of magnetite nanoparticles (MNPs) grafted with poly(poly(ethylene glycol) methyl ether methacrylate-*stat*-2-vinyl-4,4-dimethylazlactone) copolymers (poly(PEGMA-*stat*-VDM)) prepared *via* a surface-initiated atom transfer radical polymerization (ATRP) and used for the immobilization of folic acid (FA). The MNPs were synthesized using a thermal decomposition method and surface functionalized to obtain ATRP initiating sites. Molar ratio of PEGMA to VDM was systematically varied (0/100, 30/70, 50/50 and 70/30, respectively) in the copolymerization to obtain water dispersible MNP with various amounts of azlactone rings, an electrophilic moiety, on its surface. Grafting density of VDM on the particle surface increased with increased VDM loading in the copolymerization reaction. These copolymer-coated MNPs were well dispersible in water with some nano-scale aggregation after FA functionalization due to hydrophobic character of FA. Since FA is a cancer-cell targeting agent, it is anticipated that these novel FA-functionalized MNPs could be used as magnetically guidable vehicle for drug delivery, particularly for cancer treatment. The results of this study warrant a future investigation of this promising system.

#### 3.1 Experimental

##### 3.1.1 Materials

Unless otherwise stated, all reagents were used without further purification: copper(I) bromide (CuBr, 98%, Acros), triethylamine (TEA, 97%, Carlo Erba), dicyclohexylcarbodiimide (DCC, 99%, Acros), sodium hydroxide ( $\geq 98\%$ , Aldrich), 2,6-di-*tert*-butyl-*p*-cresol (BHT,  $\geq 99\%$ , Aldrich) and concentrated hydrochloric acid (conc. HCl, 37%, Sigma-Aldrich). Poly(ethylene glycol) methyl ether methacrylate (PEGMA, Aldrich) with average molecular weight  $\overline{M}_n = 300 \text{ g.mol}^{-1}$  was purified by

\*This work has been published in Journal of Nanoparticle Research, 2014, 16:2357

passing through basic alumina column and stored at  $-4^{\circ}\text{C}$  after purification. Tris-[2-(dimethylamino)ethyl]amine ( $\text{Me}_6\text{Tren}$ ) [1], 2-bromo-2-methyl-*N*-(3-(triethoxysilyl) propyl) propanamide (BTPAm) [2] and *N*-(2-aminoethyl) folic acid [3] were prepared according to previously reported procedures. *N,N*-dimethylformamide (DMF, Acros), toluene (Acros) and dichloromethane ( $\text{CH}_2\text{Cl}_2$ ,  $\geq 99.5\%$ , Sigma-Aldrich) were used as received. Acryloyl chloride was synthesized *via* the reaction between acrylic acid and benzoyl chloride at  $75^{\circ}\text{C}$  to give a colorless liquid; 60% yield.

### 3.1.2 Characterization

Fourier transform infrared (FTIR) spectroscopy was performed on Perkin-Elmer Model 1600 Series FTIR Spectrophotometer. The solid samples were mixed with KBr to form pellets. Nuclear magnetic resonance (NMR) spectroscopy was performed on a 400 MHz Bruker NMR spectrometer using  $\text{CDCl}_3$  and  $\text{DMSO}_{d6}$  as solvents. Transmission electron microscopy (TEM) was performed on a Philips Tecnai 12 operated at 120 kV equipped with a Gatan model 782 CCD camera. Thermogravimetric analysis (TGA) was performed on SDTA 851 Mettler-Toledo at the temperature ranging between 25 and  $600^{\circ}\text{C}$  at a heating rate of  $20^{\circ}\text{C}/\text{min}$  under oxygen atmosphere. Vibrating sample magnetometry (VSM) was performed at room temperature using a Standard 7403 Series, Lakeshore vibrating sample magnetometer. Hydrodynamic diameter ( $D_h$ ) and zeta potential of the particles were measured *via* photo correlation spectroscopy (PCS) using NanoZS4700 nanoseries Malvern instrument. The sample dispersions were sonicated for 30 min before the measurement at  $25^{\circ}\text{C}$ . The measurement was carried out without filtration. The amounts of azlactone groups present on the particle surfaces were quantitatively determined by a conductometric titration using Seveneasy conductometer (Mettler Toledo Bmbt 8603 Swchwerzenbach). The presence of FA was investigated using SPECORD S100 ultraviolet-visible (UV-vis) spectrophotometer (Analytikjena AG) coupled with a photo diode array detector at  $\lambda_{\text{max}} = 371 \text{ nm}$ .

### 3.1.3 Synthesis of 2-vinyl-4,4-dimethylazlactone (VDM)

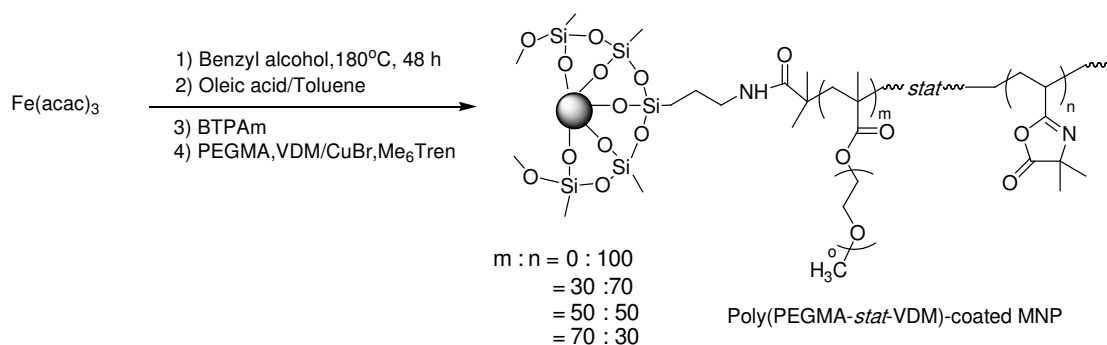
**3.1.3.1 Synthesis of *N*-acryloyl-2-methylalanine** [4]. 2-Methylalanine (5.6966 g,  $5.52 \times 10^{-2}$  mol, 1 eq.) was added into an aqueous solution of sodium hydroxide (4.4160 g,  $11.04 \times 10^{-2}$  mol, 2 eq. in 15 mL water) in the presence of BHT (0.0552 g,  $2.5051 \times 10^{-4}$  mol) as a polymerization inhibitor at 0-10°C, followed by an addition of acryloyl chloride (5 mL,  $5.52 \times 10^{-2}$  mol, 1 eq.). After 12 h stirring, conc. HCl (6.81 mL,  $6.90 \times 10^{-2}$  mol, 1.25 eq.) was added into the solution, which was kept at 10°C. The mixture was continuously stirred for another 30 min to form a white solid, which was filtered, washed with water and dried. Yield: 69-72%.  $^1\text{H}$  NMR (400 MHz, DMSO-*d*<sub>6</sub>)  $\delta_{\text{H}}$  in ppm: 1.37 (s, 6H, (C(CH<sub>3</sub>)<sub>2</sub>), 5.58 (dd,  $J_{\text{Htrans-Hcis}} = 2.1$  Hz,  $J_{\text{Htrans-Hgem}} = 10.1$  Hz, 1H, CH<sub>2</sub>=CH [trans]), 6.03 (dd,  $J_{\text{Hcis-Htrans}} = 2.1$  Hz,  $J_{\text{Hcis-Hgem}} = 17.1$  Hz, 1H CH<sub>2</sub>=CH [cis]), 6.25 (dd,  $J_{\text{Hgem-Htrans}} = 10.1$  Hz,  $J_{\text{Hgem-Hcis}} = 17.1$  Hz 1H, CH<sub>2</sub>=CH [gem]), 8.26 (s, 1H, NH), 12.16 (s, 1H, COOH).  $^{13}\text{C}$  NMR (400 MHz, DMSO-*d*<sub>6</sub>)  $\delta_{\text{C}}$  in ppm: 25.1 (C(CH<sub>3</sub>)<sub>2</sub>), 55.0 (-C(CH<sub>3</sub>)<sub>2</sub>-), 125.3 (CH<sub>2</sub>=CH), 131.8 (CH<sub>2</sub>=CH), 164.0 (COOH), 175.5 (NH-C=O). FTIR (ATR): 3337 cm<sup>-1</sup> (N-H stretching), 1707 cm<sup>-1</sup> (C=O of carboxylic acid), 1647 cm<sup>-1</sup> (C=O stretching of amide), 1599 cm<sup>-1</sup> (C=C stretching), 1551 cm<sup>-1</sup> (N-H bending).  $^1\text{H}$  NMR,  $^{13}\text{C}$  NMR and FTIR spectra are shown in the appendix B.

**3.1.3.2 Cyclization of *N*-acryloyl-2-methylalanine to form VDM.** The mixture of *N*-acryloyl-2-methylalanine (5.00 g,  $3.18 \times 10^{-2}$  mol) and BHT (0.0549 g,  $2.4912 \times 10^{-4}$  mol) in CH<sub>2</sub>Cl<sub>2</sub> (30 mL) was stirred at 0°C under argon atmosphere to form a colloidal dispersion. DCC solution (7.21 g,  $6.37 \times 10^{-3}$  mol in 40 mL CH<sub>2</sub>Cl<sub>2</sub>) was then added to the mixture with continuous stirring. After 12 h reaction, the solid dicyclohexylurea by-product was filtered off and the filtrate was evaporated to remove CH<sub>2</sub>Cl<sub>2</sub>. The VDM product was purified by distillation under reduced pressure to give a colorless mobile liquid. Yield: 60%.  $^1\text{H}$  NMR (400 MHz, CDCl<sub>3</sub>)  $\delta_{\text{H}}$  in ppm: 1.47 (s, 6H, C(CH<sub>3</sub>)<sub>2</sub>), 5.93 (dd,  $J_{\text{Htrans-Hcis}} = 2.0$  Hz,  $J_{\text{Htrans-Hgem}} = 9.9$  Hz, 1H, CH<sub>2</sub>=CH [trans]), 6.25 (dd,  $J_{\text{Hcis-Htrans}} = 2.0$  Hz,  $J_{\text{Hcis-Hgem}} = 17.6$  Hz, 1H CH<sub>2</sub>=CH [cis]), 6.27 (dd,  $J_{\text{Hgem-Htrans}} = 9.9$  Hz,  $J_{\text{Hgem-Hcis}} = 17.6$  Hz, 1H, CH<sub>2</sub>=CH [gem]).  $^{13}\text{C}$  NMR (100 MHz, DMSO-*d*<sub>6</sub>)  $\delta_{\text{C}}$  in ppm: 25.5 [C(CH<sub>3</sub>)<sub>2</sub>], 66.6 [C(CH<sub>3</sub>)<sub>2</sub>], 124.7 (CH<sub>2</sub>=CH), 129.6 (CH<sub>2</sub>=CH), 159.7 (-C=N-) and 181.5 (-C=O). FTIR: 1822 cm<sup>-1</sup> (C=O

stretching),  $1668\text{ cm}^{-1}$  (C=N stretching),  $1204\text{ cm}^{-1}$  (C-O-C stretching). This procedure was modified from the previously reported article using ethyl chloroformate as a coupling agent and giving rise to about 60% yield [4].  $^1\text{H}$  NMR,  $^{13}\text{C}$  NMR and FTIR spectra are shown in the appendix B.

### 3.1.4 Synthesis of poly(PEGMA-*stat*-VDM) copolymer coated on the MNP surface via ATRP (Scheme 3.1)

In this work, surface modification of MNPs with four different molar ratios of PEGMA to VDM (0/100, 30/70, 50/50 and 70/30, respectively) was performed. An example of surface modification of MNPs with 50/50 PEGMA/VDM copolymer was described herein. Other copolymer-MNP complexes were prepared in a similar fashion with appropriate amounts of reagents used. In a typical procedure, BTPAm-coated MNP (0.1 g) was sonicated with toluene (3.0 mL) in a Schlenk tube. A solution of PEGMA (3.6 mL, 0.11 mol), VDM (1.7 g, 0.11 mol), CuBr (0.04 g, 0.002 mol) and Me<sub>6</sub>Tren (0.05 g, 0.002 mol) in toluene (3 mL) were then syringed to the Schlenk tube. After degassing the solution by three freeze-pump-thaw cycles, ATRP was set at 30°C for 24 h.



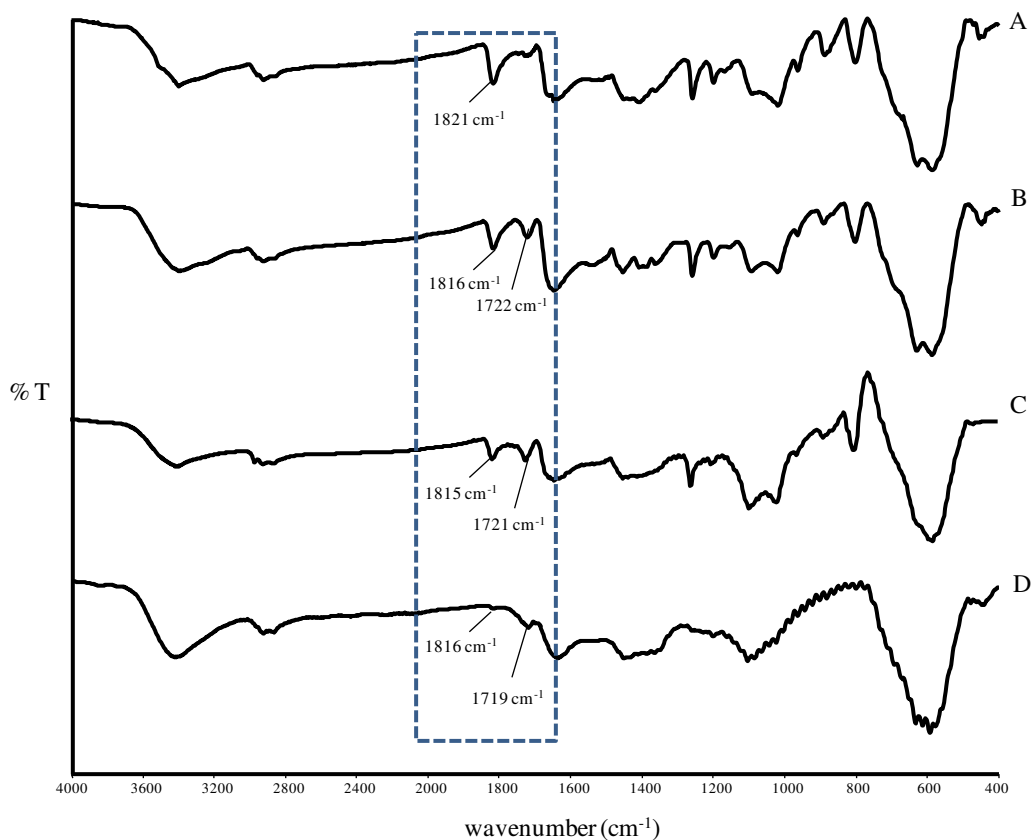
**Scheme 3.1** Synthesis of poly(PEGMA-*stat*-VDM)-coated MNPs *via* surface-initiated ATRP reaction



molecule for covalently grafting on the MNP surface through the ring-opening reaction of the VDM. Molar ratios of PEGMA to VDM on the MNPs were systematically varied (0/100, 30/70, 50/50 and 70/30, respectively) in an attempt to obtain water dispersible MNPs with various amounts of the active azlactone rings on their surface. Previous works have mostly reported the immobilization of FA on the outermost layer of polymeric surfactant coated MNPs, which might limit the grafting efficiency to the particle surface [7-9]. A promising strategy in promoting the grafting efficiency of FA to MNP surface is to have reactive functional groups along the polymer coating layers. As compared to other polymeric coatings [3, 10], the advantage of using azlactone-containing copolymers is that the azlactone rings react readily with nucleophiles at room temperature without using a catalyst or a coupling agent and leaving no by-products. Therefore, the significance of the current work is that we here report an efficient strategy to enhance the grafting efficiency of FA on water dispersible MNPs coated with well-defined copolymers. It is envisioned that the loading of FA on the poly(PEGMA-*stat*-VDM) copolymer-coated MNPs should be facilitated due to the increased amount of azlactone rings.

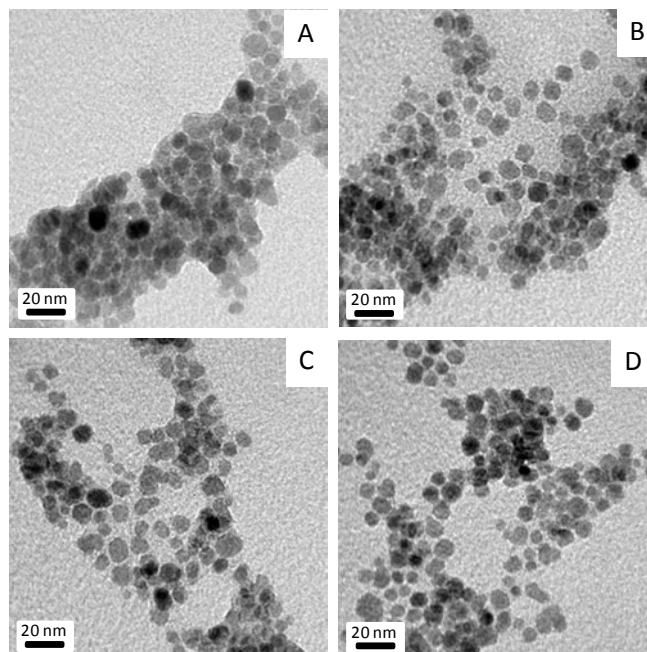
BTPAm, the initiator for ATRP, was first immobilized onto the surface of the particles through the combination of a ligand exchange reaction and condensation of triethoxysilane to obtain ATRP initiating sites on their surface, followed by surface-initiated ATRP of PEGMA and VDM. FA was then immobilized on the particle surface *via* a ring-opening reaction. Figure 3.1 shows FTIR spectra of poly(PEGMA-*stat*-VDM)-coated MNPs having the copolymer molar ratio of 0/100, 30/70, 50/50 and 70/30, respectively (Figure 3.1A-D). The success of the grafting reaction was signified by the presence of the characteristic signals of PEGMA at 1719-1722  $\text{cm}^{-1}$  (O(C=O) stretching) and those of VDM at 1815-1821  $\text{cm}^{-1}$  (C=O stretching). The decrease of the intensity of ester bonds (-O(C=O) stretching, 1719-1722  $\text{cm}^{-1}$ ) of PEGMA relative to those of the Fe-O bonds from MNP core (578  $\text{cm}^{-1}$ ) corresponds to the decrease of the amount of PEGMA units in the copolymer. Additionally, the increase of C=O signals of VDM (1815-1821  $\text{cm}^{-1}$ ) was also observed as the percentage of VDM in the copolymer was increased. It should be pointed out that the signals of the Fe-O bonds (578  $\text{cm}^{-1}$ ) of the MNP core did not significantly change in their intensity in all samples.





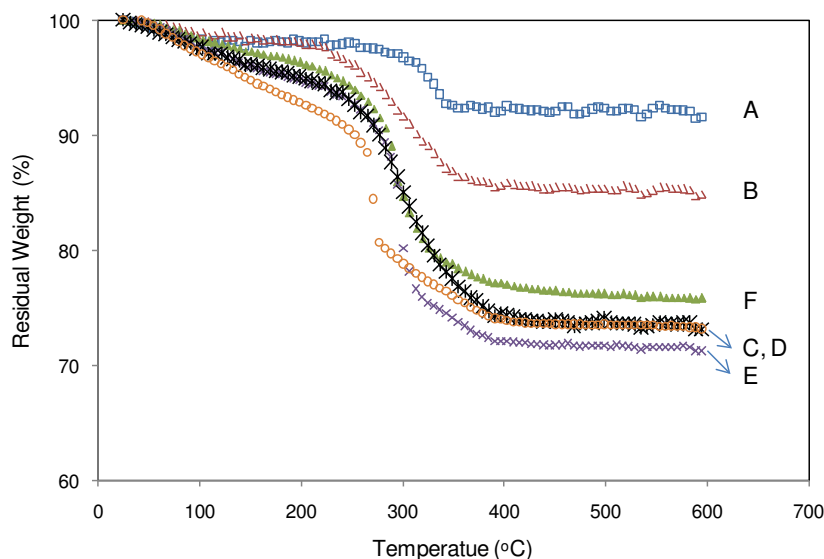
**Figure 3.1** FTIR spectra of poly(PEGMA-*stat*-VDM)-coated MNPs having molar ratio of PEGMA to VDM of A) 0/100, B) 30/70, C) 50/50 and D) 70/30, respectively

TEM images of poly(PEGMA-*stat*-VDM)-coated MNPs (0/100, 30/70, 50/50 and 70/30, respectively) are shown in Figure 3.2. The particle size is in the range of 5-10 nm with the average of  $8.0 \pm 1.2$  nm in diameter. Dispersibility of the particles in DMF improved with increasing PEGMA-to-VDM ratio in the copolymer due to the presence of higher number of polar PEGMA units on their surface. However, some nano-scale clustering of these particles was observed in TEM images and this was attributed to the existence of relatively non-polar poly(VDM) moieties on the particle surface. It should be noted that these particles were well dispersible in DMF without visually noticeable aggregation despite the observation of nanoclusters in TEM images.



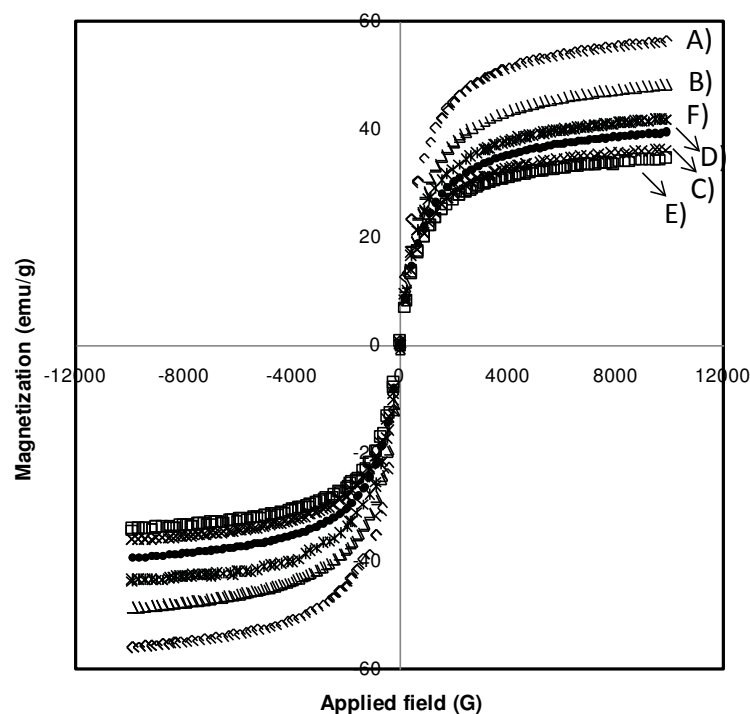
**Figure 3.2** TEM images of poly(PEGMA-*stat*-VDM)-coated MNPs having molar ratio of PEGMA to VDM of A) 0/100, B) 30/70, C) 50/50 and D) 70/30, respectively. The TEM samples were prepared from MNP-DMF dispersion.

Percent weight loss of poly(PEGMA-*stat*-VDM)-coated MNPs having different molar ratios of PEGMA to VDM was investigated to determine the relative amount of the copolymer that can be grafted on its surface. It should be noted that the particles were separated from the ungrafted species with an assistance of an external magnet. Using the hypothesis that percent char yield was the weight of magnetite core remaining at 600°C, the weight loss of the samples was thus attributed to the decomposition of organic components including BTPAm and the copolymers that partitioned to the particle surface. According to the TGA results, BTPAm content in BTPAm-coated MNP was about 7.6% and those of the copolymers were in the range of 10.5-15.3% (Figure 3.3). This result corroborates the results from FTIR suggesting that the copolymers existed on the particle surface.



**Figure 3.3** TGA curves of A) bare MNPs, B) BTPAm-coated MNPs and poly(PEGMA-*stat*-VDM)-coated MNPs having C) 0/100, D) 30/70, E) 50/50 and F) 70/30 molar ratios of PEGMA to VDM, respectively

$M$ - $H$  curves of bare MNP, BTPAm-coated MNPs and poly(PEGMA-*stat*-VDM)-coated MNPs are shown in Figure 3.4. The particles exhibit superparamagnetic behavior at room temperature as indicated by the absence of remanance and coercivity. Bare MNPs and BTPAm-coated MNPs showed relatively high saturation magnetization ( $M_s$ ) (48.9-56.3 emu/g) due to a lack of or only trace of organic component in the samples (Figure 3.4A and B). A slight decrease of  $M_s$  values of the copolymer-coated MNPs (34.4-42.8 emu/g) as opposed to their precursors was attributed to the presence of the copolymers on the particle surface, giving rise to the decrease of magnetite content in the complex (Figure 3.4C-F).



**Figure 3.4** *M-H* curves of A) bare MNP, B) BTPAm-coated MNP and poly(PEGMA-*stat*-VDM)-coated MNPs having C) 0/100, D) 30/70, E) 50/50 and F) 70/30 molar ratios of PEGMA to VDM

Grafting density of VDM on the particle surface was quantitatively determined by a conductometric titration. First, the copolymer-coated MNPs were dispersed in water, leading to a ring-opening reaction of the azlactone rings grafted on the MNP surface and giving rise to the formation of carboxyl groups. After drying to obtain the exact weight of the samples, they were then re-dispersed in a 0.005 M NaOH solution and the amounts of carboxyl groups were quantified from back titrations with a 0.005 M HCl solution. An example of the calculation of the grafting density of VDM on the MNP surface is shown in the appendix B. It was found that the VDM loading ranged between 2.67 and 4.67 mmol/g of MNPs and its grafting density consistently increased from 11.36 to 19.72 molecules/nm<sup>2</sup> as VDM in the copolymer increased from 30% to 100%, respectively (Table 3.1). This implies that the grafting density of VDM on the MNP surface can be fine tuned by simply modulating the molar ratio of VDM to PEGMA monomers in the copolymerization reaction. It should be noted that the

density of carboxyl groups on the MNP was reproducible as indicated by the low values of the standard deviations.

**Table 3.1** Grafting density of carboxyl groups on poly(PEGMA-*stat*-VDM)-coated MNPs after dispersing in water

Molar ratio of PEGMA to VDM in the copolymer coated on the MNPs	Density of carboxyl group (azlactone)	
	(mmol/g of MNPs)	(molecules/nm <sup>2</sup> of MNPs)
0/100	4.67 ± 0.00	19.72 ± 0.00
30/70	3.97 ± 0.23	16.83 ± 0.82
50/50	3.39 ± 0.17	14.86 ± 0.77
70/30	2.67 ± 0.21	11.36 ± 0.67

After the surface-initiated ATRP from the MNPs, it was envisioned that the particles having azlactone ring-enriched surface were obtained. The azlactone rings are reactive with nucleophilic functional groups such as amines, hydroxyls and thiols. In the current work, FA was covalently immobilized on poly(PEGMA-*stat*-VDM)-coated MNPs through a ring-opening reaction of the VDM moiety. Utilization of FA increasingly attracted much attention for tumor selective drug delivery applications because it provides specific sites that differentiate tumor cells from normal cells. FA also plays a role in receptor-mediated endocytosis and the process involves the access of a folate-receptor complex into the cells as a group, where it is fused with a lysosome [11-12]. In addition, FA is considered appropriate for targeted delivery because it is non-immunogenic, high binding affinity for its receptor, highly stable and inexpensive and easy to be conjugated with imaging agents [13].

In this work, FA needed to be functionalized with ethylene diamine (EDA) to contain a primary aliphatic amine group (*N*-(2-aminoethyl) folic acid or EDA-FA). This strategy enabled FA to efficiently couple with azlactone rings present on the particles. Immobilization of EDA-FA on the particle surface was carried out in *anh.* DMF at room temperature for 12 h. The  $D_h$  and zeta potential of FA-functionalized and non-functionalized MNP are given in Table 3.2. The  $D_h$  of the particles

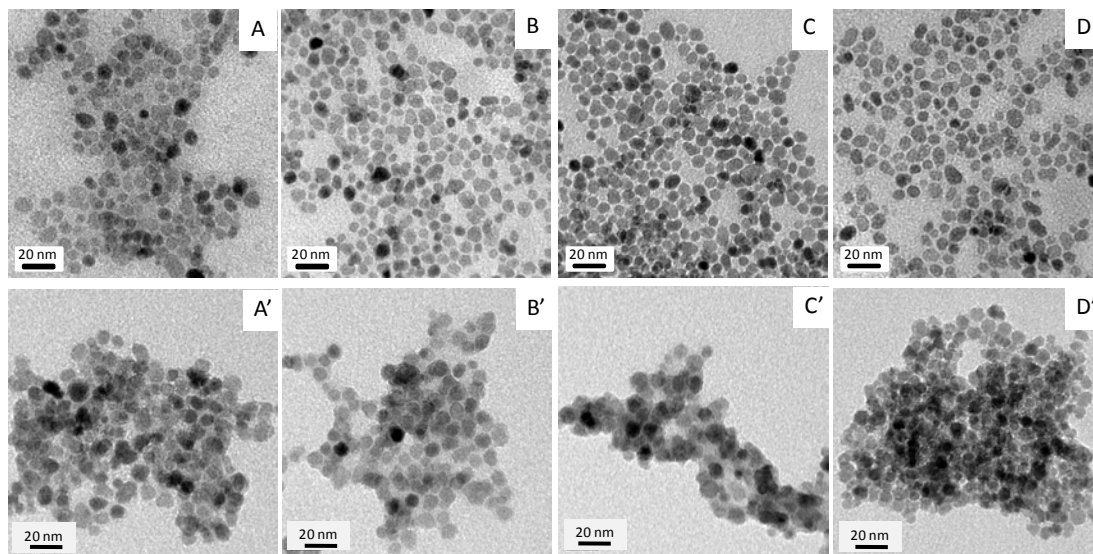
significantly increased after the FA immobilization. This was attributed to the grafting of hydrophobic FA on the particle surface and thus promoting particle agglomeration. This is in good agreement with the decrease in degree of negative charge of the FA-functionalized MNPs as compared to those before the FA functionalization, which was attributed to the presence of the pterin rings of FA after coupling reactions. It should be mentioned that the first requirement of MNPs for applicability in the biomedical field is that they should be stable in aqueous medium. In order to have the best possible transmembrane permeability, a second requirement is that the final size of the MNPs should be as small as possible. Grafting FA to MNP surface should increase the permeability into cancer cells but, due to FA hydrophobic behavior, it seemed to decrease the overall solubility of the complex. Therefore, optimization between the degree of nano-clustering, reflecting to the final size of the MNP, and FA grafting efficiency needs to be investigated. In addition, transmembrane permeability testing of the FA-grafted MNPs is warranted for future studies.

After FA immobilization, the zeta potential values of the particles decreased from -14.12 to -4.90 mV with decreasing azlactone composition in the copolymer. These values seemed to be quite low for nanoparticle stabilization *via* electrostatic repulsion, which might cause an increase in nanoparticle agglomeration tendency. However, these particles were rather well dispersible in water because of the presence of hydrophilic polymeric coating on their surface providing steric repulsion stabilization mechanism, and this might consequently enhance cell membrane penetration ability.

**Table 3.2** Hydrodynamic diameter ( $D_h$ ) and zeta potential of the MNPs in water at pH 7.4, before and after FA conjugation

MNPs (before FA conjugation)	$D_h$ (nm)	Zeta potential (mV)	MNPs (after FA conjugation)	$D_h$ (nm)	Zeta potential (mV)
poly(VDM)-coated MNPs	$96.3 \pm 1.1$	-17.39	FA-poly(VDM)-coated MNPs	$107.7 \pm 1.4$	-14.12
30/70 poly(PEGMA- <i>stat</i> -VDM)-coated MNPs	$131.0 \pm 5.0$	-15.92	FA-30/70 poly(PEGMA- <i>stat</i> -VDM)-coated MNPs	$210.3 \pm 4.5$	-9.80
50/50 poly(PEGMA- <i>stat</i> -VDM)-coated MNPs	$99.4 \pm 1.1$	-17.78	FA-50/50 poly(PEGMA- <i>stat</i> -VDM)-coated MNPs	$168.0 \pm 1.2$	-6.38
70/30 poly(PEGMA- <i>stat</i> -VDM)-coated MNPs	$114.0 \pm 4.1$	-14.12	FA-70/30 poly(PEGMA- <i>stat</i> -VDM)-coated MNPs	$270.0 \pm 7.0$	-4.90

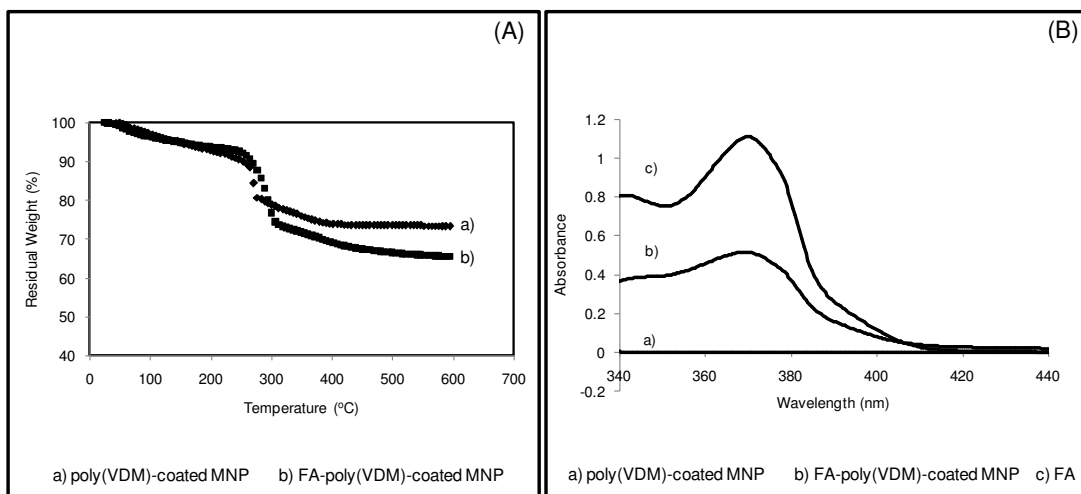
TEM images of poly(PEGMA-*stat*-VDM)-coated MNPs having 0/100, 30/70, 50/50 and 70/30 molar ratios of PEGMA to VDM, respectively, both before and after FA conjugation are shown in Figure 3.5. These TEM samples were prepared from aqueous dispersions. It was found that, before FA conjugation, all polymer-coated MNPs were well dispersible in water without aggregation (Figure 3.5A-D). After FA conjugation, some nano-scale aggregations of multiple MNPs were observed and this was attributed to the presence of hydrophobic FA coated on the particle surface (Figure 3.5A'-D'). More interestingly, according to the visual observation, FA-grafted MNP having high VDM content exhibited good particle dispersibility and stability in water. For instance, FA-poly(VDM)-coatedMNP (without PEGMA) was well dispersible in water for more than 24 h without noticeable aggregation as opposed to other samples. This result could be explained by the formation of carboxylate ions from a ring-opening reaction of the remaining VDM in water, leading to additional electrostatic repulsion stabilization and thus preventing particle agglomeration. Therefore, FA-poly(VDM)-coated MNPs were used for study of the percentage of FA in the complex discussed in the later section.



**Figure 3.5** TEM images of the poly(PEGMA-*stat*-VDM)-coated MNPs, (A-D) before and (A'-D') after the FA conjugation. The MNPs were coated with the copolymers having (A, A') 0/100, (B, B') 30/70, (C, C') 50/50 and (D, D') 70/30 molar ratios of PEGMA to VDM, respectively. All TEM samples were prepared from aqueous dispersions.

The compositions of poly(VDM) and FA on the particles were determined *via* TGA by analyzing the samples both before and after FA conjugation (Figure 3.6A). It was found that there were 12.3 wt% of poly(VDM) and 10.6 wt% FA grafted to the particles. This number corresponds to about 1.30 FA molecules/nm<sup>2</sup> of the particle surface area (260 FA molecules/particle). An example of the calculation is illustrated in the appendix B. Figure 3.6B exhibits the UV-visible spectra of poly(VDM)-coated MNP both before and after FA conjugations. FA shows a  $\lambda_{\text{max}}$  value at 371 nm (Figure 3.6B-c)), and suspension of poly(VDM)-coated MNPs after FA conjugation exhibit a weak absorbance signal at the same wavelength (Figure 3.6B-b). Poly(VDM)-coated MNPs before FA conjugation do not show any absorbance signal at the same wavelength (Figure 3.6B-a)). This result signifies that FA was, to some extent, covalently conjugated to the MNP surface.





**Figure 3.6** (A) TGA thermograms of a) poly(VDM)-coated MNP without FA and b) FA-poly(VDM)-coated MNP and (B) UV-visible absorption spectra of a) poly(VDM)-coated MNP without FA b) FA-poly(VDM)-coated MNP and c) FA

### 3.3 Conclusions

This work reports the surface modification of MNPs with poly(PEGMA-*stat*-VDM) *via* ATRP using a grafting ‘from’ strategy. The degree of the electrophilic azlactone rings could be adjusted by varying the molar ratio of PEGMA to VDM in the copolymerization. These copolymer-coated MNPs were successfully used for immobilization of FA on their surface. It was found that the particles with good dispersibility and stability in water, and with reasonable FA immobilization capability were obtained. These novel FA-functionalized MNPs might be used as efficient drug delivery vehicles, particularly for cancer treatment. Studies investigating the efficiency of treating cancer using these particles will be conducted in the future.

## References

1. Ciampolini, M.; Nardi, N. *Inorg Chem* **1966**, 5, 41.
2. Sun, Y.; Ding, X.; Zheng, Z.; Cheng, X.; Hu, X.; Peng, Y. *Eur Polym J* **2007**, 43, 762-772.
3. Rutnakornpituk, M.; Puangsin, N.; Theamdee, P.; Rutnakornpituk, B.; Wichai, U. *Polymer* **2011**, 52, 987-995.
4. Taylor, L.D.; Kolesinski, H.S.; Mehta, A.C.; Locatell, L.; Larson, P.S. *Makromol Chem Rapid Commun* **1982**, 3, 779-782.
5. Prai-in, Y.; Tankanya, K.; Rutnakornpituk, B.; Wichai, U.; Montembault, V.; Pascual, S.; Fontaine, L.; Rutnakornpituk, M. *Polymer* **2012**, 53, 113-120.
6. Ho, T.H.; Levere, M.; Soutif, J.C.; Montembault, V.; Pascual, S.; Fontaine, L. *Polym Chem* **2010**, 2, 1258-1260.
7. Lin, J.J.; Chen, J.S.; Huang, S.J.; Ko, J.H.; Wang, Y.M.; Chen, T.L.; Wang, L.F. *Biomaterials* **2009**, 30, 5114-5124.
8. Mohapatra, S.; Mallick, S.K.; Maiti, T.K.; Ghosh, S.K.; Pramanik, P. *Nanotechnology* **2007**, 18, 1-9.
9. Sahu, S.K.; Maiti, S.; Pramanik, A.; Ghosh, S.K.; Pramanik, P. *Carbohydr Polym* **2012**, 87, 2593-2604.
10. Yang, H.M.; Park, C.W.; Bae, P.K.; Ahn, T.; Seo, B.K.; Chung, B.H.; Kim, J.D. *J Mater Chem B* **2013**, 1, 3035-3043.
11. Sauzedde, F.; Elaissari, A.; Pichot, C. *Colloid Polym Sci* **1999**, 277, 846-855.
12. Sauzedde, F.; Elaissari, A.; Pichot, C. *Colloid Polym Sci* **1999**, 277, 1041-1050.
13. Low, P.S.; Henne, W.A.; Doorneweerd, D.D. *Acc Chem Res* **2008**, 41, 120-129.

## CHAPTER IV

# RECYCLABLE MAGNETIC NANOCLUSTER CROSSLINKED WITH POLY(ETHYLENE OXIDE)-*BLOCK*-POLY(2-VINYL-4,4-DIMETHYLAZLACTONE) COPOLYMER FOR ADSORPTION WITH ANTIBODY

### Abstract

Surface modification of magnetic nanoparticle (MNP) with poly(ethylene oxide)-*block*-poly(2-vinyl-4,4-dimethylazlactone) (PEO-*b*-PVDM) diblock copolymer and its application as recyclable magnetic nano-support for adsorption with antibody were reported herein. PEO-*b*-PVDM copolymers were first synthesized *via* a reversible addition-fragmentation chain transfer (RAFT) polymerization using poly(ethylene oxide) chain transfer agent (PEO-CTA) as a macromolecular chain transfer agent to mediate the RAFT polymerization of VDM. They were then grafted on amino functionalized MNP by coupling with some azlactone rings of the PVDM block on MNP to form magnetic nanoclusters with tunable cluster size. The nanocluster size could be tuned from 20 to 150 nm in diameter with 10 to 100 particles/cluster by adjusting the chain length of the PVDM block. The remaining azlactone rings of obtained clusters were hydrolyzed with water to yield negatively charged surface. Hydrodynamic diameter ( $D_h$ ) of the copolymer-coated MNP was significantly smaller than those before polymer grafting, indicating the improvement in its water dispersibility. The nanoclusters were successfully used as efficient and recyclable nano-supports for adsorption with anti-rabbit IgG antibody. They retained higher than 96% adsorption ability of the antibody during eight adsorption-separation-desorption cycles, indicating the potential feasibility in using this novel hybrid nanocluster as recyclable support in cell separation applications.

## 4.1. Experimental

### 4.1.1 Materials

Unless otherwise stated, all reagents were used without further purification: iron(III) acetylacetonate ( $\text{Fe}(\text{acac})_3$ , 99.9%, Acros), benzyl alcohol (98%, Unilab), oleic acid (90%, Fluka), (3-aminopropyl)triethoxysilane (APS, 99%, Sigma-Aldrich), triethylamine (TEA,  $\geq 99\%$ , Sigma-Aldrich), 4,4'-azobis(4-cyanovaleric acid) (ACVA,  $\geq 98\%$ , Aldrich), anti-rabbit IgG (antibody produced in goat, Sigma-Aldrich), IgG from rabbit serum (Sigma-Aldrich), Anti-IgG-HRP (Anti-rabbit IgG (whole molecule)-Peroxidase (Sigma-Aldrich), 10% BSA diluents (KPL), ABTS<sup>®</sup> Peroxidase Substrate (KPL), Bradford reagent (Sigma), bovine gamma globulin (BGG, Thermo Scientific) and 2-(*N*-morpholino)ethanesulfonic acid (MES, 99%, Acros). 2-dodecylsulfanylthiocarbonylsulfanyl-2-methylpropionic acid (DMP) [1], poly(ethylene oxide) chain transfer agent (PEO-CTA) [2] and 2-vinyl-4,4-dimethylazlactone (VDM) [3] were synthesized following the reported procedures. Pure water was obtained from a Millipore Direct Q system and had a conductivity of 18.2 M $\Omega$  cm at 25°C. 1,4-Dioxane (99.8%, Sigma-Aldrich), *n*-hexane (Acros), *N,N*-dimethylformamide (DMF, 99.8%, Aldrich), toluene (99.8%, Sigma-Aldrich) and dichloromethane ( $\text{CH}_2\text{Cl}_2$ ,  $\geq 99.5\%$ , Sigma-Aldrich) were used as received.

### 4.1.2 Characterization

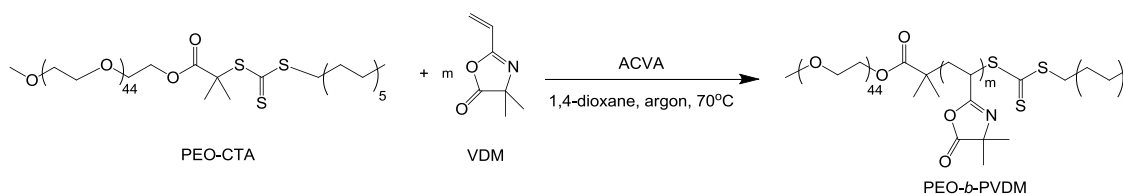
Fourier transform infrared (FTIR) spectroscopy was performed on Perkin-Elmer Model 1600 Series FTIR Spectrophotometer. The solid samples were mixed with KBr to form pellets. Nuclear magnetic resonance (NMR) spectra were performed on a 400 MHz Bruker NMR spectrometer for  $^1\text{H}$  NMR (400 MHz). Chemical shifts are reported in ppm relative to deuterated solvent resonances. Molar masses and molar mass distributions were determined *via* size exclusion chromatography (SEC) at 35°C on a system equipped with a Spectra System AS1000 autosampler with a guard column (Polymer Laboratories, PL gel 5  $\mu\text{m}$  guard, 50  $\times$  7.5 mm) followed by two columns (Polymer Laboratories, two PL gel 5  $\mu\text{m}$  Mixed-D columns, 2  $\times$  300  $\times$  7.5 mm). Polystyrene standards ( $580\text{--}483 \times 10^3 \text{ g}\cdot\text{mol}^{-1}$ ) were used to calibrate the SEC. Transmission electron microscopy (TEM) was performed on a Philips Tecnai 12 operated at 120 kV equipped with a Gatan model 782 CCD camera.

Thermogravimetric analysis (TGA) was performed on SDTA 851 Mettler-Toledo at the temperature ranging between 25 and 600°C at a heating rate of 20°C/min under oxygen atmosphere. Hydrodynamic diameter ( $D_h$ ) and zeta potential of the particles were measured *via* photo correlation spectroscopy (PCS) using NanoZS4700 nanoseries Malvern instrument. The sample dispersions were sonicated for 30 min before the measurements at 25°C without filtration. The ability of antibody adsorption to MNP was investigated by ultraviolet-visible (UV-vis) spectrophotometer on Perkin Elmer model Lambda 20 at  $\lambda = 595$  nm.

## 4.2 Syntheses

### 4.2.1 Synthesis of PEO-*b*-PVDM diblock copolymers by RAFT polymerization (Scheme 4.1)

An example of the synthesis of PEO-*b*-PVDM block copolymer using a molar ratio of  $[VDM]_0:[PEO-CTA]_0:[ACVA]_0$  equal to 100:1:0.2 molar ratio is herein explained. VDM (0.74 g,  $5.34 \times 10^{-3}$  mol), PEO-CTA (0.126 g,  $5.34 \times 10^{-5}$  mol), ACVA (3 mg,  $1.07 \times 10^{-5}$  mol), 1,4-dioxane (3.0 mL) and DMF (0.2 mL) used as an internal reference were added to a Schlenk tube equipped with a stir bar. The mixture was deoxygenated by bubbling argon for 30 min. The solution was then immersed in an oil bath thermostated at 70°C for 4 h to allow the polymerization to occur. Conversion of VDM was determined to be 41% by  $^1H$  NMR spectroscopy by comparing the integration areas of the vinylic protons of VDM at 5.93 ppm with the integral area value of the CH proton of DMF at 8.01 ppm. After precipitation in *n*-hexane, the polymer was dried *in vacuo* at room temperature for 12 h to yield a yellow powder product. The final polymer was analyzed by SEC, FTIR spectroscopy and  $^1H$  NMR spectroscopy.  $\overline{M}_n, SEC = 8800 \text{ g.mol}^{-1}$ , PDI = 1.09. FTIR ( $\nu$ ,  $\text{cm}^{-1}$ ):  $\nu_{(C=O; \text{azlactone})} = 1817$ ,  $\nu_{(C=N; \text{azlactone})} = 1699$  and  $\nu_{(C-O-C; \text{azlactone})} = 1201$ .  $^1H$  NMR (400 MHz,  $CDCl_3$ ,  $\delta$  (ppm): 1.40 ( $-OCO-(C(CH_3)_2-N=)$ ), 3.38 ( $CH_3O(CH_2-CH_2O)_{44-}$ ) and at 3.65 ( $CH_3O(CH_2-CH_2O)_{44}-CH_2CH_2-OC(O)C(CH_3)_2-$ ).



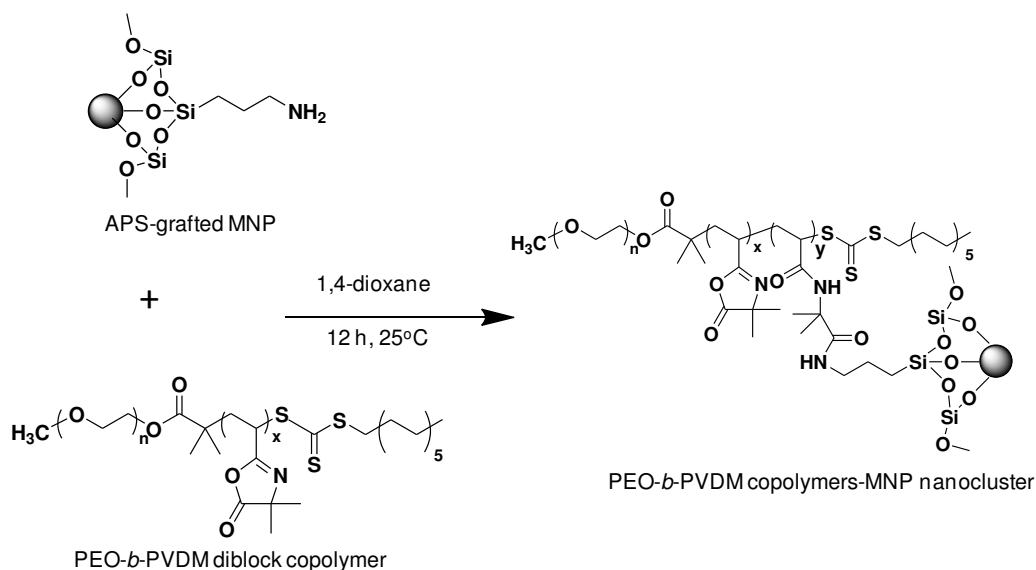
**Scheme 4.1** Synthesis of PEO-*b*-PVDM diblock copolymers by RAFT polymerization

#### 4.2.2 Synthesis of (3-aminopropyl)triethoxysilane-grafted MNP (APS-grafted MNP)

Amino-grafted MNPs were synthesized through a three-step process: (1) synthesis of MNP core, (2) grafting oleic acid onto the MNP and (3) a ligand exchange reaction with APS. First, a thermal decomposition of  $\text{Fe}(\text{acac})_3$  (5 g, 14.05 mmol) in benzyl alcohol (90 mL) was performed at 180°C for 48 h to obtain MNP core. The particle was magnetically separated from the dispersion and washed with ethanol and  $\text{CH}_2\text{Cl}_2$  repetitively to remove benzyl alcohol and then dried *in vacuo*. Oleic acid (4 mL) was then dropped to a MNP-toluene dispersion (0.8 g of MNPs in 30 mL of toluene) previously sonicated, to form oleic acid-grafted MNPs. APS (0.6 g,  $2.71 \times 10^{-3}$  mol) was then added to the oleic acid-grafted MNP dispersed in toluene (0.8 g of the MNP in 30 mL of toluene) containing 2 M TEA (5 mL) to form APS-grafted MNPs. After stirring for 24 h, the particles were precipitated in ethanol and washed with toluene to remove oleic acid and ungrafted APS from the dispersion. FTIR ( $\nu$ ,  $\text{cm}^{-1}$ ):  $\nu(\text{Fe-O}) = 586$ ,  $\nu(\text{Si-O stretching}) = 1103\text{--}1079$ ,  $\nu(\text{CH}_3 \text{ stretching}) = 2974\text{--}2886$  and  $\nu(\text{N-H stretching}) = 3363$ .

#### 4.2.3 Formation of PEO-*b*-PVDM copolymers-MNP nanocluster

APS-grafted MNP (100 mg) was dispersed in 10 mL 1,4-dioxane with sonication. Then, a PEO-*b*-PVDM diblock copolymer solution (100 mg of the copolymer in 10 mL 1,4-dioxane) was added to the APS-grafted MNP dispersion with stirring at room temperature for 12 h. The copolymer-coated MNP was magnetically separated from the dispersion and extensively washed with 1,4-dioxane. This process was repeatedly performed to remove ungrafted copolymer from the MNP nanocluster. The copolymer-MNP nanocluster was then dried *in vacuo* at room temperature for 12 h.



**Scheme 4.2** Synthesis of PEO-*b*-PVDM copolymers-MNP nanocluster

#### 4.2.4 Adsorption efficiency study of the copolymer-MNP nanoclusters with antibody

The copolymer-MNP nanocluster was first dispersed in water for 12 h to form carboxylate-enriched nanocluster due to the ring-opening reaction of the remaining azlactone rings in the copolymer on particle surface. After drying process, 10 mg of the copolymer-MNP nanoclusters were incubated in 1 mL of 10 mM MES pH 6 solution containing anti-rabbit IgG antibody for 2 h at room temperature. The Bradford assay [4] was used to determine antibody adsorption efficiency. The protein concentration of all samples was determined using a calibration curve of BGG as a protein standard. The copolymer-MNP nanoclusters after adsorption with antibody were separated from the supernatant using an external magnet. The absorption at 595 nm of the antibody solution before and after adsorption process was measured using the Bradford assay. The amount of the antibody adsorbed on the nanoclusters (in the unit of mg antibody/mg MNP) can be directly calculated from the decrease in antibody concentration in the supernatant using the following equation:

$$\text{Adsorption efficiency} = [(A-B)/A] \times 100 \dots \dots \dots (1)$$

where A is the loaded concentration of antibody and B is the concentration of adsorbed antibody.

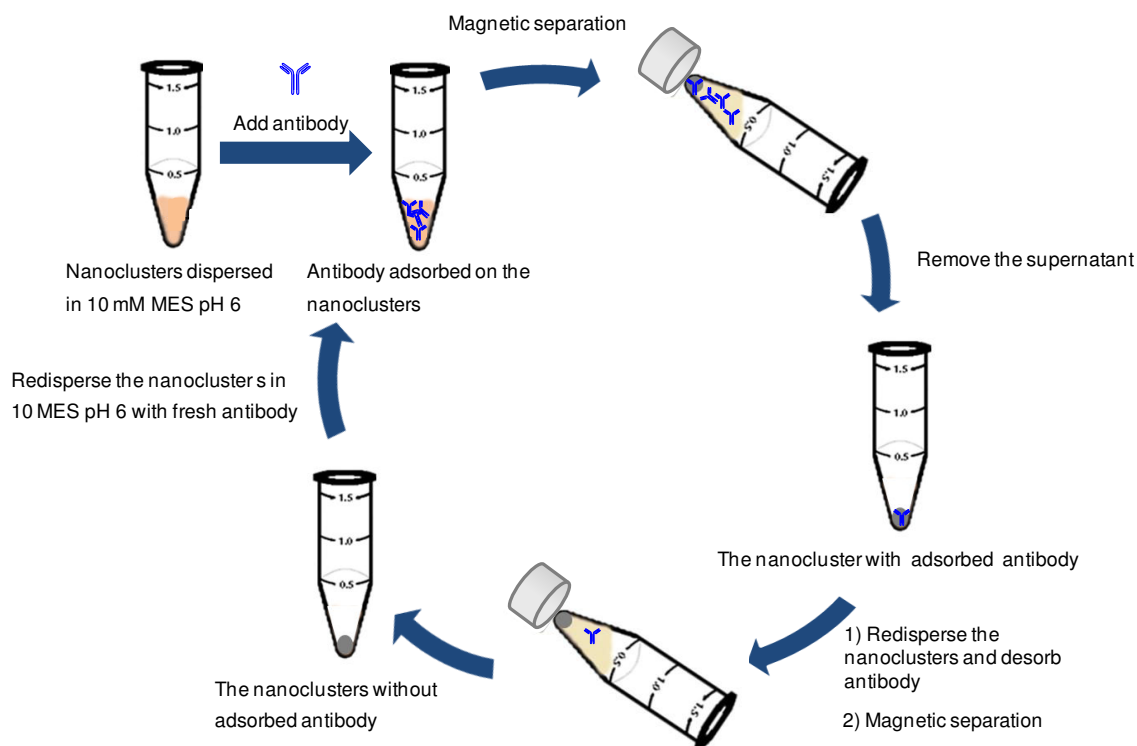
#### 4.2.5 Determination of recycling ability of the PEO-*b*-PVDM copolymer-MNP nanoclusters in adsorption with anti-rabbit IgG antibody

Copolymer-MNP nanoclusters adsorbed with anti-rabbit IgG antibody were thoroughly washed with 1 mL of a washing solution to desorb the antibody on the nanocluster surface. The amount of the antibody after desorption was determined using the Bradford assay. Desorption efficiency was determined from the following equation;

$$\text{Desorption efficiency} = (C/B) \times 100 \dots \dots \dots (2)$$

where C is the concentration of desorbed antibody and B is the concentration of adsorbed antibody

The adsorption-separation-desorption process was performed repeatedly to determine the recycling efficiency of the nanocluster (Scheme 4.3).



**Scheme 4.3** Schematic illustration of an adsorption-separation-desorption cycle of the recyclable copolymer-MNP nanocluster in adsorption with antibody (anti-rabbit IgG)



#### 4.2.6 Antigen recognition capacity study of antibody-adsorbed magnetic nanoclusters

After antibody adsorption procedure, the remaining carboxyl groups of magnetic nanoclusters were blocked with 1 mL of 1% BSA in 10 mM MES pH 6 at 25°C for 16 h. MNP nanoclusters were then washed with 10 mM MES pH 6 to remove an excess BSA. To detect the antigen recognition capacity of antibody-adsorbed MNP nanoclusters, an indirect detection method was used. First, 1 mL of 400 ppm of primary antigen (2.00 times molar excess) in 10 mM MES pH 6 was added into anti-rabbit IgG antibody-adsorbed MNP nanoclusters and incubated for 30 min. After washing the particles with 10 mM MES pH 6, they were incubated with 1 mL of 400 ppm of anti-rabbit IgG-HRP antibody for another 30 additional min. The presence of antigen on the particle surface was visualized by adding 1 mL of ABTS-H<sub>2</sub>O<sub>2</sub> solution into 10  $\mu$ l of the MNP nanoclusters dispersion.

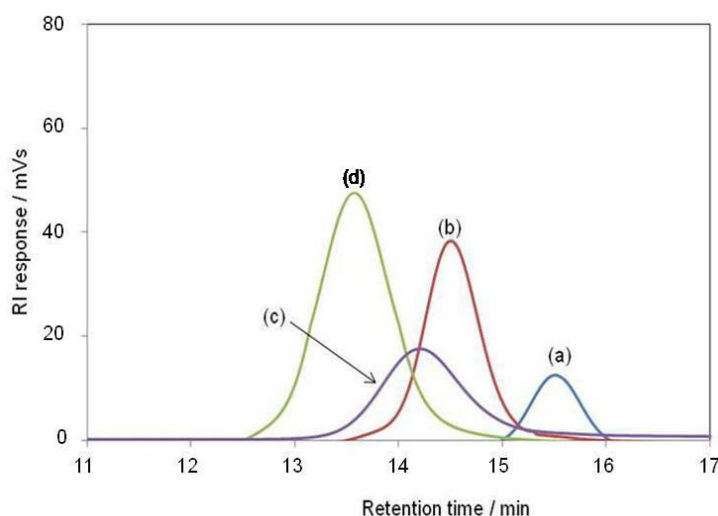
#### 4.3 Results and discussion

PEO-*b*-PVDM copolymers-MNP nanoclusters were obtained by the reaction between primary amine groups coated on MNPs surface and azlactone groups within the backbone of PEO-*b*-PVDM diblock copolymers *via* a ring-opening reaction (Scheme 4.2). In the first step, PEO-*b*-PVDM diblock copolymers were synthesized using PEO-CTA as the macromolecular chain transfer agent to mediate the RAFT polymerization of VDM in the presence of ACVA used as initiator in 1,4-dioxane at 70°C. The characteristics of the copolymers having three different PVDM block lengths are shown in Table 4.1. Theoretical number-average molecular weights ( $\overline{M}_{n,th}$ ) calculated from the monomer conversion increased as increasing the PVDM block length and this result is in good agreement with SEC results (Table 4.1). Figure 4.1 shows that SEC traces of PEO-*b*-PVDM diblock copolymers shift to earlier retention times with respect to the SEC trace of PEO-CTA maintaining low polydispersity indices (PDIs  $\leq$  1.10). This result shows that the copolymerization is well controlled leading to well-defined diblock copolymer structures.

**Table 4.1** Diblock copolymers of PEO and PVDM synthesized by RAFT polymerization at 70°C in 1,4-dioxane: experimental conditions and characterizations

Entry	Copolymer <sup>a</sup>	[VDM] <sub>0</sub> : [PEO-CTA] <sub>0</sub> : [ACVA] <sub>0</sub>	Reaction time (h)	VDM conv. <sup>a</sup> (%)	$\overline{M}_{n,th}^b$ (g/mol)	$\overline{M}_{n,SEC}^c$ (g/mol)	PDI <sup>c</sup>
1	PEO <sub>44</sub> - <i>b</i> -PVDM <sub>21</sub>	25:1:0.2	4	84	5277	7400	1.04
2	PEO <sub>44</sub> - <i>b</i> -PVDM <sub>41</sub>	100:1:0.2	4	41	8060	8800	1.09
3	PEO <sub>44</sub> - <i>b</i> -PVDM <sub>84</sub>	100:1:0.2	8	84	14083	14500	1.06

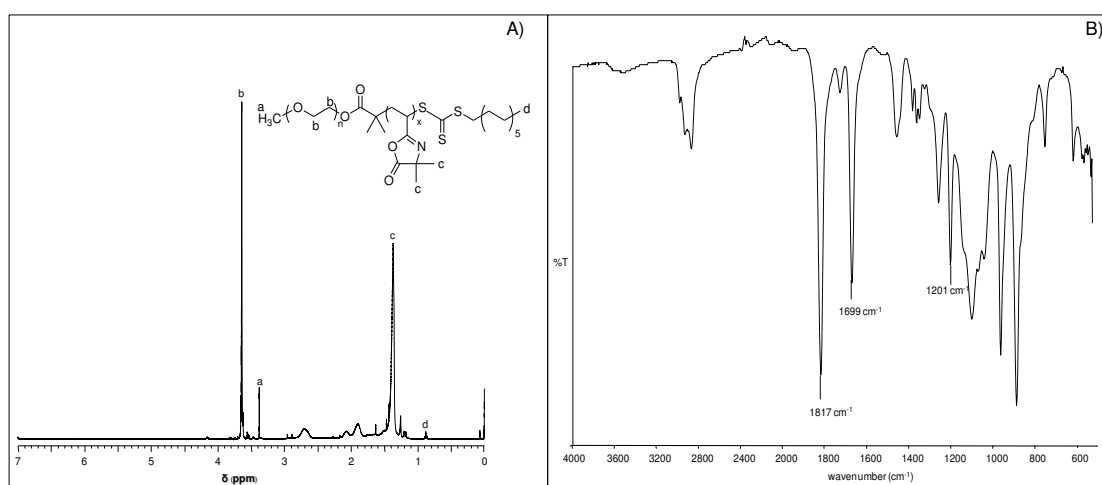
<sup>a</sup>The number of monomer units were calculated from the reaction conversion, determined by <sup>1</sup>H NMR spectroscopy. <sup>b</sup> VDM conversion determined by <sup>1</sup>H NMR spectroscopy by comparing the integration areas of the vinylic protons of VDM at 5.93 ppm with the integral area value of the CH proton of DMF at 8.01 ppm. <sup>c</sup>  $\overline{M}_{n,th} = \overline{M}_{n,NMR} \text{ of PEO-CTA} + (([VDM]_0/[PEO-CTA]_0) \times VDM_{conv.} \times M_{VDM})$ . <sup>d</sup>Determined by SEC in THF using polystyrene standard.



**Figure 4.1** Overlay SEC traces of (a) PEO<sub>44</sub>-CTA, (b) PEO<sub>44</sub>-*b*-PVDM<sub>21</sub> copolymer (Entry 1, Table 4.1), (c) PEO<sub>44</sub>-*b*-PVDM<sub>41</sub> copolymer (Entry 2, Table 4.1) and (d) PEO<sub>44</sub>-*b*-PVDM<sub>84</sub> copolymer (Entry 3, Table 4.1)

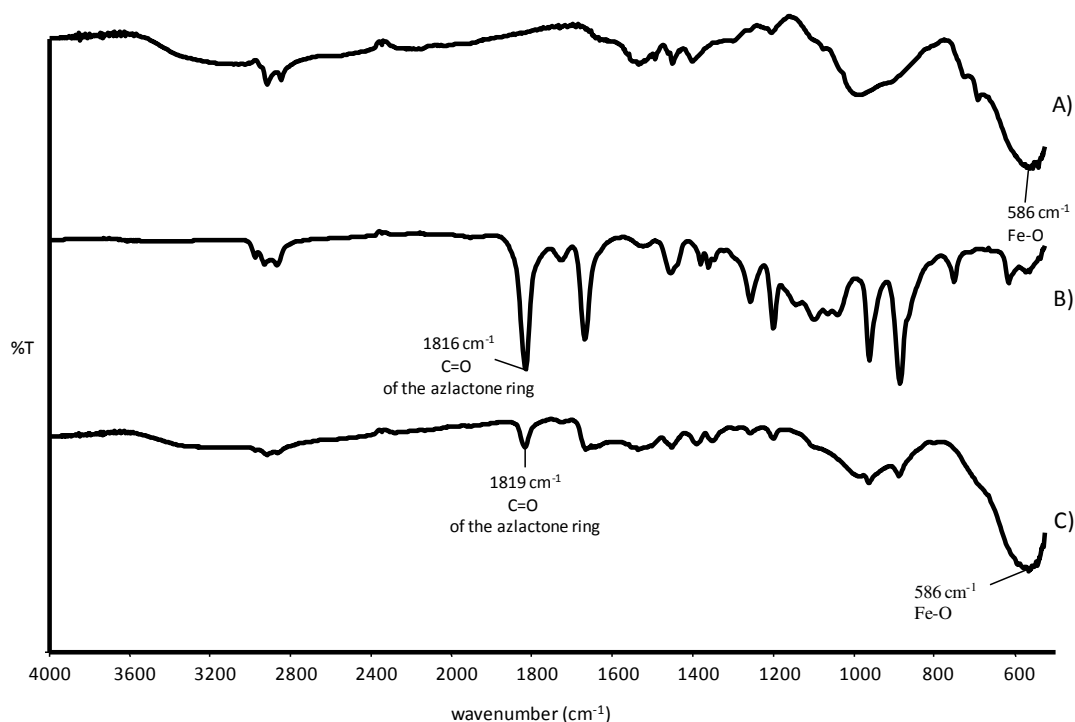
<sup>1</sup>H NMR spectrum (Figure 4.2A) of the PEO<sub>44</sub>-*b*-PVDM<sub>41</sub> copolymer (Entry 2, Table 4.1) shows the presence of signals at 3.38 ppm ( $\text{CH}_3\text{O}(\text{CH}_2\text{-CH}_2\text{O})_{44}\text{-}$ , labeled *a*) and at 3.65 ppm ( $\text{CH}_3\text{O}(\text{CH}_2\text{-CH}_2\text{O})_{44}\text{-CH}_2\text{CH}_2\text{-OC(O)C(CH}_3)_2\text{-}$ , labeled *b*), which

are characteristics of the PEO block and the presence of a signal at 1.40 ppm ( $-\text{OCO}-\text{C}(\text{CH}_3)_2-\text{N}=$ , labeled *c*), which is characteristic of PVDM block. The other two block copolymers show similar  $^1\text{H}$  NMR patterns to that of  $\text{PEO}_{44}-b\text{-PVDM}_{41}$  block copolymer with different integration ratios of signal *b* and *c*, depending on the block lengths of each copolymer. Moreover, the FTIR spectrum (Figure 4.2B) of the  $\text{PEO}_{44}-b\text{-PVDM}_{41}$  copolymer shows the characteristic bands of the azlactone rings at  $1817\text{ cm}^{-1}$  ( $\nu_{\text{C=O}}$ ), at  $1699\text{ cm}^{-1}$  ( $\nu_{\text{C=N}}$ ) and at  $1201\text{ cm}^{-1}$  ( $\nu_{\text{C-O-C}}$ ).



**Figure 4.2** A)  $^1\text{H}$  NMR spectrum of  $\text{PEO}_{44}-b\text{-PVDM}_{41}$  copolymer in  $\text{CDCl}_3$  and B) FTIR spectrum of  $\text{PEO}_{44}-b\text{-PVDM}_{41}$  copolymer

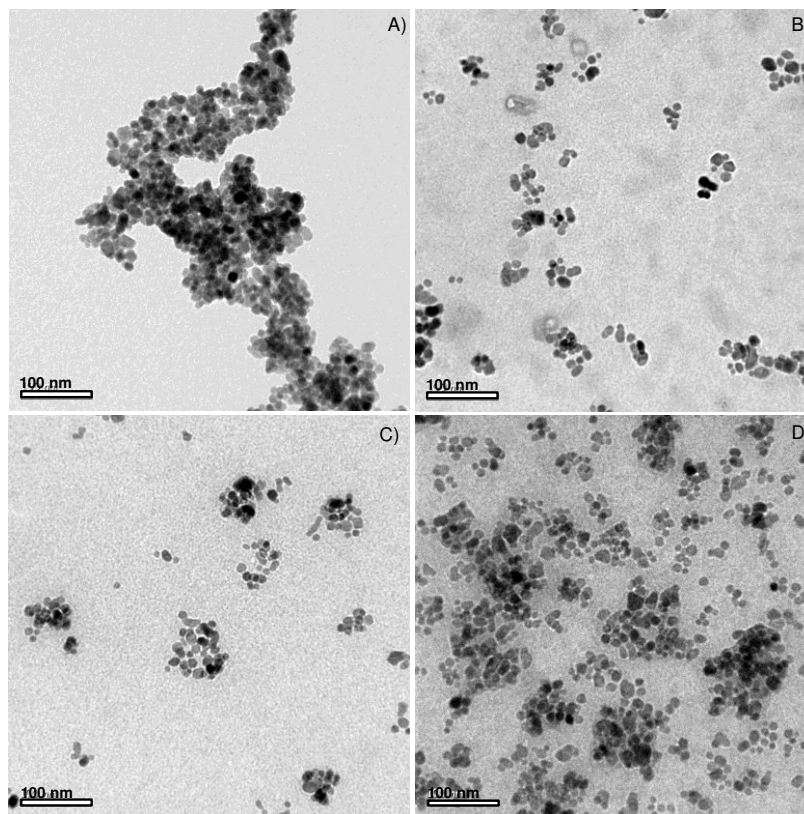
In the synthesis of  $\text{PEO}-b\text{-PVDM}$ -MNP nanoclusters, amino groups grafted on surface of APS-grafted MNP reacted with azlactone rings in PVDM blocks of the copolymers in 1,4-dioxane. The functional groups of copolymer-MNP nanoclusters were characterized by FTIR spectroscopy in comparison with those of APS-grafted MNP and  $\text{PEO}-b\text{-PVDM}$  copolymers (Figure 4.3). The spectrum of  $\text{PEO}-b\text{-PVDM}$ -MNP nanoclusters exhibited the left over azlactone rings ( $1819\text{ cm}^{-1}$ ) after the coupling reaction, indicating the availability for further hydrolysis with water to form the MNP having carboxylate-enriched surface for ionic adsorption with antibody in the next step.



**Figure 4.3** FTIR spectra of A) APS-grafted MNPs, B) PEO<sub>44</sub>-*b*-PVDM<sub>41</sub> block copolymers and C) PEO<sub>44</sub>-*b*-PVDM<sub>41</sub>-MNP nanoclusters

TEM images of APS-grafted MNPs and MNP nanoclusters coated with PEO-*b*-PVDM block copolymers containing different PVDM chain lengths are shown in Figure 4.4. It was found that large aggregations of the particles were observed for APS-grafted MNPs (Figure 4.4A). After PEO-*b*-PVDM block copolymer coating, the particle dispersibility was obviously improved due to hydrophilic PEO coating on its surface. In addition, the existence of carboxylic acid groups arising from the ring-opening reaction of azlactone rings in the PVDM block after exposure in water might also enhance water dispersibility of the particles. The ring-opening reaction between azlactone rings in the PVDM block of the copolymers and amino groups grafted on MNP surface led to the formation of the nanoclusters. The size of these nanoclusters increased from 20 to 150 nm with increasing the PVDM chain lengths: approximately 10, 50 and 100 particles/cluster were obtained for PEO<sub>44</sub>-*b*-PVDM<sub>21</sub>, PEO<sub>44</sub>-*b*-PVDM<sub>41</sub> and PEO<sub>44</sub>-*b*-PVDM<sub>84</sub> block copolymers, respectively. Increasing reactive azlactone groups in the PVDM block by increasing the PVDM length increased numbers of the MNP participating in the nanoclustering, indicating that the size of

these nanoclusters can be controlled by adjusting the number of reactive azlactone rings in the block copolymers.



**Figure 4.4** TEM images of A) APS-grafted MNP, B) PEO<sub>44</sub>-*b*-PVDM<sub>21</sub>-MNP nanoclusters, C) PEO<sub>44</sub>-*b*-PVDM<sub>41</sub>-MNP nanoclusters and D) PEO<sub>44</sub>-*b*-PVDM<sub>84</sub>-MNP nanoclusters. All TEM samples were prepared from aqueous dispersions.

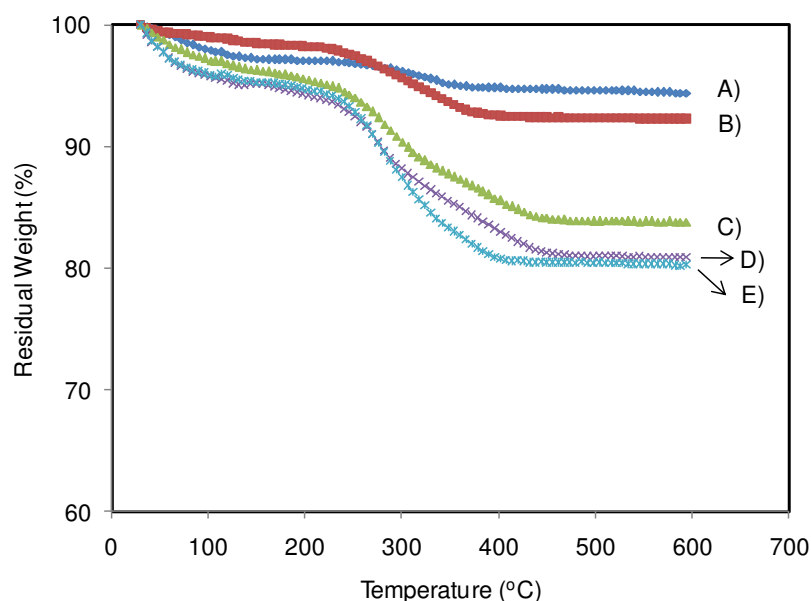
In good agreement with TEM results, hydrodynamic diameter ( $D_h$ ) of APS-grafted MNP was significantly larger than those of the MNPs coated with PEO-*b*-PVDM copolymers, indicating the improvement in water dispersibility of the particles after polymer coating (Table 4.2). Increasing PVDM block lengths in the copolymers led to the increase in  $D_h$  (97-166 nm), which corresponded to the TEM results. In addition, hydrodynamic size distributions of the copolymer-MNP nanoclusters were narrow as compared to that of APS-grafted MNP as a result of polymer coating and thus improving their water dispersibility. Zeta potential values of the nanoclusters were significantly increased after copolymer coating (-27 to -34 mV) due to the ring opening of PVDM units in the copolymers, resulting in the formation of the

nanoclusters with carboxylate-enriched surface. The negative charge of the carboxylate-coated nanoclusters was essential for magnetic separation of antibody through ionic adsorption mechanism in the next step.

**Table 4.2** Hydrodynamic diameter ( $D_h$ ), size distribution and zeta potential of the nanoclusters dispersed in 10 mM MES pH 6 solutions

Entry	Samples	$D_h$ (nm)	Size distribution	Zeta potential (mV)
1	APS-coated MNP	984.1	0.484	-3.45
2	PEO <sub>44</sub> - <i>b</i> -PVDM <sub>21</sub> -MNP nanoclusters	96.7	0.175	-27.2
3	PEO <sub>44</sub> - <i>b</i> -PVDM <sub>41</sub> -MNP nanoclusters	117.5	0.108	-28.3
4	PEO <sub>44</sub> - <i>b</i> -PVDM <sub>84</sub> - MNP nanoclusters	166.1	0.277	-33.9

TGA technique was used to calculate the percentage of organic layers bound to MNP. It was assumed that the percent weight loss was attributed to the weight of organic components and the residual weight was due to completely oxidized iron oxide in the form of magnetite. It was found that APS content in the nanoclusters was about 2.2% and the copolymers in the nanoclusters were in the range of 8.4-11.9% (Figure 4.5).

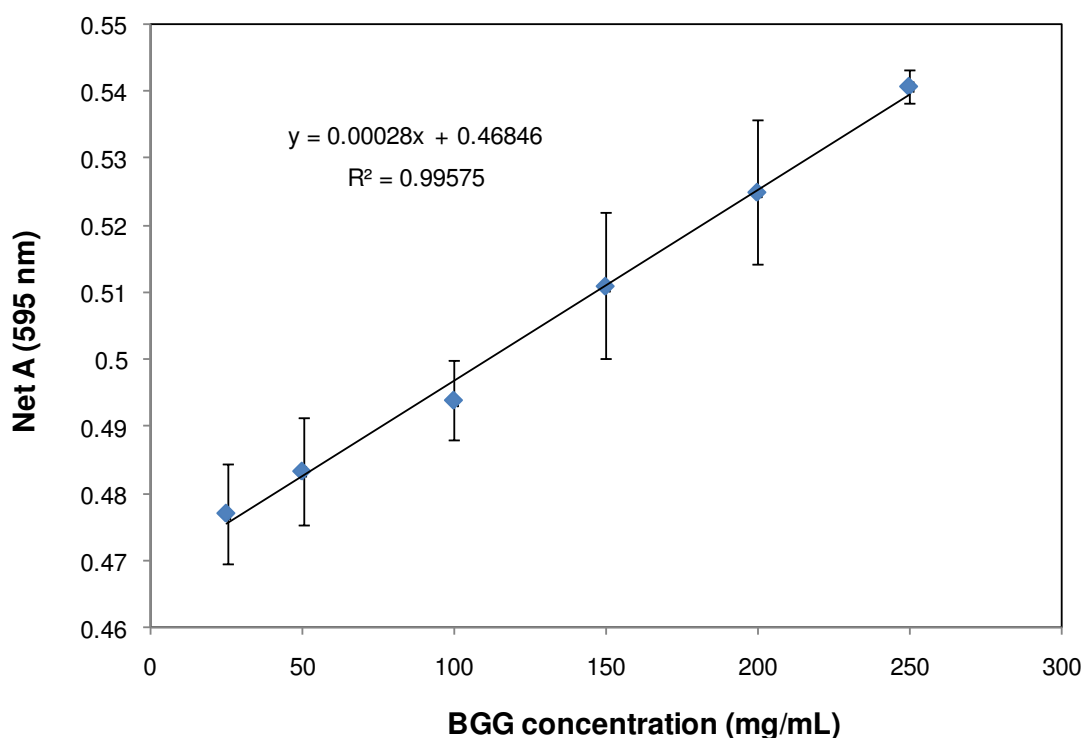


**Figure 4.5** TGA thermograms of A) bare MNPs, B) APS-grafted MNPs, C) PEO<sub>44</sub>-*b*-PVDM<sub>21</sub>-MNP nanoclusters, D) PEO<sub>44</sub>-*b*-PVDM<sub>41</sub>-MNP nanoclusters and E) PEO<sub>44</sub>-*b*-PVDM<sub>84</sub>-MNP nanoclusters

In order to use in antibody adsorption application, copolymer-MNP nanoclusters having carboxyl group-enriched surface are desirable for ionic adsorption between negatively charged MNP and positive moiety in anti-rabbit IgG antibody. Residual azlactone on the MNP surface thus was hydrolyzed to form nanoclusters with negatively charged surface due to carboxyl group coating before adsorption experiments. Nanoclusters having four different cluster sizes as shown in Table 4.2 were used as nano-solid supports in antibody adsorption experiments. It was found that APS-coated MNP was not dispersible in 10 mM MES pH 6 solution dispersing media due to a lack of polymer coating on its surface. On the other hand, the nanoclusters grafted with PEO<sub>44</sub>-*b*-PVDM<sub>21</sub> and PEO<sub>44</sub>-*b*-PVDM<sub>41</sub> copolymers were well dispersible in the media but not completely separated from the media using an external magnet. Trace of MNP in supernatant after magnetic separation and/or ultracentrifugation could interfere with Bradford assay [4]. The presence of single nanoparticles or magnetic clusters with small size possesses low magnetic sensitivity, resulting in difficulty in removal from the dispersion [5]. A compromise between good water dispersibility and magnetic sensitivity of MNP is crucial for use as a nano-solid

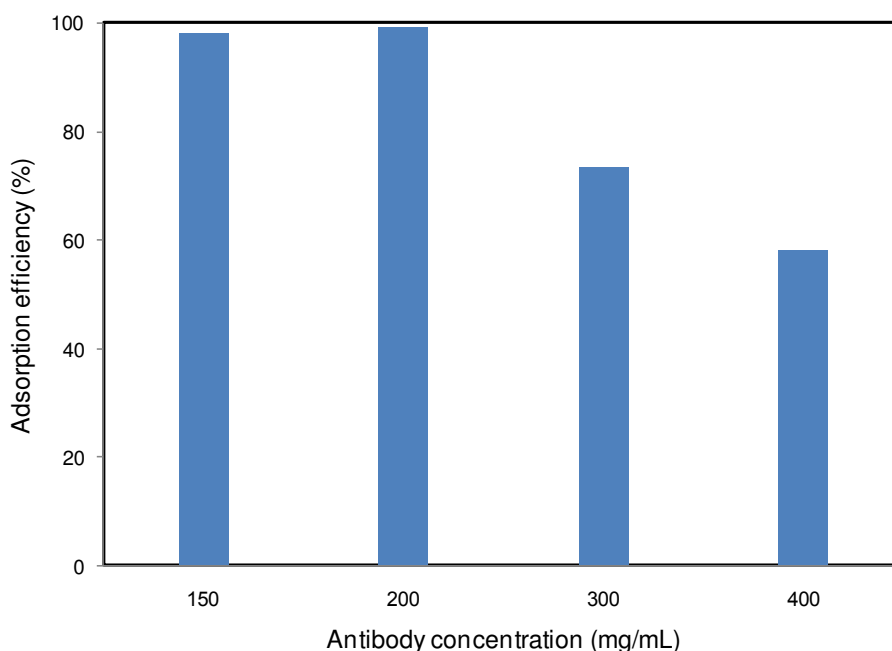
support. Therefore, the nanoclusters grafted with these two copolymers were unsuitable to be used as the supports for antibody adsorption. Interestingly, nanoclusters grafted with PEO<sub>44</sub>-*b*-PVDM<sub>84</sub> copolymer with  $D_h$  of 166 nm exhibited good dispersibility in the media and more importantly facilitated manipulation by an external magnet without trace of MNP left in the dispersion and interference with Bradford assay.

The amount of adsorbed antibody was quantified by the different concentrations of antibody in loading and in supernatant after adsorption process using the Bradford protein concentration assay [4]. The adsorption efficiency can be calculated using the Equation (1). Figure 4.6 shows the calibration of BGG standard for quantification of antibody adsorption studies. Figure 4.7 shows that 200 ppm was the maximum concentration of antibody that can bind on nanocluster surface. Increasing antibody concentration to 300 and 400 ppm resulted in the existence of un-adsorbed antibody in the dispersion. Therefore, 200 ppm antibody loading in 10 mg of PEO<sub>44</sub>-*b*-PVDM<sub>84</sub>-MNP nanoclusters would be used in other experiments.



**Figure 4.6** Calibration curve of BGG standard



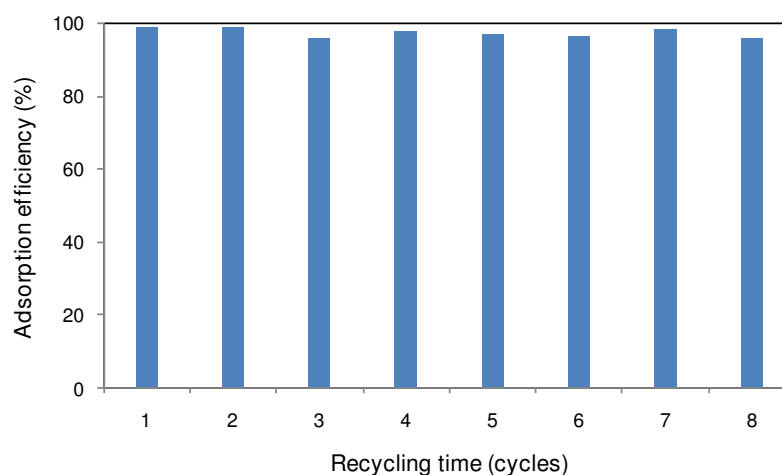


**Figure 4.7** Adsorption efficiency of PEO<sub>44</sub>-*b*-PVDM<sub>84</sub>-MNP nanoclusters for ionic adsorption with anti-rabbit IgG antibody

Because these nanoclusters possess magnetically guidable properties, which are great advantages in facilitating recycling process, the recycling ability of the copolymer-MNP nanoclusters was thus investigated. After 2 h adsorption with antibody, the nanoclusters were separated from dispersion with an assistance of a permanent magnet. To prove the recycling concept, an appropriate washing solution for desorbing anti-rabbit IgG from the nanocluster surface was then investigated. The amounts of antibody in supernatant after adsorption and desorption processes were quantitatively determined using Bradford assay and desorption efficiency was determined using the Equation (2). NaCl salt solutions at 300 mM, 1.0 and 2.5 M and pH 7, as well as 1.0 M NaCl solution at pH 12 were used for this purpose. It was found that, these salt solutions at pH 7 were unable to desorb anti-rabbit IgG antibody from the nanocluster surface probably because the solution pH was in the range of isoelectric point (pI) of the antibody (6-9) [4]. The antibody can be desorbed also by changing the global net charge of the antibody by shifting the solution pH [4]. 1.0 M NaCl solution with pH 12 exhibited a complete removal of the antibody from the surface due to the suppression in ionic adsorption between carboxylated nanoclusters

and the antibody as opposed to the situation in the pI range of the antibody. Therefore, 1 M NaCl pH 12 solution was used as a washing solution to investigate the adsorption recycling ability of the nanoclusters in the next step.

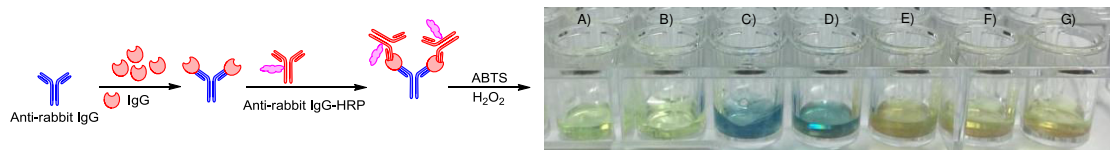
Figure 4.8 shows the antibody adsorption ability of the nanoclusters in each cycle. After adsorption-separation process, the concentration of adsorbed antibody and desorbed antibody from each cycle was determined using Bradford assay. The results showed that the particles retained higher than 96% adsorption ability of the antibody during eight adsorption-separation-desorption cycles, indicating the potential feasibility in using this novel hybrid nanocluster as recyclable support in cell separation applications.



**Figure 4.8** Recycling efficiency of PEO<sub>44</sub>-*b*-PVDM<sub>84</sub>-MNP nanoclusters in the ionic adsorption of anti-rabbit IgG antibody after 8-recycling process

The antigen recognition capacity of antibody-adsorbed MNP nanoclusters was determined from the development of a green-blue color product after the oxidation with ABTS, when reacted with horseradish peroxidase (HRP) labeled conjugates. Therefore, anti-rabbit IgG-adsorbed MNP nanoclusters were first immobilized with an IgG antigen, followed by anti-rabbit IgG-HRP as a secondary antibody for color development when reacted with ABTS. It was found that anti-rabbit IgG-adsorbed MNP nanoclusters exhibited the changing of color from light green to blue after the oxidation with ABTS (Figure 4.9D), indicating the conjugation of IgG antigen with anti-rabbit IgG adsorbed on the nanocluster surface. The MNP nanoclusters without

anti-rabbit IgG-HRP as the secondary antibody (Figure 4.9E), without IgG antigen (Figure 4.9F) and without anti-rabbit IgG (Figure 4.9G) were used as control dispersions. These dispersions showed negative results as their solution color did not change upon the oxidation with ABTS. The dispersion media (10 mM MES pH 6) (Figure 4.9A) and those with 1% BSA as a blocking reagent (Figure 4.9B) were also testified to evaluate the negative results of the control solutions. In addition, the solution of anti-rabbit IgG-HRP as the secondary antibody (without MNP nanoclusters) was also used in the testing to evaluate the color change (positive result) due to the reaction between HRP and ABTS (Figure 4.9C). Therefore, these experiments confirm that the antigen recognition of the antibody-adsorbed MNP nanoclusters was preserved. These MNP nanoclusters could be used as a recyclable magnetic marker to immobilize with other specific antibody-antigen conjugates.



**Figure 4.9** Scheme showing the indirect method used to visualize the antigen recognition capability; A) 10 mM MES pH 6, B) 1% BSA in 10 mM MES pH 6, C) anti-rabbit IgG-HRP, D) anti-rabbit IgG-adsorbed MNP nanoclusters immobilized with IgG and anti-rabbit IgG-HRP, E) anti-rabbit IgG-adsorbed MNP nanoclusters immobilized with IgG, F) anti-rabbit IgG-adsorbed MNP nanoclusters without IgG (blocked with BSA) and G) MNP nanoclusters

#### 4.4 Conclusions

Surface modification of MNP with well-defined PEO-*b*-PVDM diblock copolymer using grafting ‘onto’ strategy to form magnetic nanoclusters was described. The nanocluster size could be tuned by adjusting the amount of reactive azlactone rings in the PVDM block to obtain the size below 150 nm with a controllable fashion. The obtained nanoclusters were well dispersible in water, have good magnetic sensitivity and negatively charged surface. These properties are necessary for use these particles in magnetic separation applications. Their negatively charged surface provided adsorption capability with positively charged bio-entities. In the current

report, these novel magnetic nanoclusters were successfully used as efficient and recyclable nano-solid supports for adsorption with anti-rabbit IgG antibody. This magnetic nanocluster might be advantageous for use as a nanosolid support for efficient and facile separation of positively charged molecules.

## References

1. Lai, J.T.; Filla, D.; Shea, R. *Macromolecules* **2002**, 35, 6754-6756.
2. He, Y.; Lodge, T.P. *Chem Commun* **2007**, 2732-2734.
3. Taylor, L.D.; Kolesinski, H.S.; Mehta, A.C.; Locatell, L.; Larson, P.S. *Makromol Chem Rapid Commun* **1982**, 3,779-782.
4. Puertas, S.; Batalla, P.; Moros, M.; Polo, E.; Del Pino, P.; Guisan, J.M.; Grazú, V.; de la Fuente J.M. *ACS Nano* **2011**, 28, 4521-4528.
5. Amiri, H.; Mahmoudi, M.; Lascialfari, A. *Nanoscale* **2011**, 3, 1022-1030.

## CHAPTER V

### CONCLUSION

This research presented the surface modification of magnetite nanoparticle (MNP) with polymers *via* a grafting ‘from’ and grafting ‘onto’ controlled radical polymerization (CRP) to obtain the particle containing active functional groups on its surface. ATRP and RAFT polymerization were selected for MNP surface modification in this work.

First, surface modification of MNP *via* a grafting ‘from’ ATRP strategy with poly(poly(ethylene glycol) methyl ether methacrylate-*stat*-2-vinyl-4,4-dimethylazlactone) copolymers (poly(PEGMA-*stat*-VDM)) and its application in immobilization of thymine PNA monomer was studied. In this work, ATRP of PEGMA and VDM was first carried out in a solution system to optimize the reaction condition. It was found that 1/0.2/0.2 molar ratio of [EBiB]<sub>0</sub>/[CuBr]<sub>0</sub>/[Me<sub>6</sub>Tren]<sub>0</sub>, respectively, led to a good control of the copolymerization; the resulting polymers have  $\overline{M}_n$  close to the theoretical ones and relatively narrow polydispersity indices. The optimal condition was then applied in the surface-initiated ATRP of MNP. After the surface modification, thymine PNA monomer was then immobilized on poly(PEGMA-*stat*-VDM)-coated MNP *via* ring opening reactions with azlactone rings on the particle surface. TGA results indicated that there were 4 wt% of the PNA monomer in the complex (1.2  $\mu\text{mol/g}$  complex).

In the second work, surface modification of MNP with various degrees of PEGMA and VDM using surface initiated ATRP and its conjugation with FA were studied. It was found that the degree of PEGMA and VDM could be finely tuned by varying the molar ratio of PEGMA and VDM in the loading. TEM indicated that after the FA conjugation, FA-grafted MNP having high VDM content exhibited good particle dispersibility and stability in water. This result could be explained by the formation of carboxylate ions from a ring-opening reaction of the remaining VDM in water, leading to additional electrostatic repulsion stabilization and thus preventing the particle agglomeration.

In addition, modification of MNP surface using grafting ‘onto’ technique with PEO-*b*-PVDM diblock copolymer synthesized by RAFT polymerization was prepared. Its applications for adsorption with antibody were also studied. Three different azlactone block lengths with narrow PDI were first prepared by RAFT polymerization and then grafted onto amino-functionalized MNP to form magnetic nanoclusters with tunable cluster size. The nanocluster size could be tuned from 20 to 150 nm in diameter with 10 to 100 particles/cluster by adjusting the amounts of reactive azlactone rings in the PVDM block. After the copolymer coating, the remaining azlactone rings on the nanocluster surface were hydrolyzed with water to yield the MNP with negatively charged surface. Zeta potential values of the nanoclusters were significantly increased (-27 to -34 mV) as compared with its precursor due to the ring-opening of PVDM units in the copolymers. Then, the nanoclusters were used as recyclable nano-supports for adsorption with antibody. The result indicated that there was 96-99% adsorption ability of the antibody during eight adsorption-separation-desorption cycles.

The presence of polymeric layer not only prevents aggregation to the magnetite particles, but the active functional groups can be used for further chemical attachment with biomolecules of interest. Therefore, these novel polymer-coated MNPs can be used as an intermediate for covalent bonding with a variety of molecules containing affinity functional groups. It is anticipated that these azlactone-functionalized MNPs might be used as magnetically guidable vehicles for further attachment with active biomolecules and particularly used in biomedical applications, such as drug delivery vehicle, anticancer treatment and magnetic separation.

## **APPENDIX**

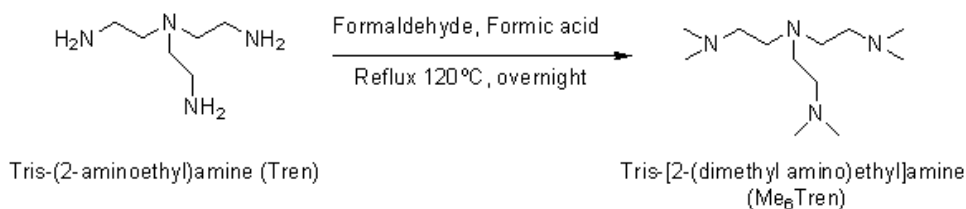


## Appendix A

### Part 1. Synthesis of tris-[2-(dimethylamino)ethyl]amine (Me<sub>6</sub>Tren) and 2-bromo-2-methyl-*N*-(3-(triethoxysilyl)propyl) propanamide (BTPAm)

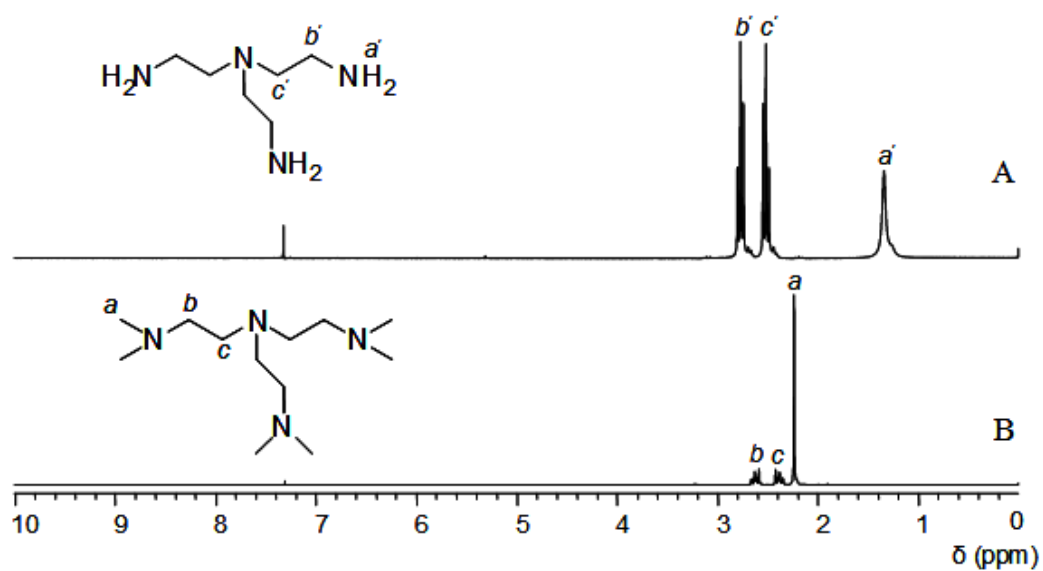
#### (A) Synthesis of tris-[2-(dimethylamino)ethyl]amine (Me<sub>6</sub>Tren) (Figure A1)

Tris-(2-aminoethyl)amine (Tren) (10 mL, 0.33 mol, 1 eq.) was slowly dropped into the mixture of formic acid (64 mL, 6.67 mol, 20 eq.) and formaldehyde (54 mL, 3.34 mol, 10 eq.) at 0°C in an ice bath. The mixture was heated to 120°C and stirred under reflux overnight. Unreacted formic acid and formaldehyde were removed by rotary evaporation. Then, the resulting orange oil was adjusted to pH 10 with saturated sodium hydroxide solution. The oily layer was extracted into diethyl ether (four times), and the volatiles removed by rotary evaporation to leave a yellow oil. The resulting oil was distilled under reduced pressure (69°C, 0.5 mmHg) to give a colorless liquid. Yield 84%.



**Figure A1** Synthesis of tris-(2-(dimethylamino)ethyl)amine (Me<sub>6</sub>Tren)

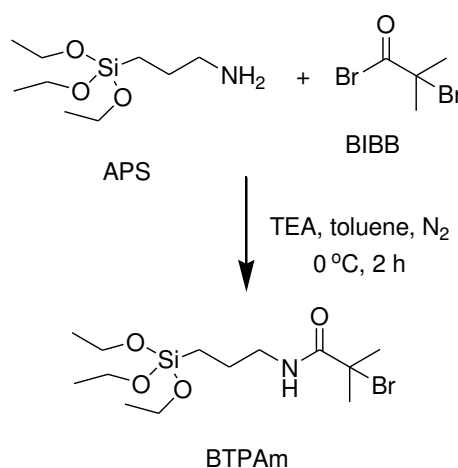
Figure A2B showed a <sup>1</sup>H NMR spectrum of Me<sub>6</sub>Tren in comparison with that of Tren starting reagent (Figure A2A), the formation of Me<sub>6</sub>Tren was identified by the presence of the methyl protons at 2.14 ppm (signal *a*). Also, the methylene protons of signal *b* (2.52 ppm) and signal *c* (2.28 ppm) confirmed the formation of Me<sub>6</sub>Tren.



**Figure A2**  $^1\text{H}$  NMR spectra of (A) tris-(2-aminoethyl) amine (Tren) (solvent:  $\text{CDCl}_3$ ), and tris-(2-(dimethylamino)ethyl) amine ( $\text{Me}_6\text{Tren}$ ) (solvent:  $\text{CDCl}_3$ )

**(B) Synthesis of 2-bromo-2-methyl-N-(3-(triethoxysilyl)propyl)propanamide (BTPAm) (Figure A3)**

To a stirred solution of (3-aminopropyl)triethoxysilane (APS) (0.18 mL, 0.8 mmol) and triethylamine (TEA) (0.12 mL, 0.8 mmol) in dried toluene (10 mL), 2-bromoisobutyryl bromide (BIBB) (0.1 mL, 0.8 mmol) in dried toluene (10 mL) was added dropwise at 0°C for 2 h under nitrogen. The reaction mixture was warmed to room temperature and stirred for 24 h. The mixture was passed through a filter paper to remove salts and the filtrate was evaporated to remove the unreacted TEA under reduced pressure. The resulting product, BTPAm, was yellowish thick liquid (78% yield).

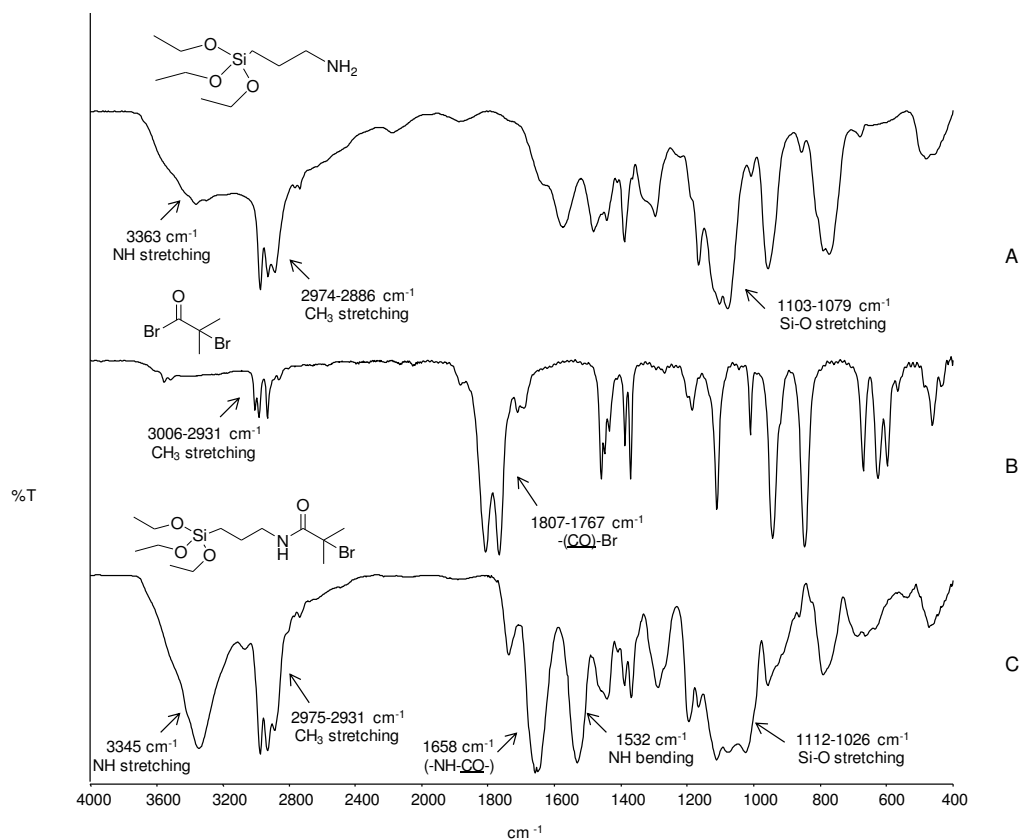


**Figure A3** Reaction between APS and BIBB to obtain BTPAm

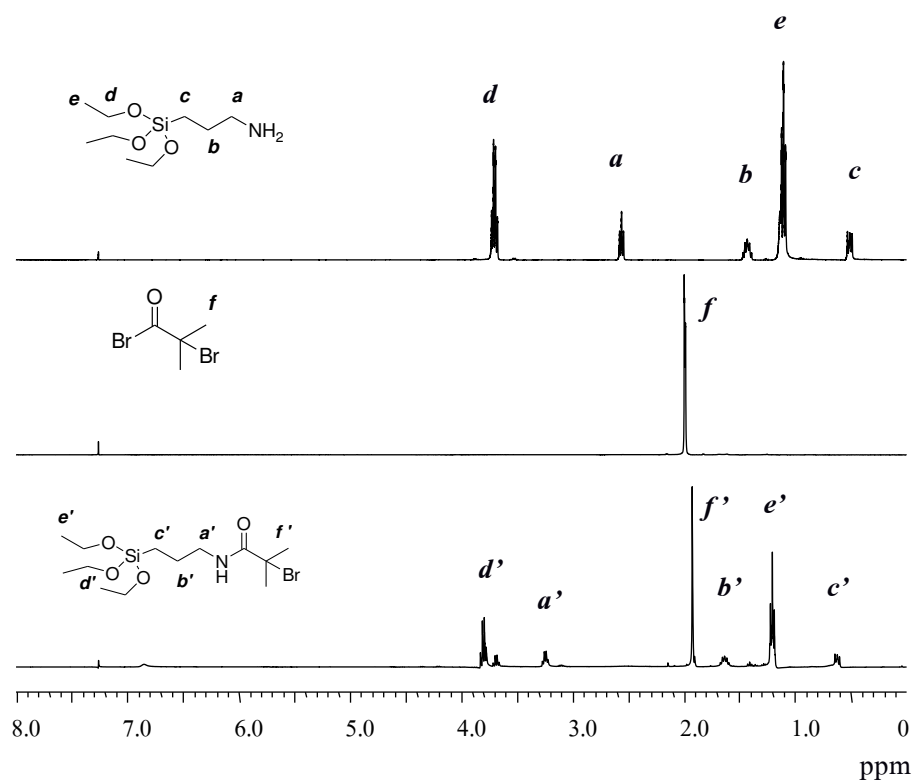
BTPAm was prepared through an amidization reaction between APS and BIBB. Comparing with the FTIR spectrum of APS and BIBB, Figure A4C showed FTIR characteristic absorption peaks of BTPAm (1658 cm<sup>-1</sup> of -NH-CO- carbonyl stretching, 1112-1026 cm<sup>-1</sup> of Si-O stretching, 1532 cm<sup>-1</sup> of N-H bending and 3345 cm<sup>-1</sup> of N-H- stretching).

Figure A5C showed a <sup>1</sup>H NMR spectrum of BTPAm in comparison with APS and BIBB starting reagents. In good agreement with FTIR results, a distinctive shift of the <sup>1</sup>H NMR signal corresponding to methylene protons adjacent to NH group (from 2.50 ppm, signal *a*, to 3.22 ppm, signal *a'*) indicated the formation of BTPAm. In addition, slight shifts of other signals such as methylene protons of signal *b* (1.45 ppm)

to signal *b'* (1.62 ppm), and methyl protons of signal *f* (2.50 ppm) to signal *f'* (2.40 ppm) also confirmed the formation of BTPAm.



**Figure A4** FTIR spectra of A) 3-aminopropyl triethoxysilane (APS), B) 2-bromoiso-butryl bromide (BIBB) and C) (2-bromo-2-methyl-N-(3-(triethoxysilyl)propanamide (BTPAm)



**Figure A5**  $^1\text{H}$  NMR spectra of A) (3-aminopropyl) triethoxysilane (APS) (solvent:  $\text{CDCl}_3$ ), B) 2-bromoisobutyryl bromide (BIBB) (solvent:  $\text{CDCl}_3$ ) and C2-bromo-2-methyl-N-(3-(triethoxysilyl)propyl) propanamide (BTPAm) (solvent:  $\text{CDCl}_3$ )

## Part 2. Synthesis of poly(PEGMA-*stat*-VDM) by ATRP in solution in different reaction conditions

### (A) Synthesis of poly(PEGMA-*stat*-VDM) by ATRP in solution

Conditions: [PEGMA]<sub>0</sub>/[VDM]<sub>0</sub>/[EBiB]<sub>0</sub>/[CuBr]<sub>0</sub>/[Me<sub>6</sub>Tren]<sub>0</sub> = 50/50/1/1/1

Temperature: 50°C

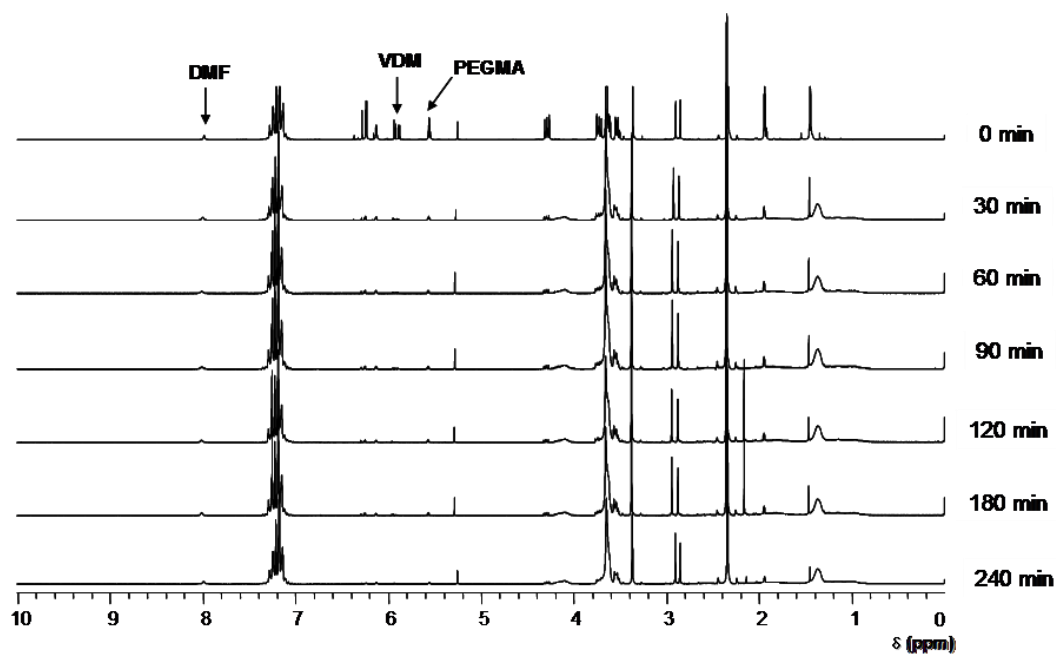
Solvent: 70% v/v toluene

Internal standard: 5% v/v DMF

**Table A1** Summary of monomer conversion, molecular weight and PDI of statistical copolymers poly(PEGMA-*stat*-VDM) obtained by ATRP using [EBiB]<sub>0</sub>/[CuBr]<sub>0</sub>/[Me<sub>6</sub>Tren]<sub>0</sub> molar ratio = 1/1/1-in toluene (70% v/v) at 50°C

time	conv. <sup>a</sup> (%)		$\overline{M}_{n,th}^b$	$\overline{M}_{n,SEC}^c$	PDI <sup>c</sup>
	PEGMA	VDM	(g/mol)	(g/mol)	
0	0	0	0	0	0
30	83	90	18705	29400	2.17
60	84	92	18994	54200	2.44
90	84	93	19064	34800	3.00
120	88	94	19733	52200	3.12
180	89	94	53122	19900	3.28
240	90	95	33327	20100	4.09
300	89	95	41552	20000	3.71

<sup>a</sup> Determined by <sup>1</sup>H NMR spectroscopy (monomer depletion monitored relative to DMF, which was used as an internal standard). <sup>b</sup>  $\overline{M}_{n,th} = ([\text{PEGMA}]_0/[\text{EBiB}]_0 \times \text{conv.}_{\text{PEGMA}} \times M_{\text{PEGMA}}) + [\text{VDM}]_0/[\text{EBiB}]_0 \times \text{conv.}_{\text{VDM}} \times M_{\text{VDM}}$ . <sup>c</sup> Measured by SEC (calibrated with polystyrene standards).



**Figure A6** Monitoring of monomers conversions by  $^1\text{H}$  NMR spectroscopy during atom transfer radical polymerization of PEGMA and VDM using DMF as an internal standard

**(B) Synthesis of poly(PEGMA-*stat*-VDM) by ATRP in solution**

Conditions: [PEGMA]<sub>0</sub>/[VDM]<sub>0</sub>/[EBiB]<sub>0</sub>/[CuBr]<sub>0</sub>/[Me<sub>6</sub>Tren]<sub>0</sub> = 50/50/1/0.5/0.5

Temperature: 30°C

Solvent: 70% v/v toluene

Internal standard: 5% v/v DMF

**Table A2** Summary of monomer conversion, molecular weight, and PDI of statistical copolymers poly(PEGMA-*stat*-VDM) obtained by ATRP using [EBiB]<sub>0</sub>/[CuBr]<sub>0</sub>/[Me<sub>6</sub>Tren]<sub>0</sub> ratio = 1/0.5/0.5 in toluene (70% v/v) at 30°C

time (min)	conv. <sup>a</sup> (%)		$\overline{M}_{n,th}^b$	$\overline{M}_{n,SEC}^c$	PDI <sup>c</sup>
	PEGMA	VDM	(g/mol)	(g/mol)	
0	0	0	0	0	0
30	46	58	10931	11244	1.40
60	60	72	14004	15281	1.48
90	70	82	16199	18604	1.72
120	88	94	16788	21743	1.96
180	89	94	18186	24390	1.95
240	90	95	18405	27781	2.04
300	89	95	18775	27799	2.19

<sup>a</sup> Determined *via* <sup>1</sup>H NMR spectroscopy (monomer depletion monitored relative to DMF, which was used as an internal standard). <sup>b</sup>  $\overline{M}_{n,th} = ([\text{PEGMA}]_0/[\text{EBiB}]_0 \times \text{conv.}_{\text{PEGMA}} \times M_{\text{PEGMA}}) + [\text{VDM}]_0/[\text{EBiB}]_0 \times \text{conv.}_{\text{VDM}} \times M_{\text{VDM}}$ . <sup>c</sup> Measured by SEC (calibrated with polystyrene standard).



**(C) Synthesis of poly(PEGMA-*stat*-VDM) by ATRP in solution**

Conditions: [PEGMA]<sub>0</sub>/[VDM]<sub>0</sub>/[EBiB]<sub>0</sub>/[CuBr]<sub>0</sub>/[Me<sub>6</sub>Tren]<sub>0</sub> = 50/50/1/0.2/0.2

Temperature: 30°C

Solvent: 70% v/v toluene

Internal standard: 5% v/v DMF

**Table A3** Summary of monomer conversion, molecular weight, and PDI of statistical copolymers poly(PEGMA-*stat*-VDM) obtained by ATRP using [EBiB]<sub>0</sub>/[CuBr]<sub>0</sub>/[Me<sub>6</sub>Tren]<sub>0</sub> molar ratio = 1/0.2/0.2 in toluene (70% v/v) at 30°C

time (min)	conv <sup>a</sup> (%)		$\overline{M}_{n,th}^b$	$\overline{M}_{n,SEC}^c$	PDI <sup>c</sup>
	PEGMA	VDM	(g/mol)	(g/mol)	
0	0	0	0	0	0
15	11	15	2693	6500	1.11
30	25	31	5905	9500	1.17
45	34	41	7950	10800	1.24
60	38	48	9036	12200	1.33
90	52	61	12040	14400	1.35
120	55	64	12698	15200	1.40
180	58	67	13357	16700	1.39
300	56	66	12987	15100	1.43

<sup>a</sup> Determined by <sup>1</sup>H NMR spectroscopy (monomer depletion monitored relative to DMF, which was used as an internal standard). <sup>b</sup>  $\overline{M}_{n,th} = ([\text{PEGMA}]_0/[\text{EBiB}]_0 \times \text{conv.}_{\text{PEGMA}} \times M_{\text{PEGMA}}) + [\text{VDM}]_0/[\text{EBiB}]_0 \times \text{conv.}_{\text{VDM}} \times M_{\text{VDM}}$ . <sup>c</sup> Measured by SEC (calibrated with polystyrene standard).

### Part 3. Calculation of the grafting density of thymine PNA monomer on the MNP surface

From TGA result, the MNP complex exhibited about 4.1 wt% of thymine PNA monomer. Weight of poly(PEGMA-*stat*-VDM)-coated MNP used was 10 mg; weight of thymine PNA monomer per gram of the complex;

$$= \left( \frac{4.1 \text{ g} \times 10 \times 10^{-3} \text{ g}}{100 \text{ g}} \right)$$

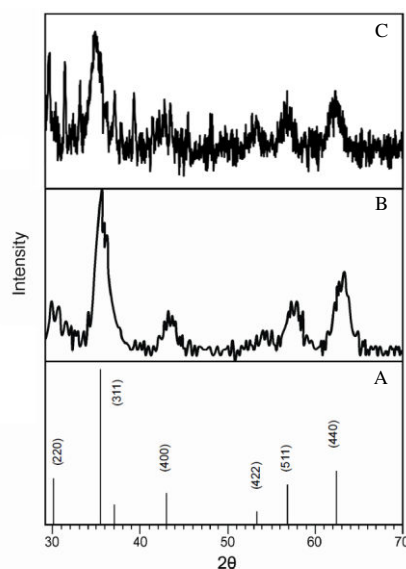
$$= 4.1 \times 10^{-4} \text{ g/g of the complex}$$

Because molecular weight of thymine PNA monomer = 338 g/mol, mole of thymine PNA monomer per gram of the complex;

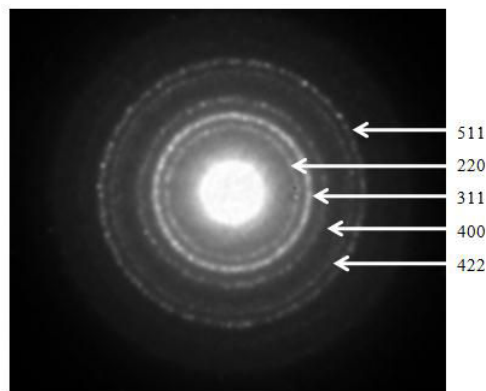
$$= \left( \frac{4.1 \times 10^{-4} \text{ g}}{338 \text{ g/mol}} \right)$$

$$= 1.2 \text{ } \mu\text{mol/g of the complex}$$

### Part 4. Determination of crystal structure of magnetite nanoparticles



**Figure A7** X-ray diffraction patterns of (A) standard magnetite powder (ICSD No. 01-075-0449), (B) bare MNP and (C) poly(PEGMA-*stat*-VDM)-coated MNP



**Figure A8** Selected area electron diffraction (SAED) pattern of poly(PEGMA-*stat*-VDM)-coated MNP immobilized with thymine PNA monomer

### Part 5. Percentage of magnetite in the complex and their magnetic properties

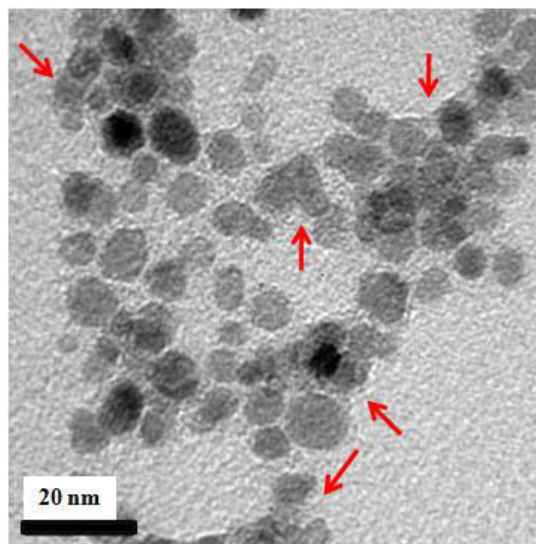
**Table A4** Composition and magnetic properties of the each complex

Type of complex	% Char yield <sup>a</sup>	% in the complex <sup>a</sup>				emu/g of complex <sup>b</sup>	emu/g of Fe <sub>3</sub> O <sub>4</sub> <sup>a,b</sup>
		Fe <sub>3</sub> O <sub>4</sub>	BTPAm	Poly(PEGMA- <i>stat</i> -VDM)	Thymine		
A) Bare MNP	92	100	-	-	-	56	56
B) BTPAm-coated MNP	85	92	8	-	-	49	53
C) Poly(PEGMA- <i>stat</i> -VDM)-coated MNP	71	77	6	17	-	36	47
D) Thymine-poly(PEGMA- <i>stat</i> -VDM)-coated MNP	68	74	6	16	4	34	46

<sup>a</sup> Estimated from % char yield at 600°C *via* TGA technique

<sup>b</sup> Estimated from  $M_s$  values at 10,000 G *via* VSM technique

**Part 6. A TEM image of poly(PEGMA-*stat*-VDM)-coated MNP**

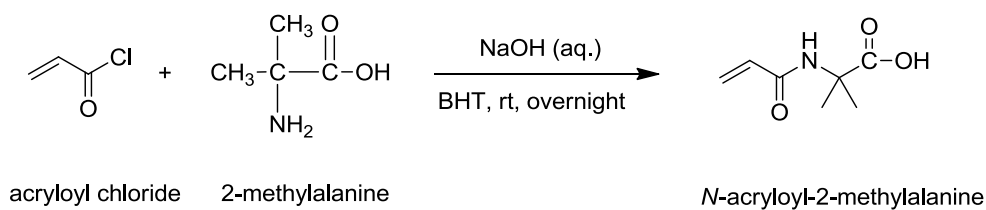


**Figure A9** A TEM image of poly(PEGMA-*stat*-VDM)-coated MNP showing the presence of polymeric thin film on the particle surface (indicated by arrows)

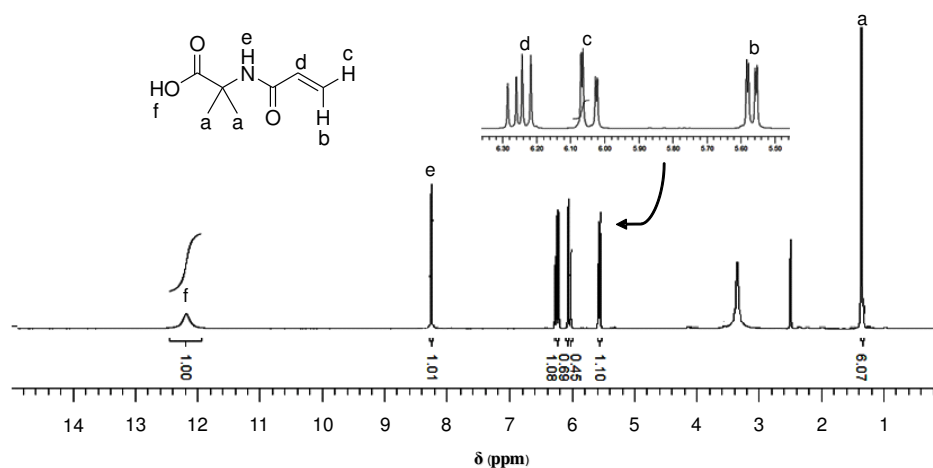
## Appendix B

### Part 1. Synthesis of 2-vinyl-4,4-dimethylazlactone (VDM) monomer

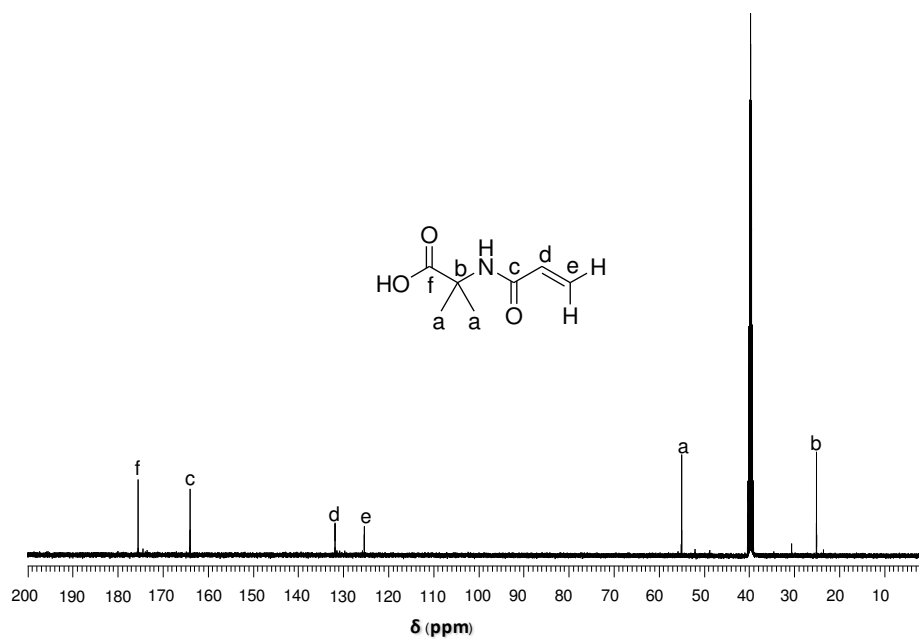
#### (A) Synthesis of *N*-acryloyl-2-methylalanine (Figure B1)



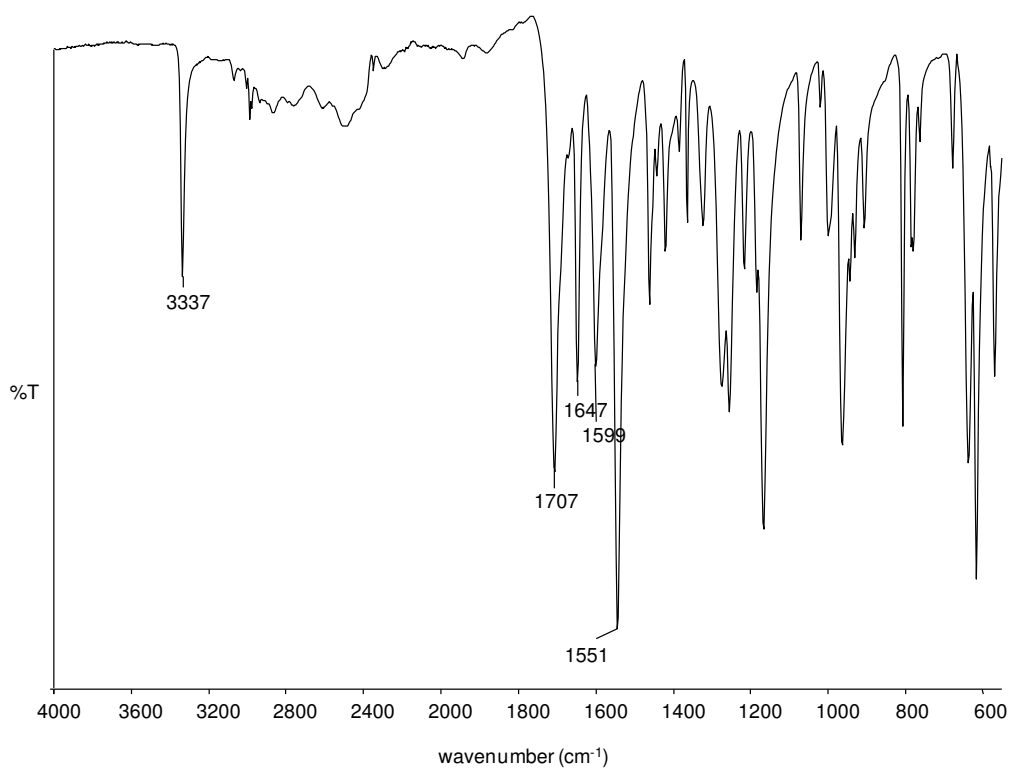
**Figure B1** Synthesis of *N*-acryloyl-2-methylalanine



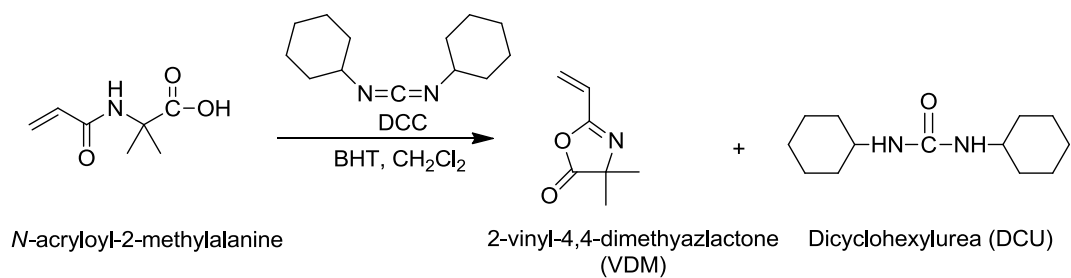
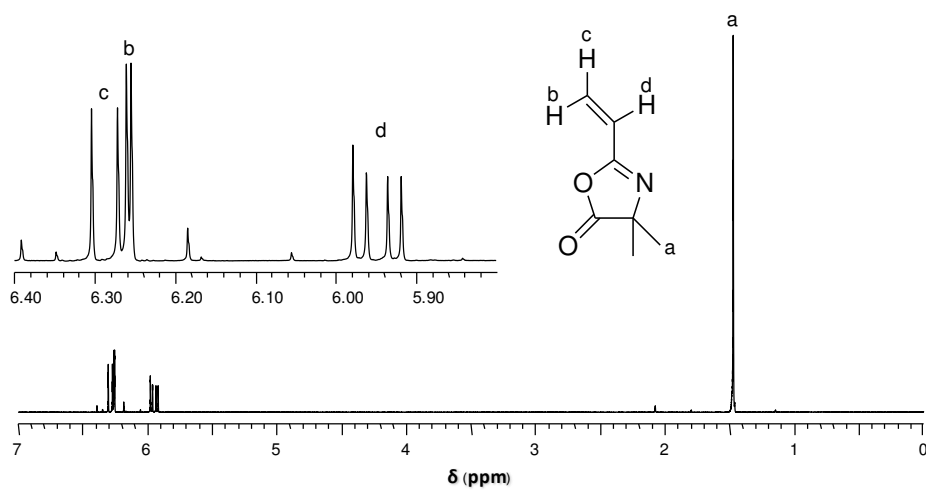
**Figure B2**  $^1\text{H}$  NMR spectrum of *N*-acryloyl-2-methylalanine in  $\text{DMSO-}d_6$

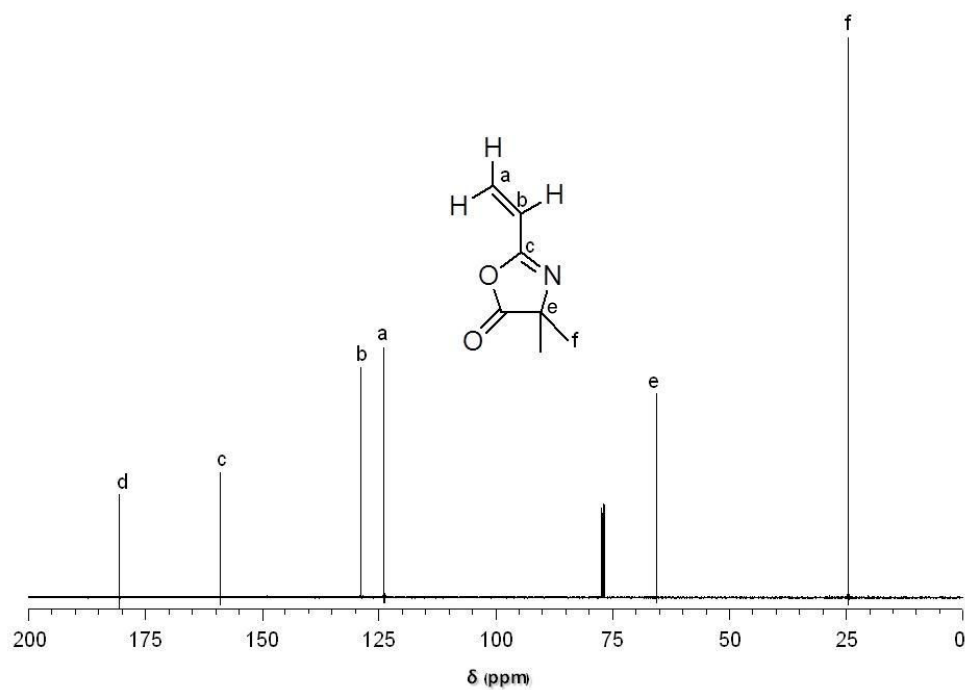


**Figure B3**  $^{13}\text{C}$  NMR spectrum of *N*-acryloyl-2-methylalanine in DMSO- $d_6$

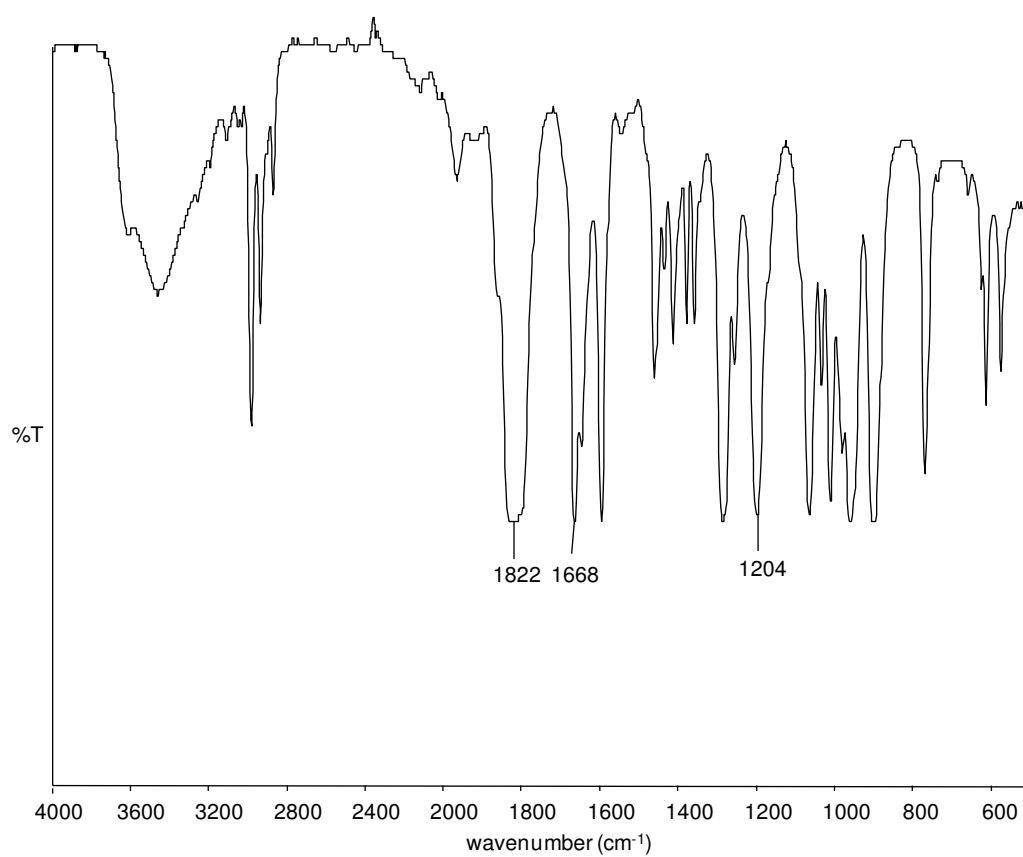


**Figure B4** FTIR spectrum of *N*-acryloyl-2-methylalanine

**(B) Cyclization of *N*-acryloyl-2-methylalanine to form VDM cyclic (Figure B5)****Figure B5** Synthesis of VDM monomer**Figure B6**  $^1\text{H}$  NMR spectrum of the VDM in  $\text{CDCl}_3$



**Figure B7**  $^{13}\text{C}$  NMR spectrum of the VDM in  $\text{CDCl}_3$

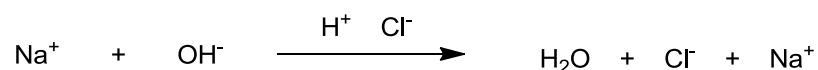


**Figure B8** FTIR spectrum of VDM



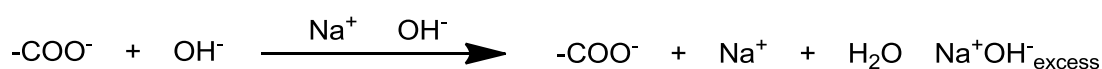
## Part 2. Calculations of the grafting density of carboxyl groups on poly(PEGMA-*stat*-VDM)-coated MNP after dispersing in water

The amounts of carboxyl groups presenting on the particle surface were quantitatively determined by a conductometric titration. Figure B9 shows the conductometric titration curve of the reaction between NaOH and HCl having a V-shape (Blank). During the titration, the reaction that takes place in the titration vessel is following:

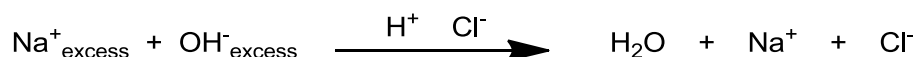


In the region I, before the end point,  $\text{OH}^-$  is removed from the solution by reaction with  $\text{H}^+$ , and  $\text{Cl}^-$  is added to the solution. The conductance of the solution decreases prior to the end point. After the end point (region II), no  $\text{OH}^-$  is available to react, and the conductance of the solution increases as a result of the additional of  $\text{H}^+$  and  $\text{Cl}^-$ .

In the case of the titration of HCl with  $-\text{COOH}$  groups on the particle surface, the conductometric titration curve exhibits three regions (Figure B9B). Before the titration of  $-\text{COOH}$  groups on the MNP surface, the  $-\text{COOH}$  grafted on the MNP surface was dispersed in an excess of NaOH solution. Thus, the reaction that takes place in the vessel is following:



In the region I of the titration, because basicity of excess  $\text{OH}^-$  in the solution is stronger than that of  $-\text{COO}^-$ , the  $\text{OH}^-$  in the solution was first neutralized when HCl was titrated.



In the region II, when the  $\text{OH}^-$  in the solution was completely neutralized, the  $\text{H}^+$  ions reacted with the  $\text{COO}^-$  groups on the MNP surface. After the  $\text{COO}^-$  groups on the MNP surface were completely reacted with  $\text{H}^+$  ions, the solution conductivity sharply increase due to the excess of  $\text{OH}^-$  and  $\text{Na}^+$  (region III). The measurement of

the amounts of –COOH groups on the surface of the polymer-grafted MNP was estimated from the following equation:

$$[Acid] = \frac{V \times M \times N_A}{SC}$$

Where,  $[Acid]$  is the number of carboxyl groups per gram sample (molecules/g)

$V$  is the consumption volume of HCl solution in the second region (region II) of the conductometric titration (L)

$M$  is the molar concentration of polyelectrolyte (mol/L)

$N_A$  is Avogadro's constant ( $6.022 \times 10^{23}$  molecules/mol)

$SC$  is the solid content or the sample (g)

From TEM analysis, particle diameter is 8 nm.

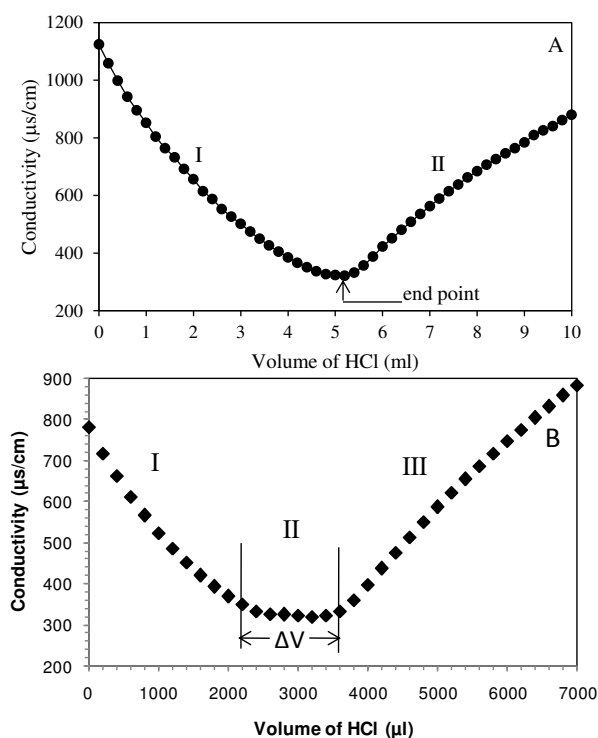
Surface area =  $4\pi r^2$ , where  $r = 4$  nm

Thus, surface area of a single particle =  $4 \times (22/7) \times 4^2 = 201 \text{ nm}^2$

For example, in the case of poly(VDM)-coated MNP (PEGMA:VDM = 0/100) :

$$\begin{aligned} [Acid] &= \frac{((3600-2200) \times 10^{-6} \text{ L}) \times (0.005 \text{ mol/L}) \times (6.022 \times 10^{23} \text{ molecules/mol})}{1.50 \times 10^{-3} \text{ g}} \\ &= 2.8103 \times 10^{21} \text{ molecules/g} \\ &= 2.8103 \times 10^{21} \text{ molecules} / 7.09 \times 10^{17} \text{ particles} \\ &= 3963.70 \text{ molecules/particle} \\ &= 3963.70 \text{ molecules} / 201 \text{ nm}^2 \\ &= 19.72 \text{ molecules/nm}^2 \end{aligned}$$

$$\begin{aligned} \text{Carboxylic acid} &= \frac{M \Delta V}{m} \\ &= \frac{0.005 \text{ mol/L} \times (1400 \times 10^{-6} \text{ L})}{0.0015 \text{ g}} \\ &= 4.67 \text{ mmol/g} \end{aligned}$$



**Figure B9** Examples of the conductometric titration curves, A) the titration curve of HCl with NaOH and B) the titration curve of HCl with carboxyl groups on the polymer-coated MNP surface

### Part 3. Example of the calculation of grafting density of BTPAm, poly(VDM) and FA

From TEM analysis, particle diameter is 8 nm.

Surface area =  $4\pi r^2$ , where  $r = 4$  nm

Thus, surface area of a single particle =  $4 \times (22/7) \times 4^2 = 201 \text{ nm}^2$

Volume =  $\frac{4}{3}\pi r^3$ , where  $r = 4$  nm

Thus, volume of a single particle =  $(\frac{4}{3}) \times (22/7) \times 4^3 = 268 \text{ nm}^3$

Because density of magnetite =  $5.26 \text{ g/cm}^3$  [reference 1-2] = mass/volume

Mass of a single particle =  $5.26 \text{ g/cm}^3 \times 268 \text{ nm}^3 = 1.41 \times 10^{-18} \text{ g}$

#### References

- [1] Tebble RS, Craik DJ. Magnetic Materials, Wiley-Interscience, London, 1969.
- [2] Cornell RM, Schertmann U. The Iron Oxides: Structure, Properties, Reactions, Occurrence and Uses, VCH Publishers, Weinheim, 1996.

From TGA result, FA-poly(VDM)-coated MNP possessed 71.5% Fe<sub>3</sub>O<sub>4</sub>, 5.6% BTPAm, 12.3% poly(VDM) and 10.6% FA

$$\begin{aligned}\text{Weight of BTPAm-coated on a single particle} &= (1.41 \times 10^{-8} \text{ g}) \times (5.6/71.5) \\ &= 1.10 \times 10^{-19} \text{ g}\end{aligned}$$

$$\text{Moles of BTPAm} = (1.10 \times 10^{-19} \text{ g}) / (156 \text{ g/mol});$$

$$\text{MW. Of BTPAm} = 156 \text{ g/mol}$$

$$\begin{aligned}&= (1.10 \times 10^{-19} \text{ g}) (6.02 \times 10^{23} \text{ molecule/mol}) / (156 \text{ g/mol}) \\ &= 424 \text{ molecules/particle} \\ &= 424 \text{ molecules}/201 \text{ nm}^2 \\ &= 2.1 \text{ molecule/nm}^2\end{aligned}$$

Similarly, weight of poly(VDM) coated on a single particle

$$\begin{aligned}&= (1.41 \times 10^{-18} \text{ g}) \times (12.3/71.5) \\ &= 2.42 \times 10^{-19} \text{ g}\end{aligned}$$

$$\text{Moles of azlactone ring} = (2.42 \times 10^{-19} \text{ g}) / (139.15 \text{ g/mol});$$

$$\text{MW. of VDM unit} = 139.15 \text{ g/mol}$$

$$\text{Number of azlactone ring} = ((2.42 \times 10^{-19} \text{ g}) \times (6.02 \times 10^{23} \text{ molecules/mol})) / (139.15 \text{ g/mol})$$

$$\begin{aligned}&= 1046.74 \text{ molecules/particle} \\ &= 1046.74 \text{ molecules}/201 \text{ nm}^2 \\ &= 5.2 \text{ molecules/nm}^2\end{aligned}$$

Similarly, weight of FA in a single particle =  $(1.41 \times 10^{-18} \text{ g}) \times (10.6/71.5)$

$$= (2.09 \times 10^{-19} \text{ g})$$

$$\text{Moles of FA} = (2.09 \times 10^{-19} \text{ g}) / (483 \text{ g/mol}) \quad ; \text{ MW. of EDA-FA} = 483 \text{ g/mol}$$

$$\text{Number of FA} = ((2.09 \times 10^{-19} \text{ g}) \times (6.02 \times 10^{23} \text{ molecules/mol})) / (483 \text{ g/mol})$$

$$\begin{aligned}&= 260.54 \text{ FA molecules/particle} \\ &= 260.54 \text{ molecules}/201 \text{ nm}^2 \\ &= 1.30 \text{ molecule/nm}^2\end{aligned}$$

## **BIOGRAPHY**

## BIOGRAPHY

<b>Name - Surname</b>	Yingrak Pray-in
<b>Date of Birth</b>	June 9, 1982
<b>Address</b>	143/3 Moo 6, Maekong, Amphoe Nongchang, Uthai thani, Thailand. 61110
<b>Education Background</b>	
2005	B.S. (Chemistry) Naresuan University, Phitsanulok, Thailand
2009	M.S. (Industrial Chemistry) Naresuan University, Phitsanulok, Thailand

### Research Output

- Prai-in, Y., Tankanya, K., Rutnakornpituk, B., Wichai, U., Montembault, V., Pascual, S., Fontaine, L., Rutnakornpituk, M. (2012). Azlactone functionalization of magnetic nanoparticles using ATRP and their bioconjugation. **Polymer**, 53, 113-120
- Pray-in, Y., Rutnakornpituk, B., Wichai, U., Vilaivan, T., Rutnakornpituk, M. (2014). Hydrophilic azlactone-functionalized magnetite nanoparticle for conjugation with folic acid. **Journal of Nanoparticle Research**, 16:2357
- Pray-in, Y., Rutnakornpituk, B., Wichai, U., Montembault, V., Pascual, S., Fontaine, L., Rutnakornpituk, M. Recyclable magnetic nanocluster crosslinked with poly(ethylene oxide)-*block*-poly(2-vinyl-4,4-dimethylazlactone) copolymer for adsorption with antibody. (draft manuscript)

### Presentations

- Pray-in, Y., Tankanya, K., Rutnakornpituk, B., Wichai, U., Montembault, V., Pascual, S., Fontaine, L., Rutnakornpituk, M. “**Hydrophilic azlactone functionalized magnetic nanoparticles and their application as scavengers**”, Poster presentation at Pure and Applied Chemistry International

Conference 2012 (PACCON 2012), Chiang mai, Thailand, 11-13<sup>th</sup> January 2012.

- Pray-in, Y., Tankanya, K., Rutnakornpituk, B., Wichai, U., Montembault, V., Pascual, S., Rutnakornpituk, M., Fontaine, L. “**Azlactone functionalization of magnetic nanoparticles using ATRP and their bioconjugation**”, Poster presentation at European Polymer Congress (epf2013), Pisa, Italy, 16-21<sup>st</sup> June 2013.
- Pray-in, Y., Rutnakornpituk, B., Wichai, U., Montembault, V., Pascual, S., Rutnakornpituk, M., Fontaine, L. “**Azlactone functionalization of magnetic nanoparticles using CRP techniques**”, Oral presentation at Journées de l’Ecole Doctorale (JED2013), Angers, France, 24-25<sup>th</sup> June 2013.

# Thèse de Doctorat

Yingrak PRAY-IN

## Az lactone functionalization of magnetic nanoparticles using crp techniques and their bioconjugation

### Fonctionnalisation de l'az lactone de nanoparticules magnétiques à l'aide de techniques de crp et de leur bioconjugation

#### Résumé

Nous rapportons ici la modification de surface de nanoparticule de magnétite (MNP) avec des copolymères contenant des noyaux d'azlactone actifs par greffage «from» et greffage Polymérisation radicalaire contrôlée «sur» (CRP) à utiliser comme support nano-solide pour immobilisation avec des biomolécules. Trois approches différentes ont été présentées comme suivant.

Premièrement, la synthèse du méthacrylate de méthyléther-stat-2- de poly (éthylène glycol) méthylque vinyl-4,4-diméthylazlactone) (PNG-PEGMA-stat-VDM) greffée via un greffage «à partir d'atome»

polymérisation radicalaire par transfert (ATRP) et son application comme plateforme de conjugaison. Le monomère d'acide nucléique peptidique (PNA) de thymine a été présenté. ATRP de PEGMA et VDM a d'abord été réalisée en solution pour optimiser les conditions de réaction. Cela a été trouvé le rapport molaire 1 / 0,2 / 0,2 du [bromure de cuivre-éthyl-2-bromoisobutyrate (EBiB)] 0 / [cuivre (I)]

(CuBr)] 0 / [tris- [2- (diméthylamino) éthyle] amine (Me6Tren)] 0, respectivement, ont conduit à un bon contrôle de la copolymérisation; les polymères résultants ont un poids moléculaire (n M) proches des valeurs théoriques et des indices de polydispersité relativement étroits (PDI = 1,11-1,43). La condition optimale a ensuite été appliquée dans l'ATRP du MNP initié en surface.

La transformation de la coque en polymère sur le noyau de la MNP était indiquée par la transformation de Fourier la spectroscopie infrarouge (FTIR) et les techniques de magnéto-métrie à échantillon vibrant (VSM).

Après immobilisation du monomère thymine-PNA, analyse thermogravimétrique (TGA) Les résultats ont montré que le complexe contenait 4% en poids de monomère de PNA (1.2 μmol / g complexe). La présence du monomère PNA a également été confirmée par FTIR et VSM.

Dans le deuxième travail, la synthèse de MNP greffés avec PEGMA et VDM via ATRP pour une conjugaison avec l'acide folique (FA) a été étudiée. Un greffage «from» a été appliqué pour la copolymérisation de PEGMA et de VDM à partir de la surface des particules avec diverses compositions molaires de PEGMA à VDM (0/100, 30/70, 50/50 et 70/30, respectivement). L'existence de PEGMA et de VDM dans la structure a été caractérisée par FTIR, TGA et VSM. Il a été trouvé que le degré de PEGMA et de VDM pouvait être ajusté avec précision en faisant varier le rapport molaire PEGMA et VDM dans la copolymérisation. Après la conjugaison de FA, le résultat de TEM indiquait que le MNP conjugué à FA ayant une teneur élevée en VDM présentait une bonne dispersibilité dans l'eau.

Troisièmement, la synthèse de MNP greffé avec un copolymère dibloc poly (oxyde d'éthylène) -bloc-poly (2-vinyl-4,4-diméthylazlactone) (PEO-b-PVDM) via une stratégie de greffage "sur" et son application en tant que source magnétique recyclable nano-support pour l'adsorption avec des anticorps ont été étudiés. Les copolymères diblocs PEO-b-PVDM ont d'abord été synthétisés en utilisant une polymérisation réversible par transfert de chaîne par addition (RAFT), puis greffés sur du MNP à fonctionnalité amino par couplage avec des noyaux azlactone du bloc PVDM. La TEM a été utilisée pour étudier le nanocluster de particules et sa distribution. Il a été constaté que l'augmentation de la longueur de la chaîne PVDM augmentait la taille des nanoclusters de MNP de 20 à 150 nm; environ 10, 50 et 100 particules / groupe pour le copolymère dibloc PEO-b-PVDM21, PEO-b-PVDM41 et PEO-b-PVDM84, respectivement. De plus, les images TEM et la technique de spectroscopie par photo-corrélation (PCS) ont indiqué une amélioration de la dispersibilité des particules dans l'eau après revêtement avec les copolymères. Les nanoclusters avec revêtement de copolymère dibloc PEO-b-PVDM84 ont été utilisés en tant que nano-supports magnétiques recyclables pour une adsorption avec un anticorps. Les résultats montrent qu'il y avait une capacité d'adsorption de 96 à 99% au cours de huit cycles d'adsorption-séparation-désorption.

#### Mots clés

**Magnétite, nanoparticule, ATRP, polymérisation RAFT, PNA, acide folique, anticorps.**

#### Abstract

We herein report the surface modification of magnetite nanoparticle (MNP) with copolymers containing active azlactone rings via a grafting 'from' and grafting 'onto' controlled radical polymerization (CRP) for use as a nano-solid support for immobilization with biomolecules. Three different approaches were presented as following.

First, synthesis of poly(poly(ethylene glycol) methyl ether methacrylate-stat-2-vinyl-4,4-dimethylazlactone) (PEGMA-stat-VDM)-grafted MNP via a grafting 'from' atom transfer radical polymerization (ATRP) and its application as a platform for conjugating thymine peptide nucleic acid (PNA) monomer were presented. ATRP of PEGMA and VDM was firstly carried out in a solution system to optimize the reaction condition. It was found that 1/0.2/0.2 molar ratio of [ethyl-2-bromoisobutyrate (EBiB)]/[copper(I) bromide (CuBr)]/[tris-[2-(dimethylamino)ethyl]amine (Me6Tren)] 0, respectively, led to a good control of the copolymerization; the resulting polymers have molecular weight (n M) close to the theoretical ones and relatively narrow polydispersity indices (PDIs = 1.11-1.43). The optimal condition was then applied in the surface-initiated ATRP of MNP.

The presence of polymeric shell on MNP core was indicated by fourier transform infrared spectroscopy (FTIR) and vibrating sample magnetometry (VSM) techniques.

After immobilization of thymine PNA monomer, thermogravimetric analysis (TGA) results showed that there were 4 wt% of the PNA monomer in the complex (1.2 μmol/g complex). The presence of the PNA monomer was also confirmed via FTIR and VSM.

In the second work, the synthesis of MNP grafted with PEGMA and VDM via ATRP for conjugation with folic acid (FA) was studied. A grafting 'from' was applied for the copolymerization of PEGMA and VDM from the particle surface with various molar compositions of PEGMA to VDM (0/100, 30/70, 50/50 and 70/30, respectively). The existence of PEGMA and VDM in the structure was characterized by FTIR, TGA and VSM. It was found that the degree of PEGMA and VDM could be finely tuned by varying the molar ratio of PEGMA and VDM in the copolymerization. After the FA conjugation, TEM result indicated that the FA-conjugated MNP having high VDM content exhibited good dispersibility in water.

Third, the synthesis of MNP grafted with poly(ethylene oxide)-block-poly(2-vinyl-4,4-dimethylazlactone) (PEO-b-PVDM) diblock copolymer via a grafting 'onto' strategy and its application as recyclable magnetic nano-support for adsorption with antibody were studied. PEO-b-PVDM diblock copolymers were first synthesized using a reversible addition-fragmentation chain transfer (RAFT) polymerization and then grafted onto amino-functionalized MNP by coupling with some azlactone rings of the PVDM block. TEM was used to investigate the particle nanoclustering and its distribution. It was found that increasing the PVDM chain length increased the size of MNP nanoclusters from 20 to 150 nm; approximately 10, 50 and 100 particles/cluster for PEO-b-PVDM21, PEO-b-PVDM41 and PEO-b-PVDM84 diblock copolymer, respectively. Moreover, TEM images and photo correlation spectroscopy (PCS) technique indicated an improvement in the particle dispersibility in water after coating with the copolymers. The nanoclusters with PEO-b-PVDM84 diblock copolymer coating were used as recyclable magnetic nano-supports for adsorption with antibody. The results show that there was 96-99% adsorption ability during eight adsorption-separation-desorption cycles.

#### Key Words

**Magnetite, nanoparticle, ATRP, RAFT polymerization, PNA, folic acid, antibody.**